

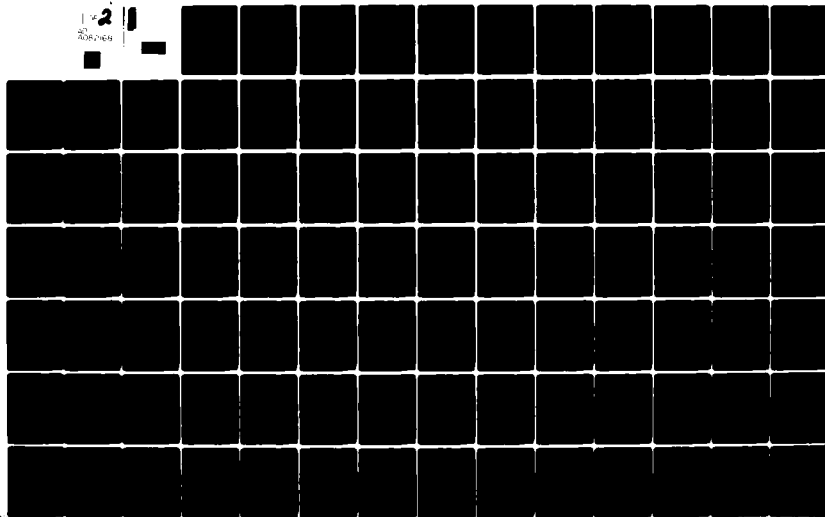
AQ-A082 168

AIR FORCE INST OF TECH WRIGHT-PATTERSON AFB OH SCHOO--ETC F/G 20/4
INITIAL DEVELOPMENT FOR A FLUTTER ANALYSIS OF DAMAGED T-38 HORI--ETC(U)
MAR 80 J O LASSITER
AFIT/6AE/AA/80M-2

UNCLASSIFIED

NL

2
AD
A082/168



AFIT/GAE/AA/80M-2

(1)

DTIC
RECEIVED

(1) INITIAL DEVELOPMENT FOR
A FLUTTER ANALYSIS OF DAMAGED
T-38 HORIZONTAL STABILATORS
USING NASTRAN.

THESIS

AFIT/GAE/AA/80M-2

John O./Lassiter
2d Lt USAF

(1) 11

(11)

Approved for Public Release; Distribution Unlimited

012000

AFIT/GAE/AA/8QM-2

INITIAL DEVELOPMENT FOR
A FLUTTER ANALYSIS OF DAMAGED
T-38 HORIZONTAL STABILATORS USING NASTRAN

THESIS

Presented to the Faculty of the School of Engineering
of the Air Force Institute of Technology

Air University
in Partial Fulfillment of the
Requirements for the Degree of
Master of Science

by
John O. Lassiter, B.S.A.E.
2d Lt USAF
Graduate Aerospace Engineering
March 1980

Approved for Public Release; Distribution Unlimited

Preface

Accession For	NTIS C-141	
DDC TAB	Unannounced	
Justification		
By		
Distribution/		
Availability Codes		
Dist	Avail and/or special	A

The author owes his thanks and appreciation to his thesis advisor, Captain Hugh C. Briggs, whose guidance and interest in this thesis greatly helped the author with his first "real world problem." I am grateful for having had such an advisor.

A special word of thanks goes to Dr. V. Venkayya, Mr. J. R. Johnson, Mr. Bernard H. Groomes, Mrs. Victoria Tischler, and Cheryle Mummert of the Air Force Flight Dynamics Laboratory. Their help with NASTRAN and STAGING proved to be invaluable.

To Sharon Gabriel I extend my deep appreciation for her forbearance in typing the many aspects of this thesis. Without her help, putting together this work would have been much harder.

Also, I would like to thank 1st Lieutenant William Rohlman of the Air Force Armament Laboratory, Eglin Air Force Base, Florida, for the very useful data that appears in the Modal Analysis section of this thesis.

Space prohibits mentioning the many other people, both at Wright-Patterson AFB and at Kelly AFB, who have helped me greatly. To these I say a hearty thank you.

John O. Lassiter

Contents

	<u>Page</u>
Preface-----	ii
List of Figures-----	v
List of Tables-----	viii
List of Symbols-----	ix
Abstract-----	xi
I. INTRODUCTION-----	1
Initial Request of Sponsor-----	1
Background and Statement of Problem-----	1
General Approach to the Problem-----	3
Assumptions and Restrictions-----	5
Computer Software and Hardware-----	6
Literature Review-----	7
II. A FINITE ELEMENT MODEL OF THE HORIZONTAL STABILATOR-----	8
Introduction-----	8
Description of the Stabilator-----	8
The Finite Element Model-----	11
III. FINITE ELEMENT MODEL VERIFICATION USING AN INFLUENCE COEFFICIENT AND MASS DISTRIBUTION CHECK-----	22
Introduction-----	22
Static Analysis Using Influence Coefficients---	22
Weight, Center of Gravity, and Mass	
Distribution Check-----	37
IV. MODAL ANALYSIS OF THE FINITE ELEMENT MODEL-----	45
Introduction-----	45
Modal Analysis Using NASTRAN-----	45
Rigid Root Modal Analysis-----	47
Flexible Root Modal Analysis-----	65
Results and Conclusions of the Modal Analysis---	91
V. DOUBLET LATTICE AERODYNAMIC MODEL AND FLUTTER ANALYSIS-----	93
Introduction-----	93
Doublet Lattice Aerodynamic Model-----	93

Contents (Cont'd)

	<u>Page</u>
NASTRAN Flutter Analysis of an Undamaged Horizontal Stabilator-----	95
Methods of Simulating a Damaged Horizontal Stabilator-----	96
VI. RESULTS-----	98
VII. CONCLUSIONS-----	99
Bibliography-----	101
APPENDIX A: Stabilator Physical Properties and NASTRAN Bulk Data Deck Generating Program-----	103
APPENDIX B: Experimental Modal Analysis-----	108
Vita-----	109

List of Figures

<u>Figure</u>		<u>Page</u>
1	Series 2 Stabilator-----	9
2	Series 3 Stabilator-----	12
3	Torque Tube and Grid Point Locations-----	16
4	Basic Finite Element Model Showing Grid Points-----	17
5	Basic Finite Element Model Showing Elements-----	18
6	Coordinate System of Finite Element Model--	19
7	Influence Coefficient Load and Deflection Points-----	25
8	Influence Coefficient Finite Element Model Showing Grid Points-----	26
9	Influence Coefficient Finite Model Showing Elements-----	27
10	400 lb Load at Grid Point 149-----	32
11	400 lb Load at Grid Point 153-----	33
12	400 lb Load at Grid Point 155-----	34
13	1200 lb Load at Grid Point 162-----	35
14	1200 lb Load at Grid Point 106-----	36
15	Basic Finite Element Model Showing Lump Parameter Sections Relative to the Elastic Axis-----	40
16	NASTRAN 1st Bending, 23.05 Hz-----	51
17	Converted NAI 1st Bending, 27.08 Hz-----	52
18	NASTRAN 1st Torsion, 51.05 Hz-----	53
19	Converted NAI 1st Torsion, 62.35 Hz-----	54
20	NASTRAN 2nd Bending, 73.11 Hz-----	55

List of Figures (Cont'd)

<u>Figure</u>		<u>Page</u>
21	Converted NAI 2nd Bending, 101.41 Hz-----	56
22	NAI Lump Parameter Model, 2nd Bending (Ref 9:37)-----	57
23	Converted NAI 2nd Bending Viewed from Leading Edge-----	58
24	NASTRAN/GVT Torque Tube Bending, 12.95 Hz----	59
25	Converted GVT 1st Mode, 13.61 Hz-----	60
26	NASTRAN/GVT 2nd Bending, 45.99 Hz-----	61
27	Converted GVT 2nd Mode, 55.67 Hz-----	62
28	NASTRAN/GVT 3rd Torsion, 116.49 Hz-----	63
29	Converted GVT 3rd Mode, 99.21 Hz-----	64
30	Case 1, NASTRAN 1st Bending, 15.56 Hz-----	70
31	Case 1, NAI 1st Bending, 18.80 Hz-----	71
32	Case 1, NASTRAN 1st Torsion, 32.47 Hz-----	72
33	Case 1, NAI 1st Torsion, 44.89 Hz-----	73
34	Case 1, NASTRAN 2nd Bending, 56.08 Hz-----	74
35	Case 1, NAI 2nd Bending, 78.76 Hz-----	75
36	Case 2, Measured Symmetric Flexible Root Modes (Ref 14:6-7)-----	76
37	Case 4, 1st Modes NASTRAN/GVT 1st Bending, 16.92 Hz-----	77
38	Case 4, 1st Modes Eglin GVT 1st Bending, 18.52 Hz-----	78
39	Case 4, 2nd Modes NASTRAN/GVT 1st Torsion, 35.37 Hz-----	79
40	Case 4, 2nd Modes Eglin GVT 1st Torsion, 50.20 Hz-----	80

List of Figures (Cont'd)

<u>Figure</u>		<u>Page</u>
41	Case 4, 3rd Modes NASTRAN/GVT 2nd Bending, 56.22 Hz-----	81
42	Case 4, 3rd Mode Eglin GVT 2nd Bending, 70.69 Hz-----	82
43-46	FEM Flexible Root Modes, Symmetrical Boundary Conditions, One Hydraulic System Operating-----	83-86
47-50	FEM Flexible Root Modes, Anti-Symmetrical Boundary Conditions, One Hydraulic System Operating-----	87-90
51	Horizontal Stabilator Physical Dimensions and Properties-----	104

List of Tables

<u>Table</u>		<u>Page</u>
I	Series 2 Stabilator Part List-----	10
II	Series 3 Stabilator Part List-----	13
III	Influence Coefficient Loads and Loading Points-----	31
IV	Total Weight, CG, and Weight Distribution Comparison-----	41
V	Comparison of Lump Parameter Model Inertia to the NASTRAN FEM-----	44
VI	Comparison of NASTRAN Modal Analysis Results to the Two Rigid-Root Cases-----	50
VII	Comparison of NASTRAN Modal Analysis Results to the Calculated and GVT Flexible-Root Cases-----	68

List of Symbols

A	Applied forces in the stiffness method
AFFDL	Air Force Flight Dynamics Laboratory
CDC	Control Data Corporation
CG	Center of gravity
CL	Aircraft centerline
D	Displacements in the stiffness method
$f(t)$	Temporal part of assumed solution in the eigenvalue problem
FEM	Finite element model
FS	Fuselage station
g	Acceleration of gravity
GP	Grid point
GVT	Ground vibration test
HSS	Horizontal stabilator station
Hz	Hertz, cycles per second (cps)
K	Stiffness matrix in eigenvalue problem
l	distance of stabilator CG relative to pivot point
M	Mass matrix in the eigenvalue problem
NAI	Northrop Aircraft Industries
NASA	National Aeronautics and Space Administration
NASTRAN	<u>NASA Structural Analysis</u>
S	Stiffness matrix in the displacement method
SAALC	San Antonio Air Logistics Center
STAGING	<u>Structural Analysis Via Generalized Interactive Graphics</u>

List of Symbols (Cont'd)

T	period (in seconds)
u	Eigenvector
w	Eigenvector before being normalized by its largest element
π	3.14159
ω	Frequency rad/sec
λ	Shift point in eigenvalue frequency range
n	Iteration number

Abstract

This thesis demonstrates the development and response of a finite element model of the T-38 horizontal stabilator using NASTRAN. The finite element model is to be used in a flutter analysis of damaged or repaired stabilators. The objective of the flutter analysis is to determine absolute values and degradations of the flutter speed due to different types of damages and repairs.

Development of a finite element model with two dimensional quadrilateral and bar elements is described. For verification, a static analysis of the finite element model yielded for the most part qualitatively agreeable values in comparison to an influence coefficient study.

For showing the dynamic response of the finite element model, a modal analysis using both rigid and flexible root boundary conditions is used. The rigid root analysis shows agreement between the first two modes and the flexible root compares favorably up to three and possibly four modes. With these results, it is decided to use the finite element model in an initial flutter analysis.

In the flutter analysis a doublet lattice aerodynamic model is combined with the finite element model for an undamaged stabilator. Poor agreement of the NASTRAN flutter speed with other available data indicates possible camber effects and the need for a verification of the aerodynamic

model using steady and unsteady airloads. A brief description of a method of simulating repairs and damages of a horizontal stabilator is included.

INITIAL DEVELOPMENT FOR
A FLUTTER ANALYSIS OF DAMAGED
T-38 HORIZONTAL STABILATORS USING NASTRAN

I. Introduction

Initial Request of Sponsor

San Antonio Air Logistics Center (SAALC) has the primary responsibility for all engineering and maintenance for the Northrop/United States Air Force T-38 Talon supersonic jet trainer. Currently, SAALC has the requirement to have a more advanced method for performing flutter analyses on the T-38's horizontal stabilator. This control surface has severe limits of repair due to flutter criticality.

It is the intent of this thesis to upgrade the current method of analysis by developing and verifying a finite element model that can be used to determine degradations in flutter characteristics. Damages to the stabilator such as punctures, skin delamination, water absorption of the honeycomb core, and corrosion of metal parts due to water can cause these degradations. The degradations, specifically decreases in flutter speed, can be caused by repairs for the damages as well as the damages themselves.

Background and Statement of Problem

Since 1971, SAALC has had in use a flutter analysis that could be performed on stabilators with added uniform

mass to the trailing edge due to standard repair procedures for delamination (Ref 1:1-5). This analysis is a two-dimensional "typical section" analysis which provides relatively accurate and conservative answers for decrements (relative changes) in flutter speeds. These decrements are caused by any changes in mass and stiffness properties. In comparing this method to a more complex one, such as collocation, a section analysis using unsteady aerodynamic theory will produce much lower absolute values for predicted flutter speeds. But, since the intent of this analysis is to only determine decrements in flutter speed, no attempt was made to take into account corrections for compressibility, finite aspect ratio, and/or elastic axis sweep effects.

SAALC has requested that a more accurate and versatile analysis be developed so that reliable absolute flutter speeds can be obtained. The analysis should be able to determine any changes in flutter speed for a horizontal stabilator which has been subjected to any type of damage or repair. Since a method that reflected the state of the art was desired, a computer oriented finite element analysis was the likely candidate.

A major benefit to be obtained from such an analysis would be a more reliable prediction of changes in flutter speeds. This benefit would in turn produce cost savings since any uncertainty in the flutter speed of a stabilator would cause an immediate removal and replacement.

General Approach to the Problem

Today the use of finite elements in structural analysis is widely accepted among the aerospace community. Coupled with the use of digital computers, finite element methods provide a wide range of capabilities in solving various types of structural analysis problems. Heat transfer and fluid flow solution capabilities are provided as well. Finite elements and associated structural analysis computer programs represent the state of the art in its associated field. Therefore, a finite element analysis is quite appropriate to be used for the previously stated problem.

NASTRAN (NASA Structural Analysis) is a very comprehensive finite analysis program used extensively in the aerospace industry. It was initially developed by NASA and was later contracted out to private companies for development. Because of its wide range of capabilities, NASTRAN will be used to provide a computer package to the user (i.e., SAALC) that can be used to perform the necessary analysis in order to solve the prescribed problem. It is assumed that the user (and reader) has a working knowledge of NASTRAN as well as applicable finite element methods.

NASTRAN itself is used to develop a finite element model of the horizontal stabilator using NASTRAN specific finite elements. Of course, the finite element model is the basis for the entire problem and it is used in each of the analyses. These analyses and the associated NASTRAN Rigid Format are listed as follows.

1. The finite element model of the structure is confirmed with respect to both stiffness and mass distribution using influence coefficients and reported mass distributions, respectively. Rigid Format 1 (Static Analysis) is used for the influence coefficient study.

2. Natural frequencies and mode shapes are used for a flutter analysis. Therefore, the eigenvalue problem for the stabilator is solved using the Modal Analysis (Rigid Format 3).

3. The flutter analysis requires an interface between the finite element structural model and a finite section (finite sections of the planform) aerodynamic model. This aerodynamic model will be generated using the doublet lattice method. Rigid Format 10 (Flutter Analysis) is applied.

4. Once the aerodynamic model is confirmed with existing airloads data, it is combined with the finite element structural model. Then a NASTRAN flutter analysis can be done using Rigid Format 10.

5. Changes in the structural model simulating various repairs and damages will be made. The absolute values and changes in flutter speeds that can occur will be found from the flutter analysis.

Assumptions and Restrictions

The following three sections list the assumptions and restrictions for the finite element model, eigenvalue problem, aerodynamic model, and the flutter analysis.

1. Finite Element Model and Eigenvalue Problem

- (a) Linear elastic plane elements used
- (b) Torque-tube and actuator assembly modeled
- (c) Fuselage motions ignored
- (d) Changes in mass and stiffness distribution to simulate damages and repair
- (e) Lower eigenvectors used in flutter analysis

2. Doublet Lattice Aerodynamic Model

- (a) Subsonic conditions
- (b) Thin airfoil theory
- (c) Unsteady airloads, potential flow
- (d) Boundary layer effects neglected
- (e) Wing and fuselage interference neglected

3. Flutter Analysis

- (a) Only a few speeds and altitudes simulated
- (b) 0.0% - 2.0% structural damping to show sensitivity of flutter

Computer Software and Hardware

Since the current state-of-the-art in structural analysis relies heavily upon the computer and associated programs, SAALC would in effect need a computer package to perform all the analyses up to and including the flutter analysis. This section will briefly describe the computer software and hardware used in this thesis.

As mentioned previously, NASTRAN is used for all the needed structural analyses. NASTRAN, Level 17, currently exists on the Aeronautical System's Division's Control Data Corporation (CDC) Cyber 175 computer system, located at Wright-Patterson Air Force Base, Ohio. The associated NASTRAN manuals, in particular the User's Manual and Theoretical Manual, were utilized. These manuals and other documents on NASTRAN are listed in the Bibliography.

Most of the undeformed plots of the finite element model were obtained from a Calcomp plotter using a batch program called EZPLOT. EZPLOT is also currently on the CDC Cyber 175, and it was developed under the auspices of the Air Force Flight Dynamics Laboratory (AFFDL), Wright-Patterson Air Force Base, Ohio.

A highly versatile interactive graphics program was utilized to obtain the mode shapes generated in the modal analysis. STAGING, Structural Analysis via Generalized Interactive Graphics, was developed for AFFDL by Battelle Columbus Laboratories, Columbus, Ohio. It is also on the CDC Cyber 175.

Several other supporting programs were written to provide necessary data and data conversion or reduction. These were written in FORTRAN and they are mentioned in the appropriate sections where they were used.

Literature Review

A primary source of literature was the technical library located at SAALC. The literature obtained from this source consisted of Northrop technical reports on the horizontal stabilator, written during the initial aircraft development. Such aspects as structural properties, static, modal and flutter analyses are contained in these reports.

The sponsor at SAALC provided other documents pertaining to current methods of analysis and repair methods. Aperture cards of blueprints of the stabilator were also provided by the sponsor.

Other documents were obtained from AFFDL, Eglin Air Force Base, Florida, and Northrop Corporation. NASTRAN literature and manuals were obtained from the Aerospace Structures Information and Analysis Center which is located at AFFDL.

II. A Finite Element Model of the Horizontal Stabilator

Introduction

The development of a finite element model of an actual structure depends heavily upon how the structure is made; that is, what its individual components are. Once this is known, the appropriate type of finite elements can be used. Also, the mesh size and location of boundary conditions can be determined. With this information, a finite element model can then be developed.

Description of the Stabilator

The T-38A Talon, which was developed for the U.S. Air Force by the Northrop Corporation, has an all-movable (free-flying) horizontal stabilator which is powered by a system of dual hydraulic actuators. These actuators are located in the fuselage tail cone. A significant feature of the stabilator is that it is a lightweight, honeycomb structure whose stiffness was chosen to meet flutter requirements instead of load considerations.

There are two basic structural designs of the stabilator. The initial design, which was for aircraft N5101 to N5205, utilized intermediate ribs and an auxiliary spar (Fig. 1). A redesign of the stabilator for aircraft N5206 and subsequent aircraft deleted the intermediate ribs and auxiliary

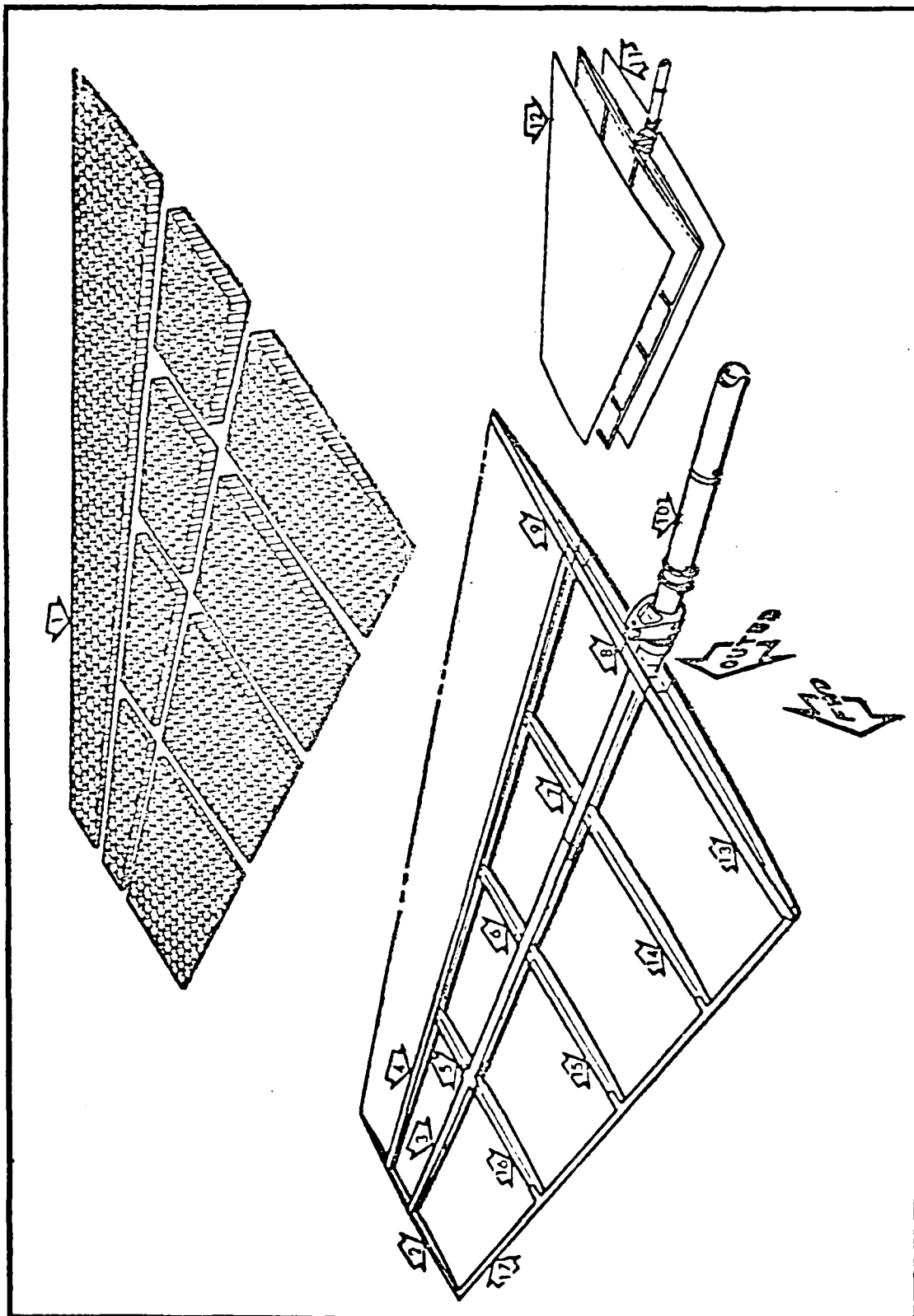


Figure 1. Series 2 Stabilator
(Ref 2: Sect IV)

TABLE I
SERIES 2 STABILATOR PART LIST (REF 2: SECT IV)

INDEX NO.	PART NO.	NOMENCLATURE	GAGE	MATERIAL
1	3-32301	Honeycomb Core	0.0007 P Foil 0.125 Cell	Aluminum Alloy
2	2-32303	End Rib	Machined Bar	Rolled Bar Aluminum Alloy 7075-T6
3	2-32307	Main Spar	Machined Bar	Rolled Bar Aluminum Alloy 7075-T6
4	2-32306	Auxiliary Spar	0.050	Sheer Alclad 7075-T6
5	2-32315	Rib	0.050	Sheet Alclad 7075-T6
6	2-32313	Rib	0.050	Sheet Alclad 7075-T6
7	2-32311	Rib	0.050	Sheet Alclad 7075-T6
8	2-32308	Rib	0.080	Sheet Alclad 7075-T6
9	2-32308	Rib	0.025	Sheet Alclad 2024-T4
10	2-32317	Hinge Fitting	Tube	Steel 43M30
11	2-32304	Lower Skin	See Fig 4-36	Sheet Alclad 7075-T6
12	2-32304	Upper Skin	See Fig 4-36	Sheet Alclad 7075-T6
13	2-32310	Rib	Machined Forging	Die Forging Aluminum Alloy 2014-T6
14	2-32311	Rib	0.071	Sheet Alclad 7075-T6
15	2-32313	Rib	0.063	Sheet Alclad 7075-T6
16	2-32315	Rib	0.050	Sheet Alclad 7075-T6
17	2-32302	Leading Edge	Machined Plate	Plate Aluminum Alloy 7075-T6

spar as seen in Figure 2. The listings after each figure can be used to identify assembly numbers of the two designs and also for part types and materials. (Ref 2: Sect IV)

Since most of the T-38 aircraft have the newer stabilator (designated Series 3 in this thesis), SAALC requested that all analyses be conducted for this design. Henceforth, any mention of static and dynamic properties is for the newer design unless stated otherwise.

In order to model the stabilator correctly, blueprints (Ref 3) of each of the components were used to obtain dimensions as accurately as possible. These are listed in Appendix A, as well as other properties and algorithms that describe physical dimensions. Also, NAI-57-59 (Ref 4) was used to obtain and confirm properties common to both designs.

The Finite Element Model

Figure 2 can be used in determining what finite elements can be used to model the components of the stabilator. These elements and their corresponding stabilator components are as follows:

1. Plate bending elements with in-plane stiffness model quadrilateral sections of the skin-honeycomb core combination.
2. Bar elements model the hinge fitting (torque tube and main spar to HSS 48.0), main spar outboard of

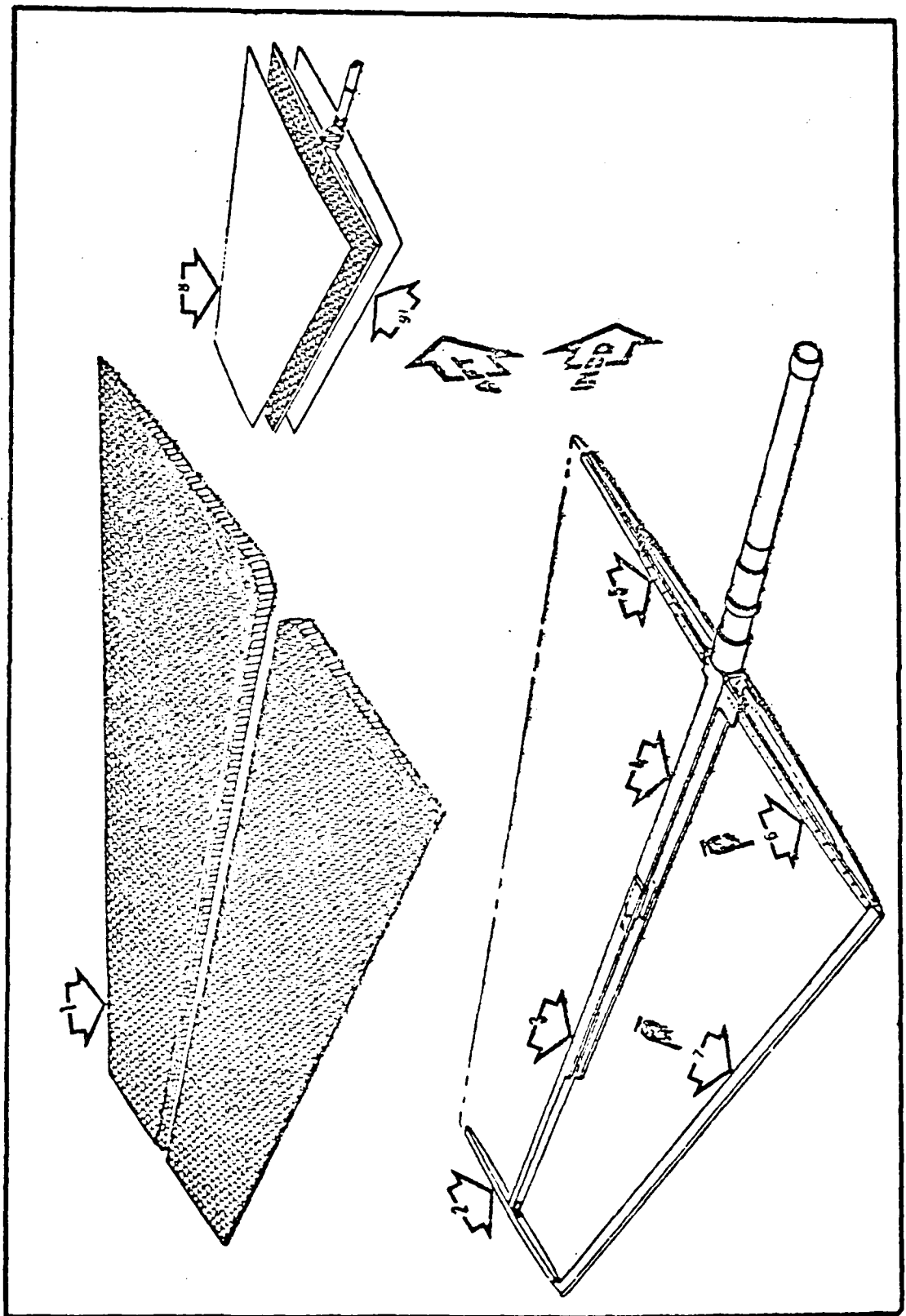


Figure 2. Series 3 Stabilator
(Ref 2: Sect IV)

TABLE II

SERIES 3 STABILATOR PART LIST (REF 2: SECT IV)

INDEX NO.	PART NO.	NOMENCLATURE	GAGE	MATERIAL
1	3-32350	Honeycomb Core	0.0007 P Foil 0.125 Cell	Aluminum Alloy 5052-H39
2	3-32353	Rib	Machined Bar	Bar Aluminum 7075-T6
3	3-32356	Main Spar	Machined Bar	Rolled Bar Aluminum Alloy 7075-T6
4	3-32317	Hinge Fitting	Tube	Steel 43M30
5	3-32352	Rib	0.025	Sheet Alclad 7075-T6
6	2-32310	Rib	Machined Forging	Die Forged Aluminum Alloy 2014-T6
7	3-32357	Leading Edge	Machined Plate	Plate Aluminum Alloy 7075-T6
8	3-32355	Upper Skin	See Fig 4-45	Sheet Alclad 7075-T6
9	3-32355	Lower Skin	See Fig 4-45	Sheet Alclad 7075-T6

HSS 48.00, leading edge extrusion, trailing edge closure, root rib and tip rib.

It should be pointed out that these elements produce a two-dimensional model of the stabilator. From an analysis point of view, this is an improvement from the section analysis model that SAALC has in its current method.

As mentioned in the introduction, NASTRAN. Level 17, is used for all the major analyses of this thesis. The elements and methods of developing a finite element model provided by NASTRAN are, therefore, utilized. The basic elements are listed as follow:

QUADI - quadrilateral membrane and bending
element

BAR - simple beam element

A FORTRAN program was written that generated the NASTRAN Bulk Data Deck. This program contains separate parts (modules) that produce the connectivity and property cards for the elements corresponding to each assembly of the stabilator. Also, the grid point cards and material cards are generated.

Appendix A gives an outlined procedure of the type of checks performed on this program to insure that its input data are accurate descriptions of the actual stabilator physical dimensions.

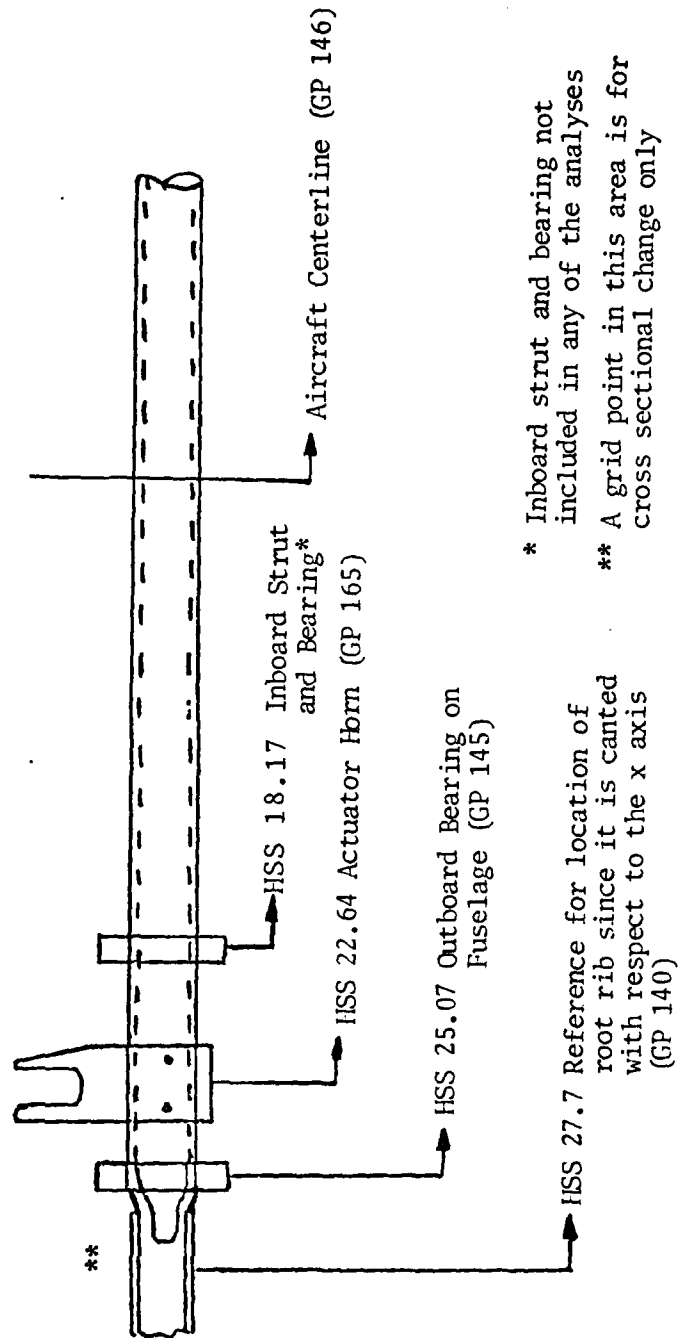
Several aspects of this program should be mentioned at this time. The main aspect is that the properties of each element (quantities on the NASTRAN property cards) were calculated using the physical dimensions (airfoil thickness, flange or web thickness, etc.) at the elements' center. For the most part these dimensions are obtained using an interpolating routine. That is, once a certain element center is found in terms of percent chord or horizontal stabilator station, the dimensions at that particular point are found from interpolating between dimensions from known locations as shown in the blueprints. Since the possibility of changing mesh sizes exists, the program was written in a general sense so that the initial 15 element spanwise by 8 element chordwise mesh size could be increased.

For the torque tube, the grid point, element, and property cards were generated by hand. Figure 3 shows the torque tube and locations of grid points. The particular parts of the torque tube-actuator assembly located at each grid point are indicated in this figure. Future reference to this figure will be made when constraint conditions are discussed.

Other cards appearing in a Bulk Data Deck, such as Force, Load, SPC, and also those cards appearing in the Executive and Case Control portions of the NASTRAN deck, are produced by hand.

Figures 4 and 5 show the Finite Element Model generated for the T-38 Horizontal Stabilator. A few physical features were

(REF 2:B-36)



* Inboard strut and bearing not included in any of the analyses
 ** A grid point in this area is for cross sectional change only

Figure 3. Torque Tube and Grid Point Locations

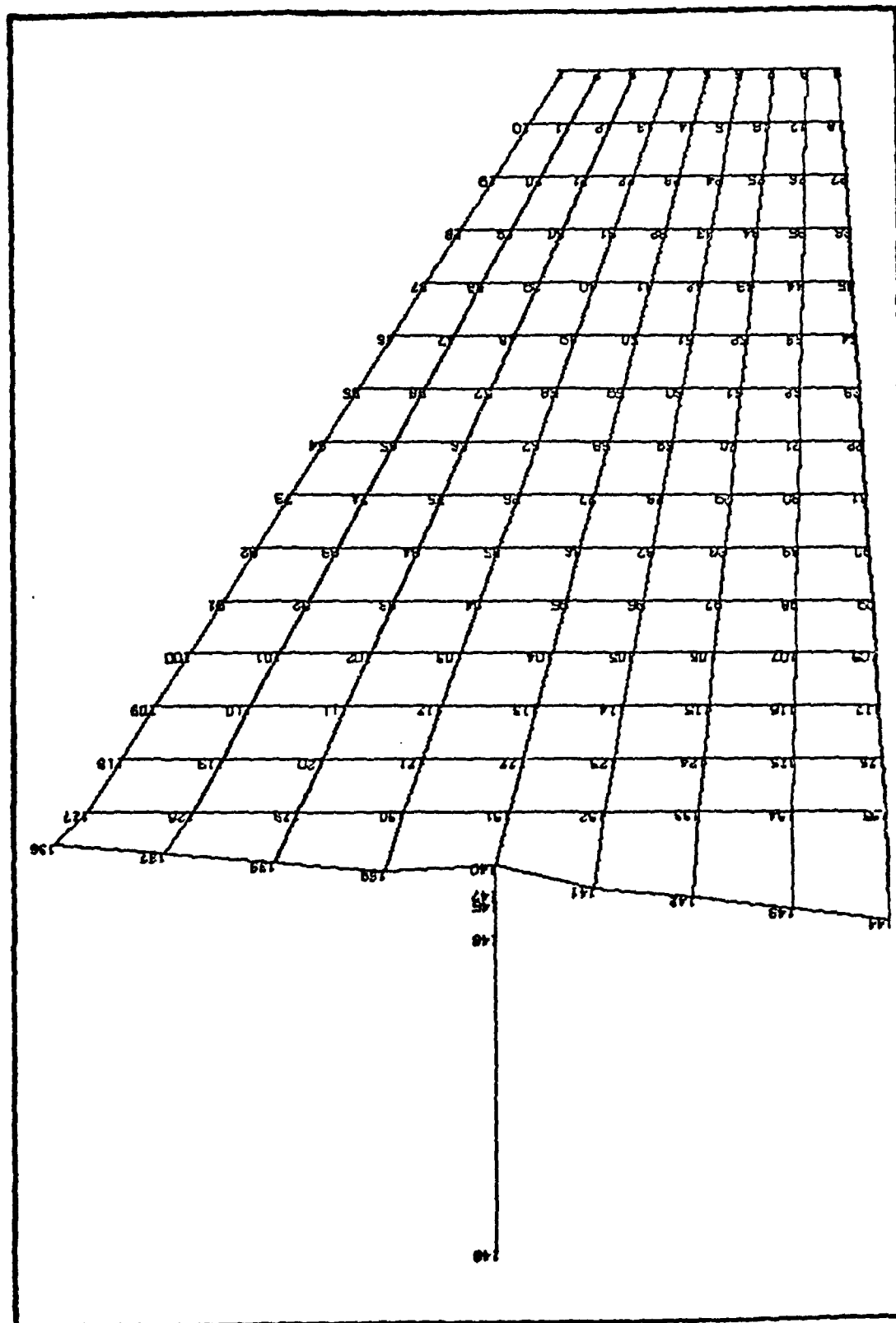


Figure 4. Basic Finite Element Model
Showing Grid Points

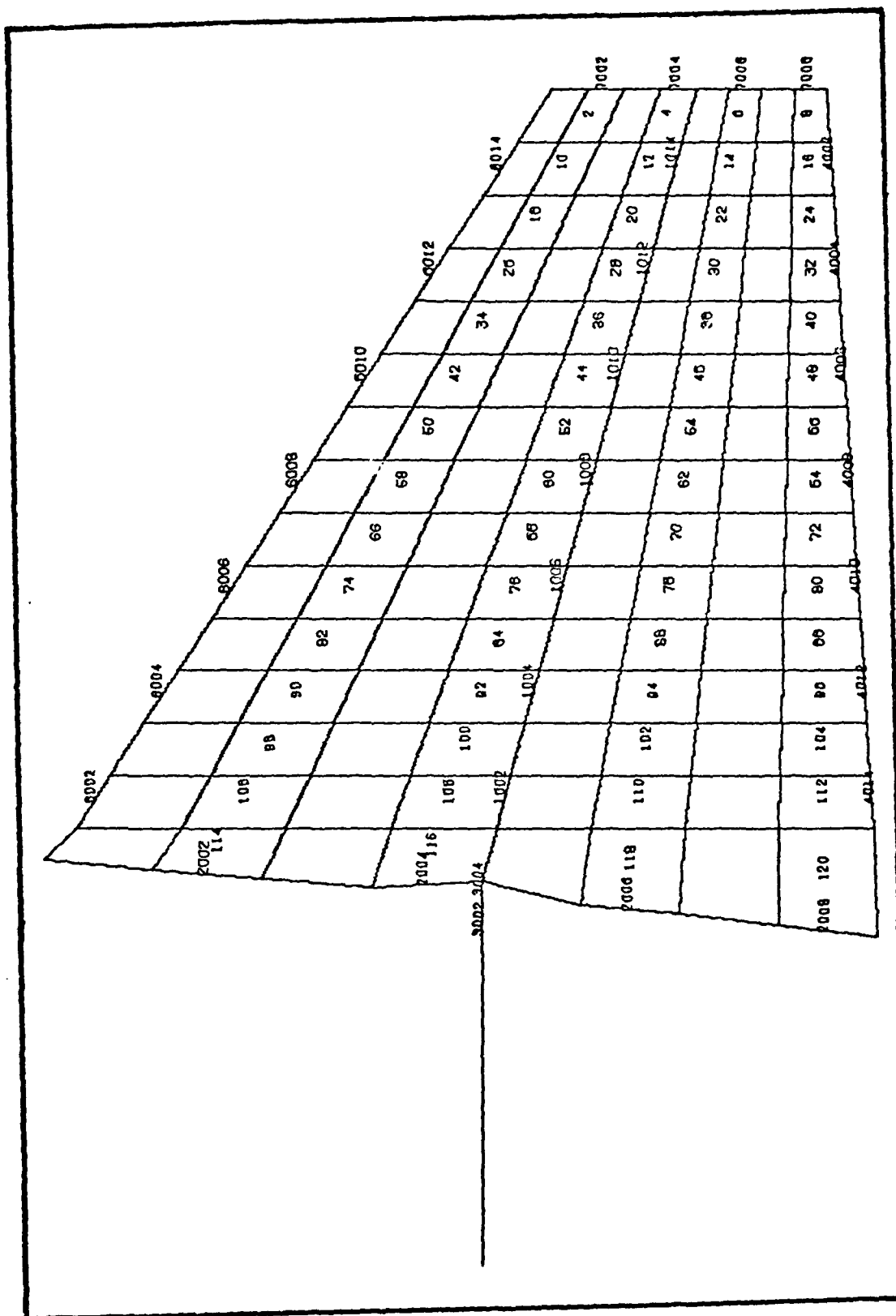


Figure 5. Basic Finite Element Model
Showing Elements

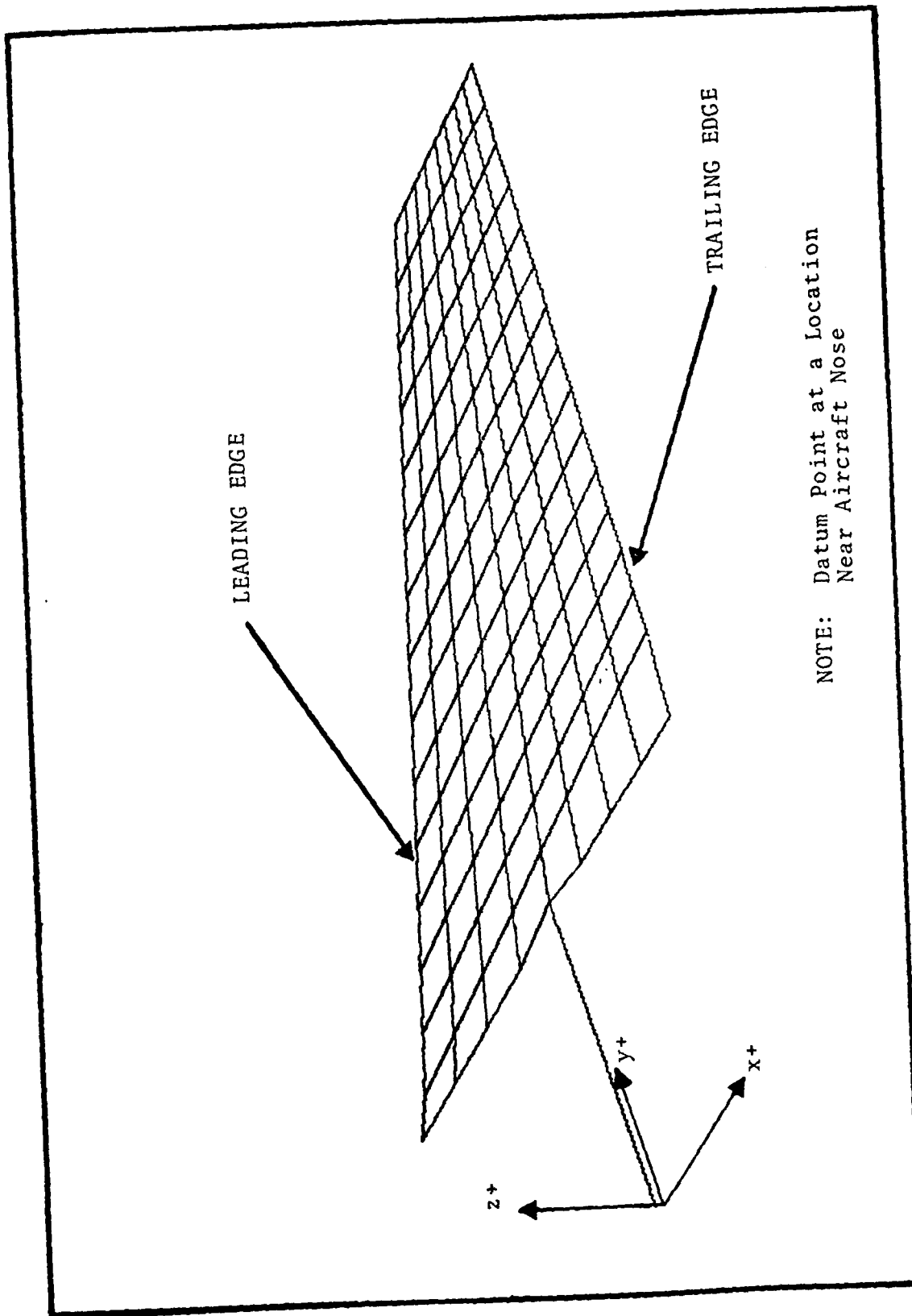


Figure 6. Coordinate System of Finite Element Model

omitted and some inaccuracies have been found. These are listed as follows:

1. Three cross sections are used to model the torque tube length of the hinge fitting assembly. Due to the complex cross section of the hinge fitting near the root rib, only a few elements are used. For torque tubes CBAR 3002 and 3003, a section directly inboard of the support bearing (Grid Point 145) is used. CBAR 3001 uses a section at HSS 25.07 (directly at the bearing) and CBAR 3004 uses a section at HSS 25.8 (Ref 4:B-36-B-44, Ref 3 and Fig 3).

2. Several dimensions, such as chord length at a certain HSS station, have been found to be in error of about .25 to .6 in. with comparison to the actual stabilator.

3. A small skin pad just aft of the hinge fitting and adjacent to the root rib has been omitted since it is small relative to the other elements.

4. Forward of the torque tube and along the root rib is a "tongue" that extends about 4 in. This part connects the forward root rib to the hinge fitting (torque tube-main spar assembly). Since it is relatively small (Ref 3), it was not put in the model.

5. Since the root rib is not parallel to the fuselage centerline (due to the fuselage boat-tail), interpolating

values for FS and HSS values were used to obtain the necessary shape. These interpolating values cause the visible differences in the FEM root rib in comparison to the actual stabilator.

III. Finite Model Verification

Using An Influence Coefficient and Mass Distribution Check

Introduction

Even though a static analysis is not used explicitly for a flutter analysis, it can be useful in comparing the structural response of the FEM to the response of the actual structure. Therefore, a static analysis using influence coefficients was performed as a check on the performance of the model and to try to locate modeling errors.

Static Analysis Using Influence Coefficients

During the initial development of the T-38, Northrop performed a static test on the entire airframe. Both influence coefficients and deflections due to design load conditions were obtained for each of the aircraft's substructures. The final results were reported in NOR-60-6 (Ref 5). The type of loading conditions, methods of obtaining data, and the stabilator series used were obtained from this report.

In the section concerning the static test using the design loads, it is found that the Series 2 stabilator (Figure 1) was the article tested. Further investigation, using the blueprints (Ref 3), revealed that the only difference between the two series, other than the deletion of the intermediate ribs and auxillary spar, is a minor

decrease in skin thickness aft of the main spar. Additional inquiries as to reason for the deletion of these components brought the conclusion that they did not appreciably add to the stiffness of the structure. The ribs could have possibly affected the rate at which the shear flow was distributed to the root rib and the spar, but evidently this aspect was not strong enough to justify including them in the stabilator. Their deletion can also be seen to make fabrication easier.

Even with these deletions, the two stabilators have the same stiffness according to the NAI-57-59 report (Ref 4:V). Further discussion on this aspect will be given as the results of the influence coefficient study are presented.

A careful study was made of the static analysis report to insure that the proper boundary conditions were used in this analysis. These boundary conditions depend not only on the nature of the actual structure, but also on the method of obtaining data and the relation of the stabilator to other substructures such as the actuator assembly.

The report, in the section pertaining to influence coefficients, mentions that the actuator assembly was pressurized in order to provide a resistive moment at the actuator horn. But the servo mechanism was not functioning properly. This indicates that the actuator was not able to maintain the desired deflection in pitch (angle of attack) of the stabilator commanded by a control input,

even though the loading on the stabilator may cause it to have a different deflection. From this information it is concluded that the actuator provides a partially clamped condition and its equivalent spring stiffness does contribute to the structure stiffness.

Symmetric boundary conditions are assumed for the static loading. This is supported by the fact that the opposite stabilator had a load applied to it also, but its deflections were of no concern. In the FEM, this symmetric loading is accomplished by applying these constraints to the following grid points (Figure 3).

- (1) GRID POINT 146 - 246
- (2) GRID POINT 145 - 13

The characteristic feature of the constraints at grid point 146 is that no rotation of the torque tube about the X-axis is allowed at the aircraft centerline. The constraints at grid point 145 are typical for a bearing, except in this case axial displacements of the torque tube are allowed.

For each static load in the influence coefficient study, the deflections at 25 points were measured. Since these points (Figure 7) do not correspond to any of the existing grid points, new grid points were included in the FEM at the locations of these 25 points. This produced the FEM shown in Figures 8 and 9. A FORTRAN program was written that made the majority of the changes to the basic Bulk Data Deck in order to produce the Influence

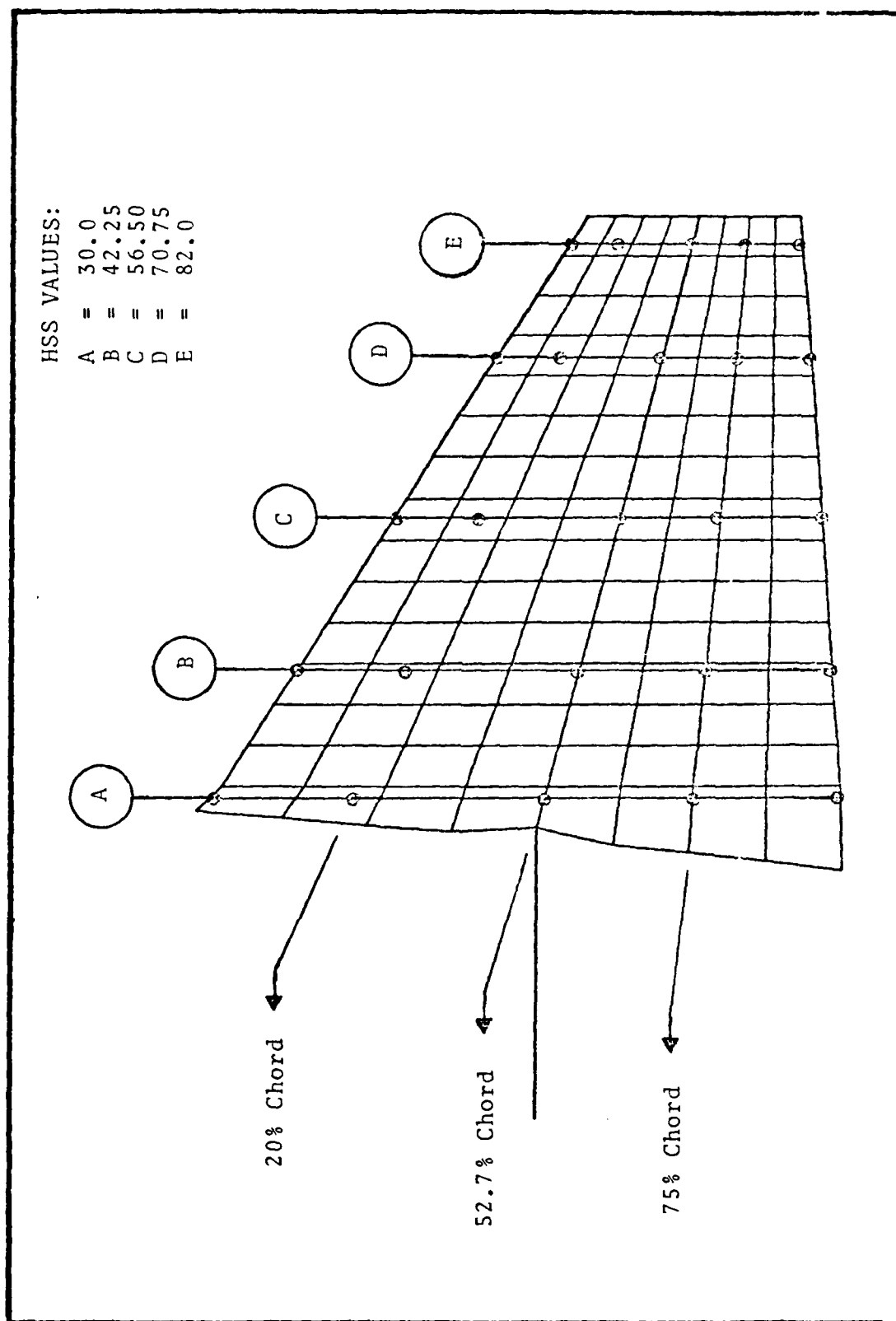


Figure 7. Influence Coefficient Load and Deflection Points

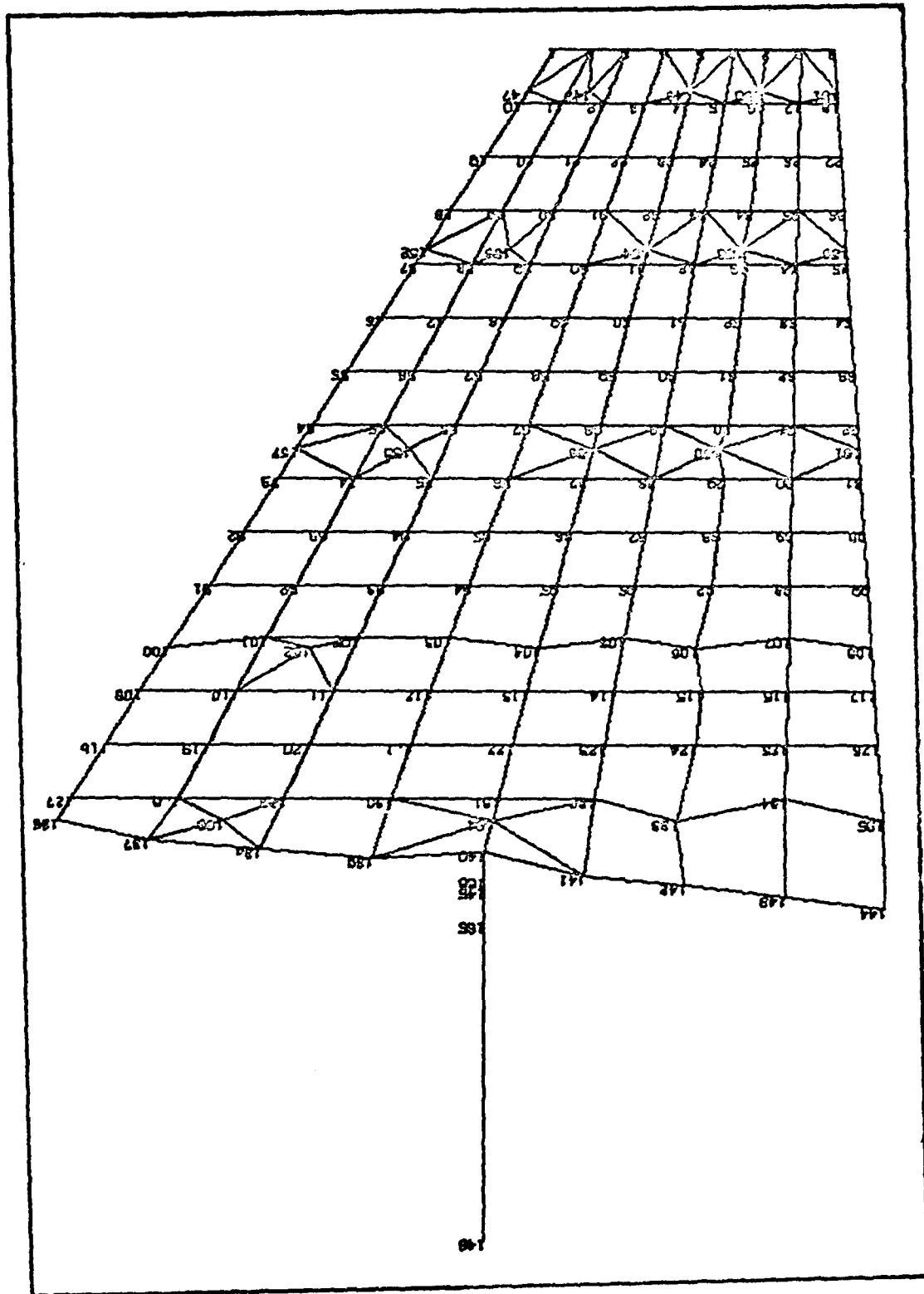
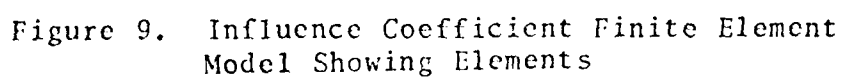


Figure 8. Influence Coefficient Finite Element Model Showing Grid Points



Coefficient FEM. Since an additional grid point is added to several of the quadrilateral membrane elements, triangular membrane elements are needed. Therefore, NASTRAN particular CTRIAL and corresponding PTRIAL cards are used.

For the Northrop report the location of each deflection point is taken with respect to percent chord at HSS 30.00. By using a mirror-transit arrangement (Ref 5:33), the translation and rotation of this chordline could be determined. This rotation is present due to the fact that the servo mechanism could not provide the desired stabilator angle of attack, which is most likely to be zero. These displacements are subtracted from the displacements of each point. Therefore, the reported results show the structural response of the stabilator outboard of HSS 30.00. With respect to the FEM, this is accomplished by constraining degree of freedom 5 (rotation about the Y-axis) at grid point 140. This grid point is used because it lies on the pitch axis of the torque-tube.*

With respect to both finite element models, the mathematical formulation is based on the linear theory of elasticity, i.e., linear (stress-strain) relationships and linear material properties. In NASTRAN there are two Rigid Formats that have these constraints. Rigid Format 1 was used to perform the influence coefficient study for the FEM verification.

* 5 constrained at Grid Point 140 has the same effect as 5 constrained at the actuator horn and subtracting the rotation of the chord at HSS 30.00 from each grid point. Subtraction of this rotation also removes any effect of the actuator pitch stiffness.

The FEM stiffness matrix is created by defining element connections via the Bulk Data Deck. This stiffness matrix, which is associated with all grid point degrees of freedom, is modified by specifying various constraints (NASTRAN single point constraints) and partitioning operations. The remaining set of displacements after these modifications is called the 1-set and is the solution set for the static analysis. (Ref 6:CH 12)

For the static loads, only concentrated forces applied to the appropriate grid points are used. By using transformations defined by constraints and partitioning specifications, the 1-set node point forces is reduced to that associated with the 1-set of displacements. The form of the resulting equations is

$$\{A\} = [S] \{D\}$$

which is the basic form of the equilibrium equations of the stiffness method. The vectors A and D are the forces and displacements, respectively, and the S matrix is the model stiffness matrix. In order to solve this set of equations, the stiffness matrix is first decomposed into its lower and upper triangular factors. For all load subcases that have the same constraints, which is the case here, a forward-backward substitution is performed.

An arbitrary load was applied to determine any gross errors which could cause NASTRAN to abort an attempt to execute. A successful run with NASTRAN executing and producing the desired output was obtained with this arbitrary load.

Figures 10 through 14 show the results of the influence coefficient study. The five loads that were used and their locations are shown in Table III. From these results, it is seen that the model yields greater deflections than those of the actual stabilator that was tested. By referring to the deflection curve for the chordline that a particular load is applied, it is seen that the errors are more pronounced near the location of the load. An example of this is the curve for HSS 42.25 as shown in Figure 14. The load for this case is on the designated chordline.

These errors could be attributed largely to model inaccuracies which result from the use of finite elements with element properties found at the center of each element. For instance, the apparent rigid body rotation shown in the curves for HSS 82.00 and HSS 70.75 in Figure 14 is most likely caused by "root rib" wind up and errors near the root rib. This is supported by the observation that no suspected rigid body rotation is present in the chord sections further inboard.

For the most part, the results can be considered qualitatively acceptable. One significant aspect that

TABLE III

INFLUENCE COEFFICIENT LOADS AND LOADING POINTS (REF FIG 7)

LOAD (1b)	HSS	% CHORD	GRID POINT NR.	FIGURE
400	82.0	52.7	149	10
400	70.75	20.0	153	11
400	70.75	75.0	155	12
1200	42.25	20.0	162	13
1200	42.25	75.0	106	14

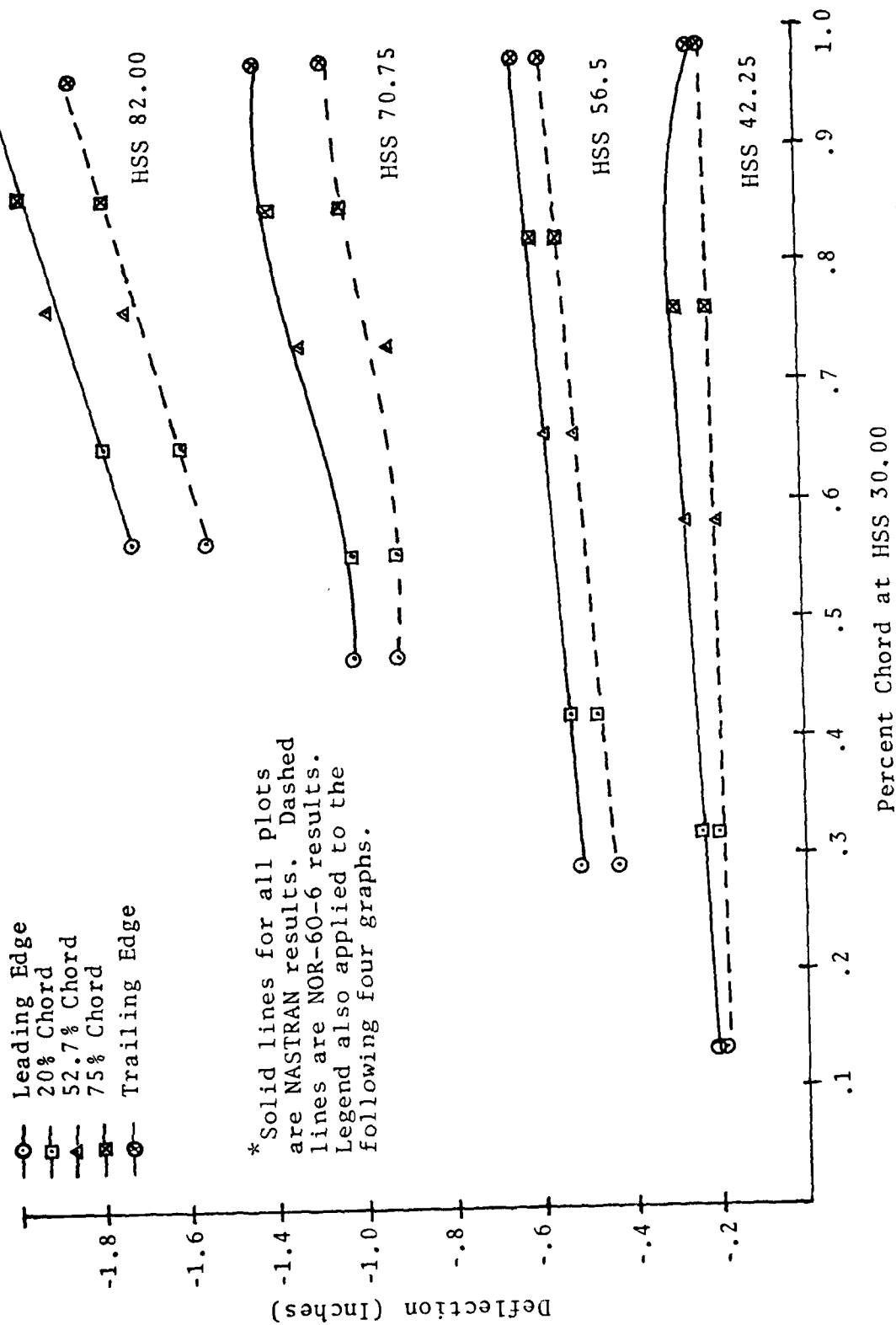


Figure 10. 400 Lb Load at Grid Point 149

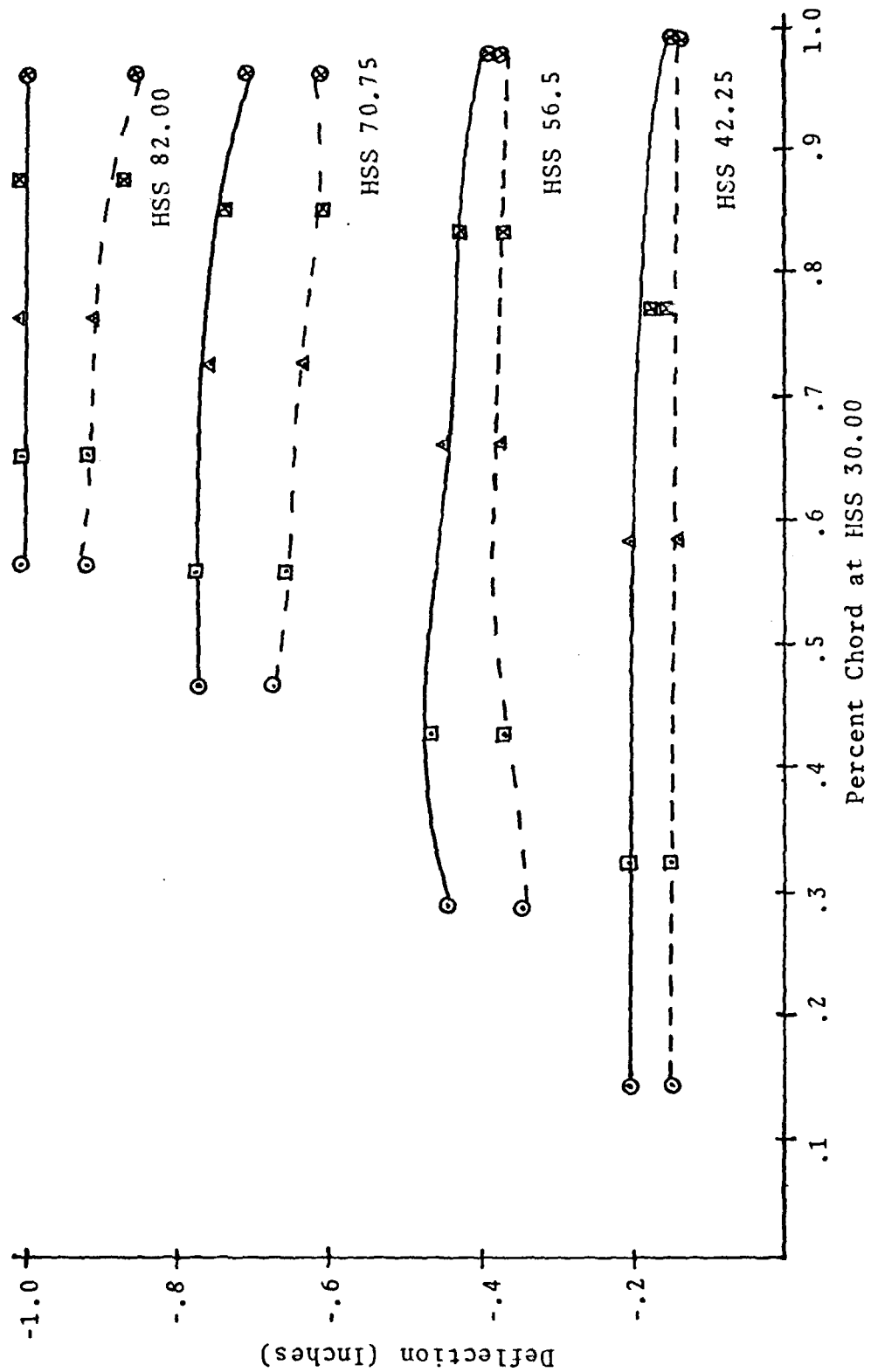


Figure 11. 400 Lb Load at Grid Point 153

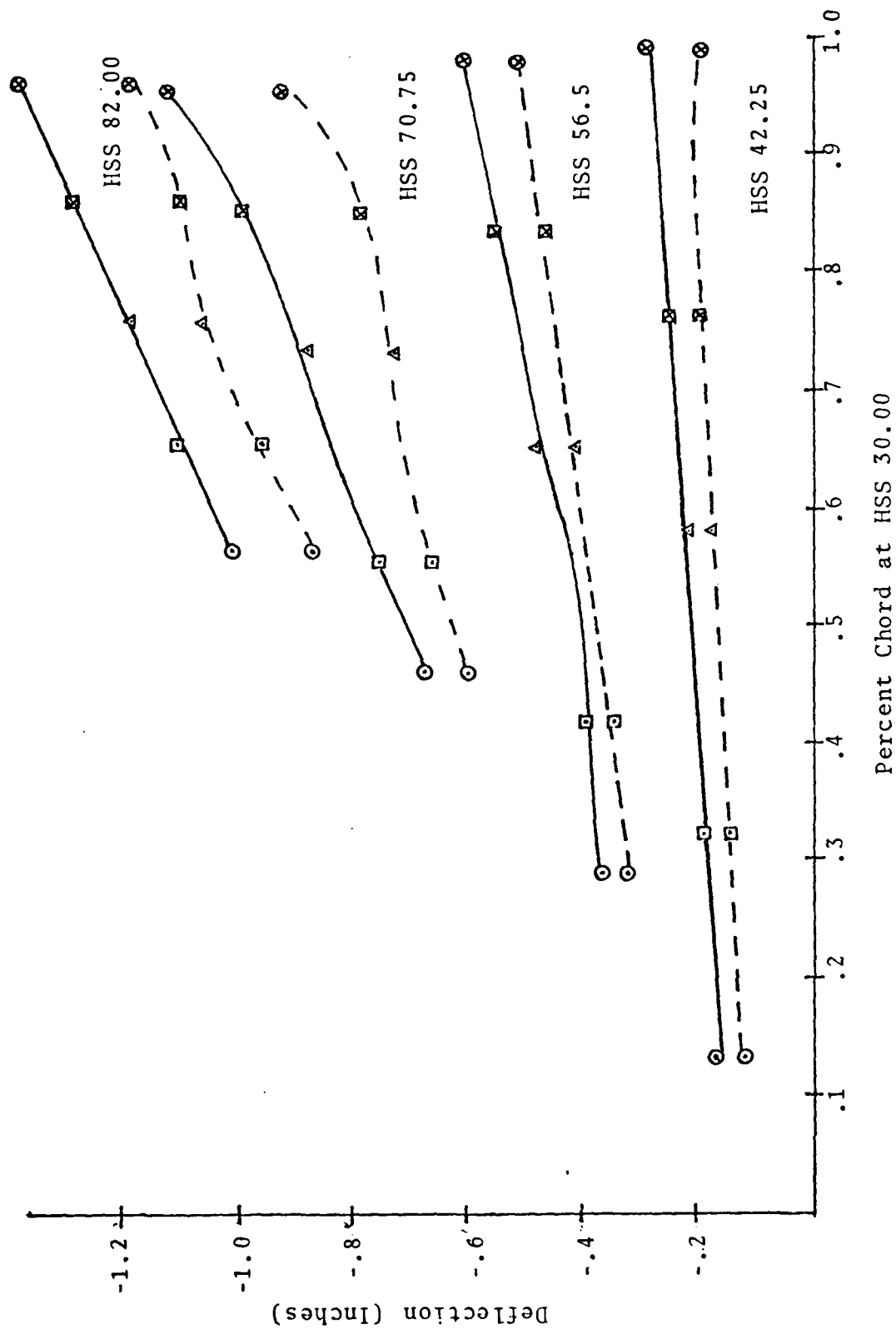


Figure 12. 400 Lb Load at Grid Point 155

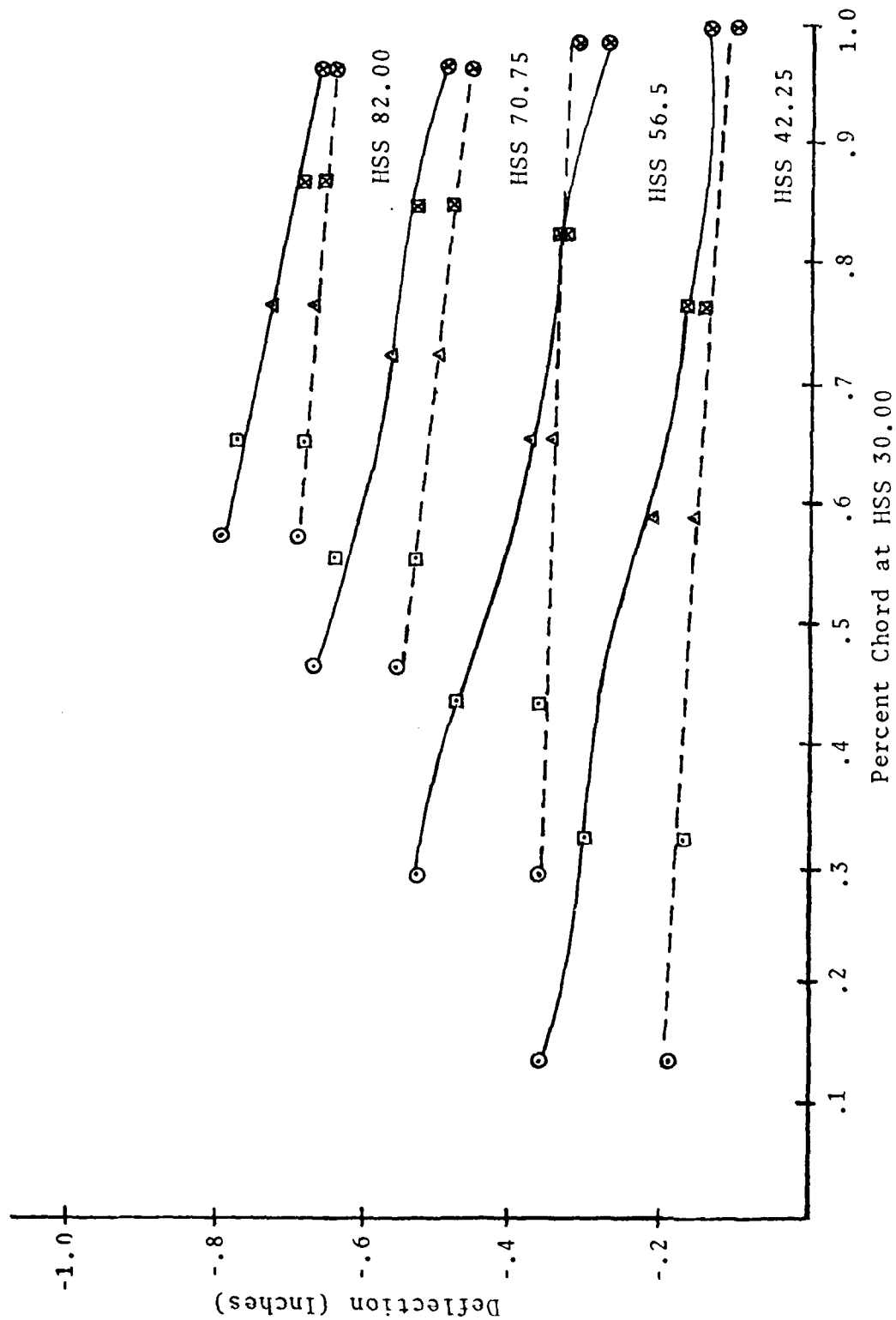


Figure 13. 1200 Lb Load at Grid Point 162

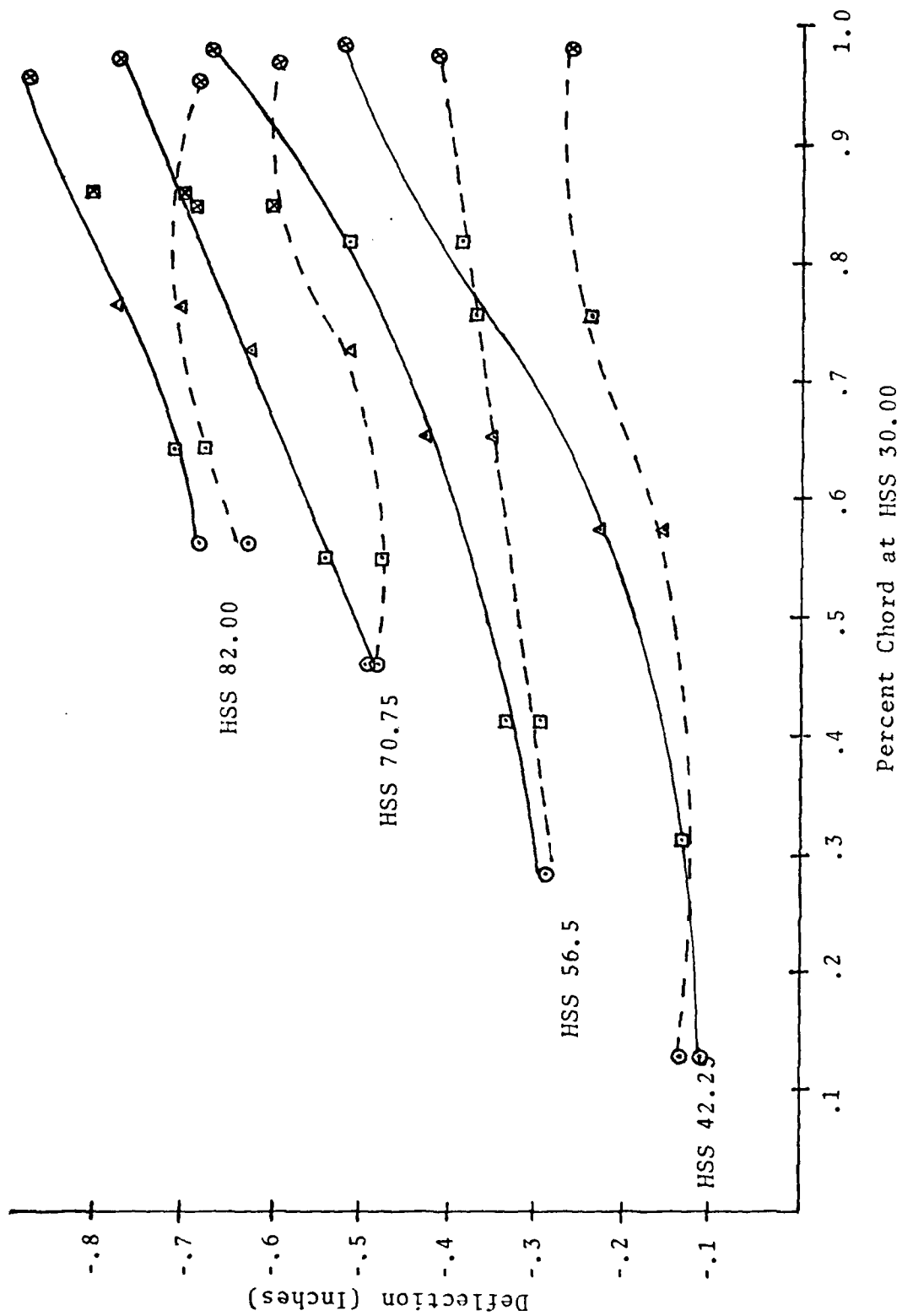


Figure 14. 1200 Lb Load at Grid Point 106

could be obtained from this analysis is determining any changes in camber of a chordline. This is extremely important since the slope (camber) of an airfoil is contained in the boundary condition which is used in thin-airfoil theory. In developing this concept further, it is seen that the camber affects the aerodynamic loading which in turn affects the dynamic response of the structure. In light of the previously discussed results, it cannot be determined if significant camber changes will occur due to typical aerodynamic loading. A further study of camber changes will be included in the flutter analysis.

Monotonical or oscillational convergence to the correct answer by increasing the mesh size cannot be predicted. This could be the reason the displacements for the finite element model are larger. Of course, in the limit, as the elements become smaller, the model will yield the correct answers assuming there are no model errors. Thus, the discrepancies in the present answers are primarily due to the mesh size and any model errors.

Weight, Center of Gravity, and Mass Distribution Check

Weight and mass distribution are of equal importance as stiffness is when a modal analysis of a structure is involved. In order to facilitate this part of the verification, two stabilators were obtained from SAALC for the purpose of weight, center of gravity, and modal analysis

studies. One of the stabilators had the standard repairs for delaminated skin at the trailing edge and, because of these repairs, it was not tested.

The test stabilator was weighed using a set of standard balance scales. To determine the CG location, a simple lump mass pendulum analogy was used. That is, the stabilator was hung from the end of the torque tube by putting a bolt through the most inboard hole which is for one of the two tapered pins used to join the torque tubes of the left and right stabilators in a male-female type connection (Ref 4:B-36, B-44). The torque tube was allowed to swing as freely as possible about the bolt (about an axis perpendicular to the torque tube longitudinal axis). The period of a simple pendulum (Ref 7:357-358) is

$$T = 2\pi \sqrt{\frac{l}{g}}$$

where l will be the distance the CG is from the pivot point which is the hole for the tapered pin. Dividing both sides by 2π and taking the reciprocal of both sides yields

$$\frac{2\pi}{T} = \frac{g}{l}$$

where $\frac{2\pi}{T}$ is the frequency in radians/sec. Several measurements of frequencies in cycles per second were measured visually using a stopwatch, and the average value

is used.

In the NASTRAN Static Analysis Rigid Format, one of the parameters that can be used is the Grid Point Weight Generator. This is the means of obtaining the model total mass, weight, and CG coordinates. All of these measurements are taken with respect to the aircraft centerline which is GP 146.

For the vibration analysis done by Northrop during the initial aircraft development, a lump parameter model of the stabilator assembly minus the torque tube was used (Ref 8:9). Bending and torsional stiffness are represented at ten discrete locations along the straight swept elastic axis. Corresponding to each of these elastic axis locations are strips perpendicular to the elastic axis. Surface mass distributions are represented by the inertial equivalence of these strips. Concentrated inertia loads are applied to the elastic axis by each chordwise segment at the centerline of each segment. Figure 15 shows these ten strips of the basic model, the grid points in these strips, and the elastic axis.

Table IV compares the total weights, CG locations and the weights of each strip for the actual stabilator, NAI study, and the finite element model. The following conclusions can be made from these results.

(1) The total weight of the stabilator from NASTRAN is approximately 3.9 lb more than the actual stabilator weight. For the given mesh size, this is considered to be

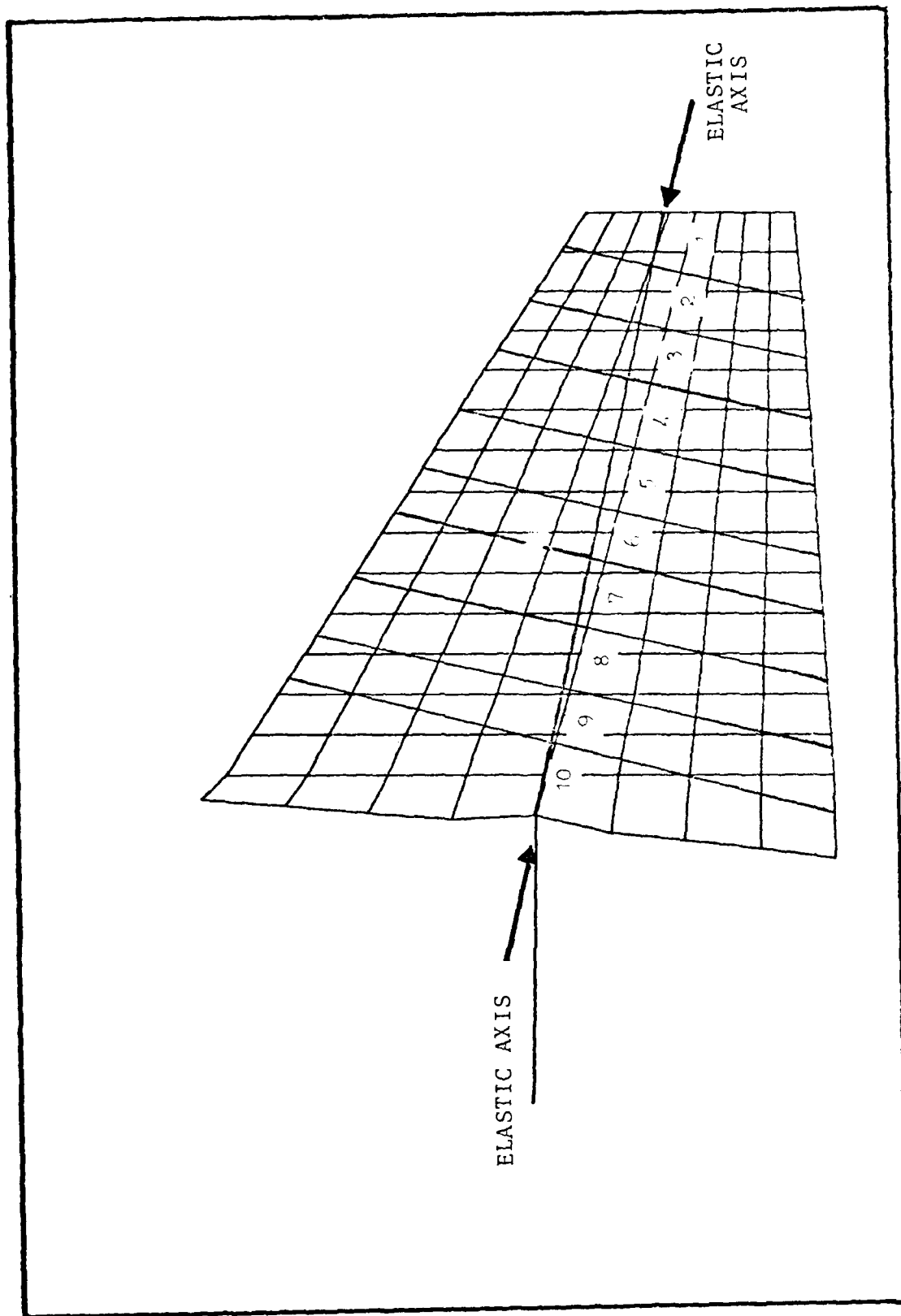


Figure 15. Basic Finite Element Model
Showing Lump Parameter Sections
Relative to the Elastic Axis

TABLE IV

TOTAL WEIGHT, CG, AND WEIGHT DISTRIBUTION COMPARISON

TOTAL STABILATOR WEIGHT

<u>Source</u>	<u>Weight (Lb)</u>	<u>Stabilator Minus Torque Tube Weight</u>
Measured	68.1494	52.0091
NASTRAN	72.0517	55.9114
NAI-58-6	62.3753	46.2350

STABILATOR CG LOCATION

<u>Source</u>	<u>CG (In, HSS Value, Outboard of Aircraft Centerline)</u>
Measured	42.6902
NASTRAN	40.9677

STABILATOR WEIGHT DISTRIBUTION

(Compared to NAI Lump Parameter Model Using the Basic FEM)

<u>Section</u>	<u>NAI-58-6 (Lb)</u>	<u>NASTRAN (Lb)</u>
1	2.2120	3.5244
2	2.0290	2.3396
3	2.8580	2.6820
4	3.0630	4.0616
5	3.5630	3.6170
6	4.4690	4.3983
7	4.7860	5.9411
8	6.4120	8.1998
9	6.3210	6.3459
10	10.5220	16.2630

NOTE: The NASTRAN section weights do not add up to exactly the NASTRAN stabilator weight minus torque tube due to the torque tube's contribution to particular grid points in Section 10.

good results. Also, it must be remembered that the characteristics of each element are taken at the element's center. Therefore, those elements in a region of the stabilator where the thickness changes more quickly, both spanwise and chordwise, such as the area aft of the main spar, will have a thickness that is larger than an average thickness that can be obtained for these elements.

(2) The given NAI weight (46.2350 lb) is the weight of the stabilator planform (Ref 8:29) without the torque tube. Using the data in the Bulk Data Deck, the torque tube was found to weigh 16.1403 lb. The two added yields a weight which is approximately 5.7 lb lighter than the actual stabilator. The reason for this error may be due to the fact that the root rib and the section of the torque tube near the root rib may have been eliminated from the vibration analysis. The same comparison made in parts (1) and (2) above apply also to the stabilator weights minus the torque tube.

Table IV compares the 10 section weights for both the NAI model and the NASTRAN finite element model. Good agreements are obtained with the exception of sections 1, 4, 7, 8, and 10. Because both the end sections and two intermediate sections are involved, the probable reason for these errors could be due to the fact that the elements' weights are lumped at each of its nodes. This means that a section contributes weight to its adjacent section(s).

Moment of inertia data are also given for each section (Ref 8:29). Because the 10 sections are perpendicular with respect to the elastic axis, the moment of inertias are also with respect to the elastic axis. Once the algorithm for the elastic axis was obtained (in terms of the FS-HSS coordinate frame), a FORTRAN program was written to calculate the distance each grid point lies from the elastic axis and the resulting moment of inertia. Input data were the GRID cards from the Bulk Data Deck and the punch output from the NASTRAN Dead Weight Load Vector (using the OLOAD card). The inertia value for each section is then found by adding the inertias of the grid points located in each particular section.

The results for each section are shown in Table V. These results are also in good agreement with the NAI study. Those sections in the finite element model that are different from the NAI results are due to the larger mass content as explained previously.

TABLE V
COMPARISON OF LUMP PARAMETER
MODEL INERTIA TO THE NASTRAN FEM
(SLUG-FT²)

Section	NAI-58-6	NASTRAN
1	.2519	.2983
2	.3769	.3207
3	.6256	.6400
4	.8529	.8996
5	1.1993	1.0354
6	1.7252	1.5215
7	2.0446	2.0423
8	2.7626	3.2485
9	2.8175	2.8649
10	4.0831	7.7411

IV. MODAL ANALYSIS OF THE FINITE ELEMENT MODEL

INTRODUCTION

The modal analysis of the finite element model is an important step in the process of performing a flutter analysis. Theoretically, this is because the response of a structure to forced vibration (i.e., flutter) is taken to be the infinite sum of the structure's free vibration mode shapes. Therefore, it is important that verified mode shapes for the proper boundary conditions be obtained and passed on to the flutter analysis.

MODAL ANALYSIS USING NASTRAN

NASTRAN Rigid Format 3, Normal Mode Analysis, is used to solve the eigenvalue problem. This rigid format utilizes three eigenvalue extraction techniques; the determinant, inverse power, and the Given's triangularization method. The first two are root tracking techniques, and the last method transforms the eigenvalue problem to standard form (Ref 6:305-309).

Since the basic FEM has approximately 550 degrees of freedom and less than 10 eigenvalues are found for each type of boundary condition, the inverse power method is used. This extraction technique works well with large problems where only a few eigenvalues are to be obtained.

The algorithm also takes advantage of stiffness matrix bandwidth size. Minimum bandwidth is achieved by numbering the grid points chordwise instead of spanwise.

In order to eliminate problems in finding rigid body modes and slow convergence for closely spaced roots, a method where eigenvalues are found relative to a shift point is utilized. The iterating equation for the eigenvector u_n is then put in the form

$$w_{n+1} = (K - \lambda_o M)^{-1} M u_n$$

where λ_o is the shift point in the range of eigenvalues. The shift points can be changed at any stage in the solution in order to improve both convergence rate and accuracy.

The algorithm starts searching for eigenvectors at a starting point. Then it may shift to another point (another starting point) when convergence appears too slow. The number of these starting points depends directly on the number of estimated roots (NE on the EIGR card) in the frequency range. Any number of starting points divides the frequency range into smaller regions. This idea enables the inverse power method to iterate at enough shift points to where it will shift to a point outside the frequency range. Once this occurs, the extraction technique will find one or more eigenvalues outside the frequency range and then terminate. Therefore, one is sure that all the eigenvalues for the problem have been found in the desired frequency range.

The user can be sure of obtaining this termination by letting NE equal to an integer larger than the probable number of eigenvectors in the frequency range (Ref 6: 316-320).

RIGID ROOT MODAL ANALYSIS

As a check on the modal analysis problem of this finite element model, two different sets of rigid root boundary conditions are used. The first set has all the grid points of the torque tube (145, 146, 147, 148 and 140) constrained in all six degrees of freedom. These constraints simulate the NAI lump parameter model shown in Figure 15 which was used in the initial modal analysis of the stabilator (Ref 9).

A ground vibration test (GVT) was also performed using one of the stabilators obtained from SAALC. The clamped torque tube of this analysis (see Appendix B) is simulated by constraining grid point 146, which is at the aircraft centerline, in all six degrees of freedom. Only a five by five mesh of deflection points was used in the GVT because of the small number of accelerometers and the amount and type of hardware that was available.

At first qualitative studies were made in comparing NASTRAN mode shapes to those of the NAI lump parameter model (Ref 9:35-40). Similarities in relative magnitudes of translation, bending and pitch (torsion), sign changes, and zero displacements (smallest numerical values of any displacement) for node lines were attempted to be found. This method became increasingly harder as the mode shapes became more

complex and therefore it was abandoned.

NASTRAN has its own capability to produce deformed plots (i.e., mode shapes) using an on-line plotter. But, by using STAGING, the mode shapes together with the undeformed structure for direct comparisons can be obtained from any interactive terminal with a screen and hard copy unit. Since STAGING can display the output of a structural analysis program such as NASTRAN once it is converted to a form STAGING can interpret, pictures of mode shapes can be obtained quite easily. All the pictures of mode shapes in this section were obtained using this interactive program.

In Reference 9, the mode shapes for the lump parameter model are given. The translation, bending and pitch (torsion) of the center of each of the ten sections are plotted versus the elastic axis position of the centers. This elastic axis position is taken with respect to the root rib (see Figure 15) going outboard. Since only one dimension is involved, these mode shapes are essentially one-dimensional. Figure 22 is an example of one of the lump parameter model mode shapes.

In order to view a NAI mode shape as if it were one for a finite element model, a FORTRAN program was written that gave each grid point of the FEM an interpolated translation (T3 in NASTRAN). These interpolated values were found by using the lump parameter model mode shapes and the elastic axis position of each grid point. For instance, the translation and pitch about the elastic axis for a grid point with a

certain elastic axis position is found by interpolating between these values which are obtained from the lump parameter mode shape curves. Once the translation values in the z direction due to bending and torsion are found, the two values are added together. This addition results in a total z displacement which is T3 in NASTRAN for each grid point. Output for all grid points is put into the form of NASTRAN output which is then converted for use by STAGING.

For converting the GVT modes, a two dimensional interpolating subroutine is used. By doing this, the GVT grid size is changed to that of the FEM.

The following table and figures compare the FEM to the two rigid-root conditions that have been previously described. A summary of the results will be given at the end of this section. Case 1 is the modal analysis simulating the NAI conditions and Case 2 is the GVT of the stabilator clamped near the location of aircraft centerline (Ref Figure 3). Each mode is presented by first showing the FEM mode shape. Following this picture is the appropriate NAI or GVT mode shape which has been converted to two dimensions as previously described. Figure 23 is included as a better representation of the results of the program that changes the NAI shapes to those of a finite element model. NASTRAN/GVT indicates the NASTRAN simulation of the GVT.

TABLE VI

COMPARISON OF NASTRAN MODAL ANALYSIS RESULTS
TO THE TWO RIGID-ROOT CASES

CASE 1 - NASTRAN Compared to NAI

DESCRIPTION OF MODE	NAI MODE #	NAI FREQ (cps)*	NASTRAN MODE #	NASTRAN FREQ (cps)*
1st Bending	1	27.08	1	23.05
1st Torsion	2	62.35	2	51.05
2nd Bending	3	101.41	4	73.31

CASE 2 - NASTRAN Compared to GVT

DESCRIPTION OF MODE	GVT MODE #	GVT FREQ (cps)	NASTRAN MODE #	NASTRAN FREQ (cps)
Torque Tube Bending at Root Rib	1	13.61	1	12.95
2nd Bending	2	55.67	4	45.99
3rd Torsion	3	99.21	8	116.49

* cps = cycles per second

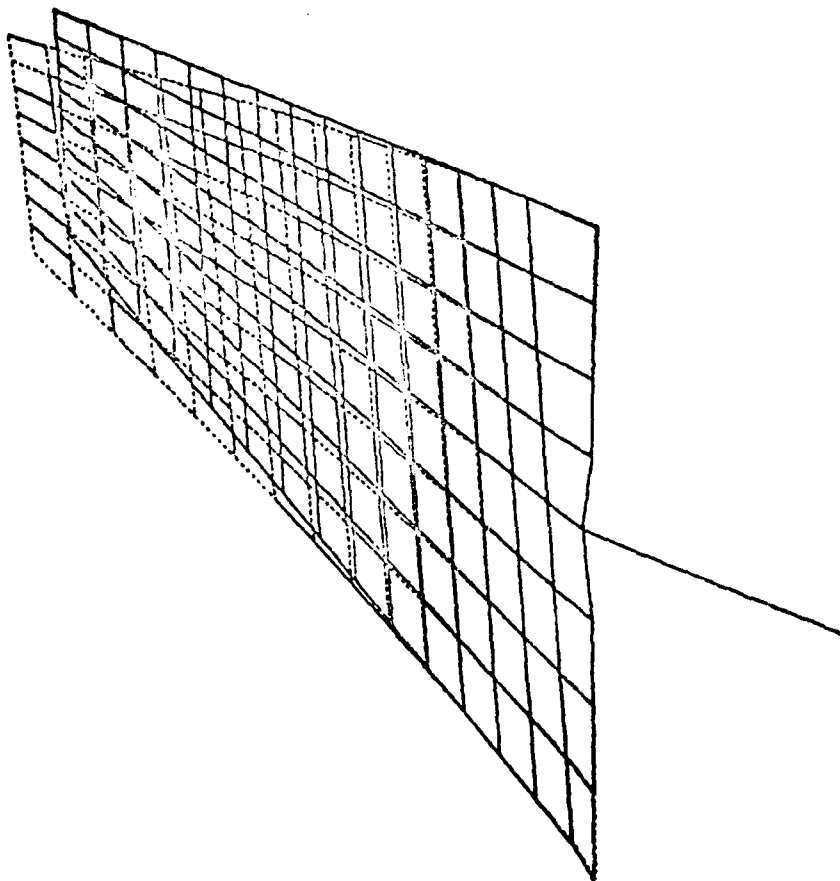


Figure 16. NASTRAN 1st Bending 23.05 Hz

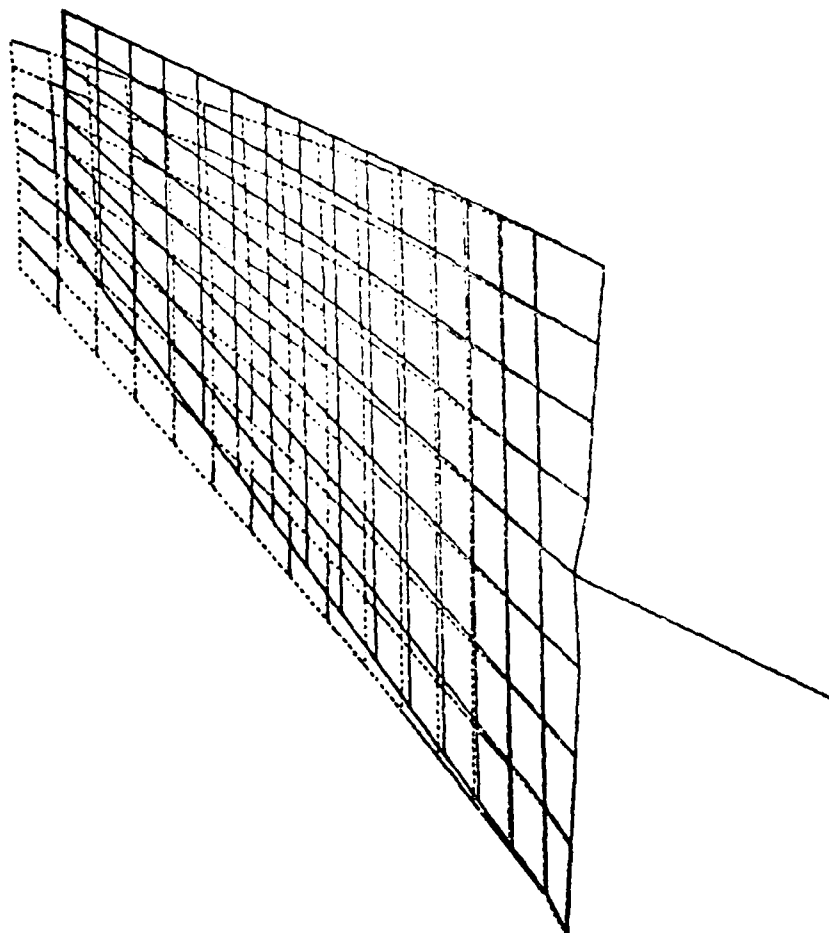


Figure 17. NAI 1st Bending 27.08 Hz

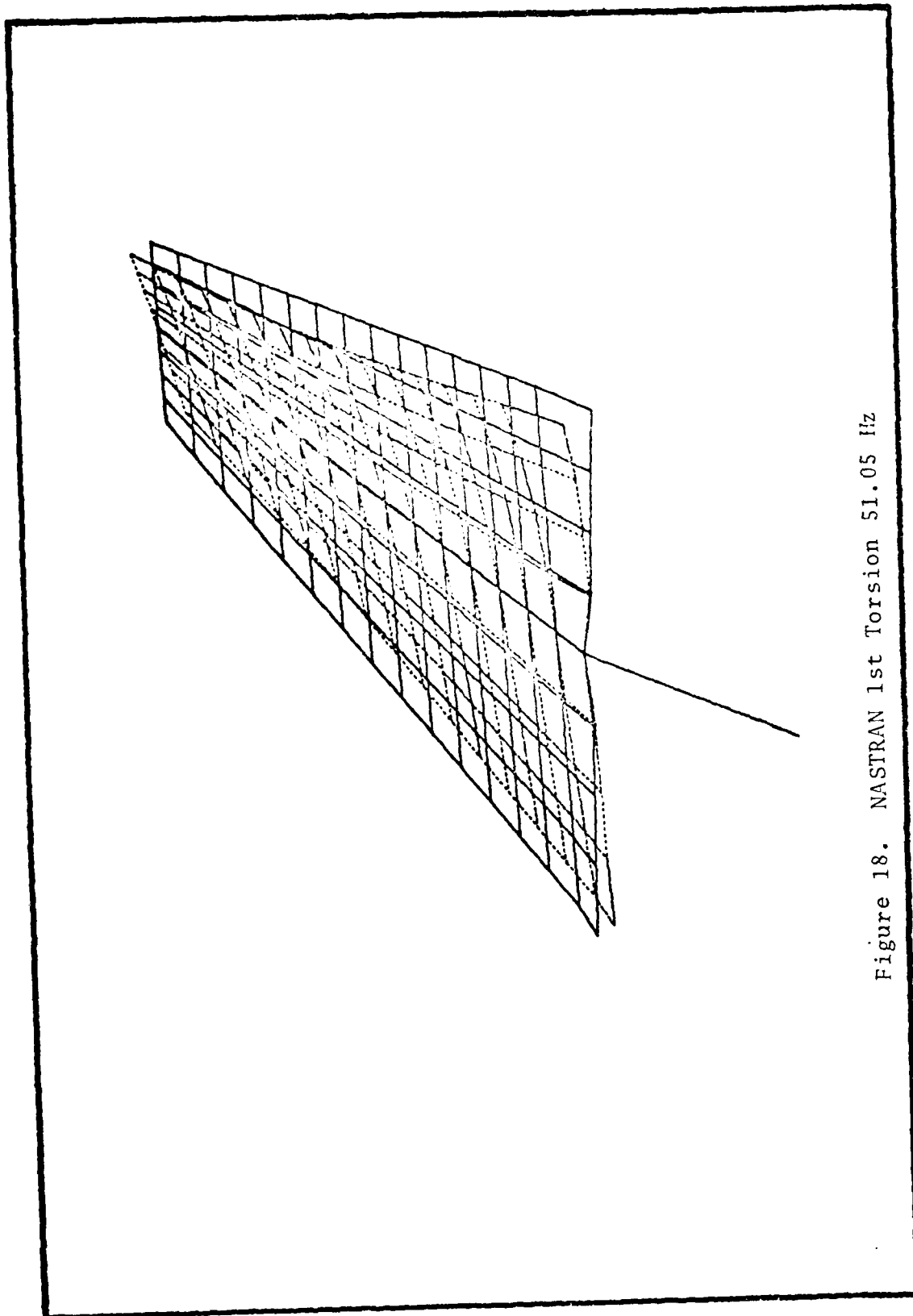


Figure 18. NASTRAN 1st Torsion 51.05 Hz

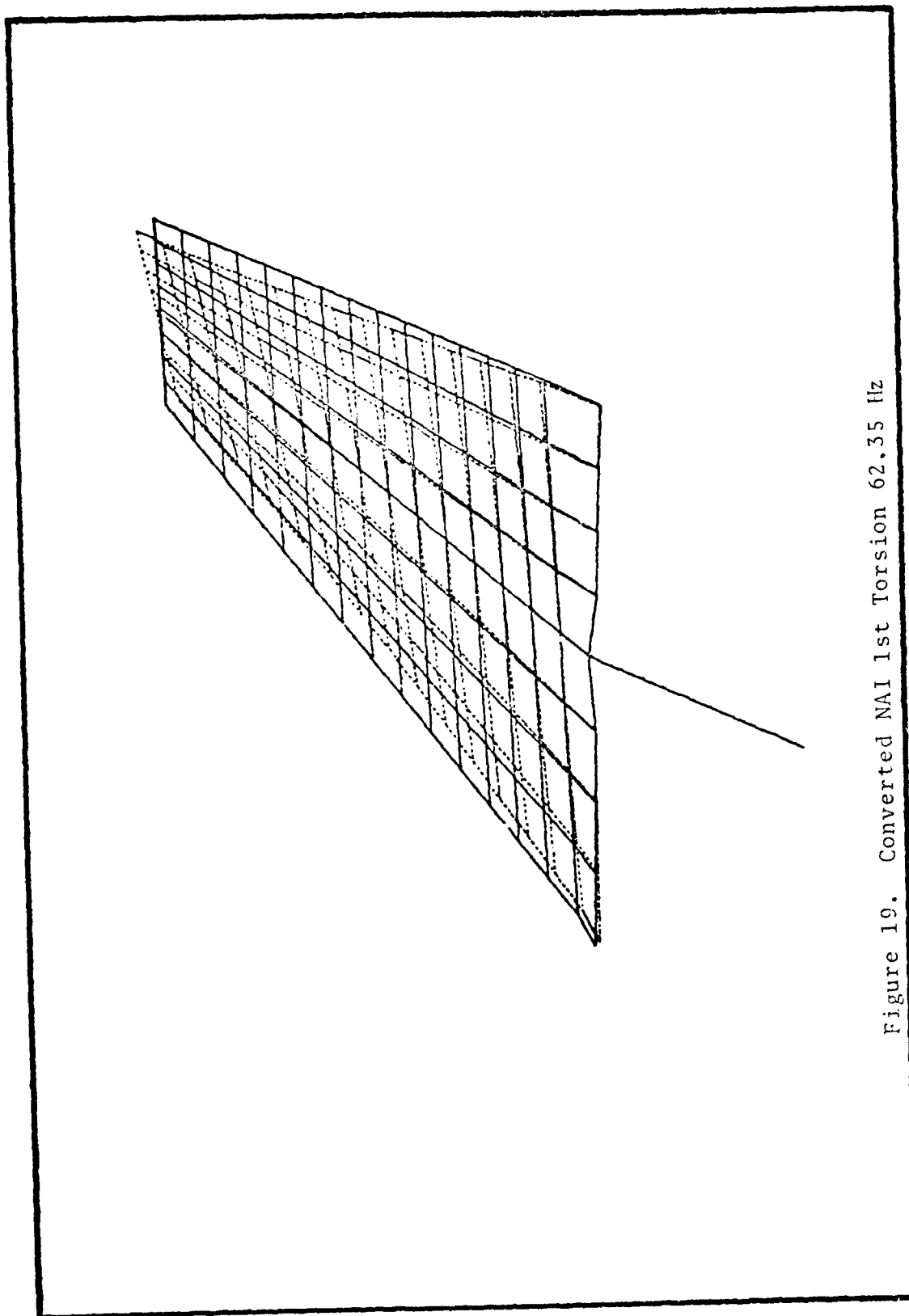


Figure 19. Converted NAI 1st Torsion 62.35 Hz

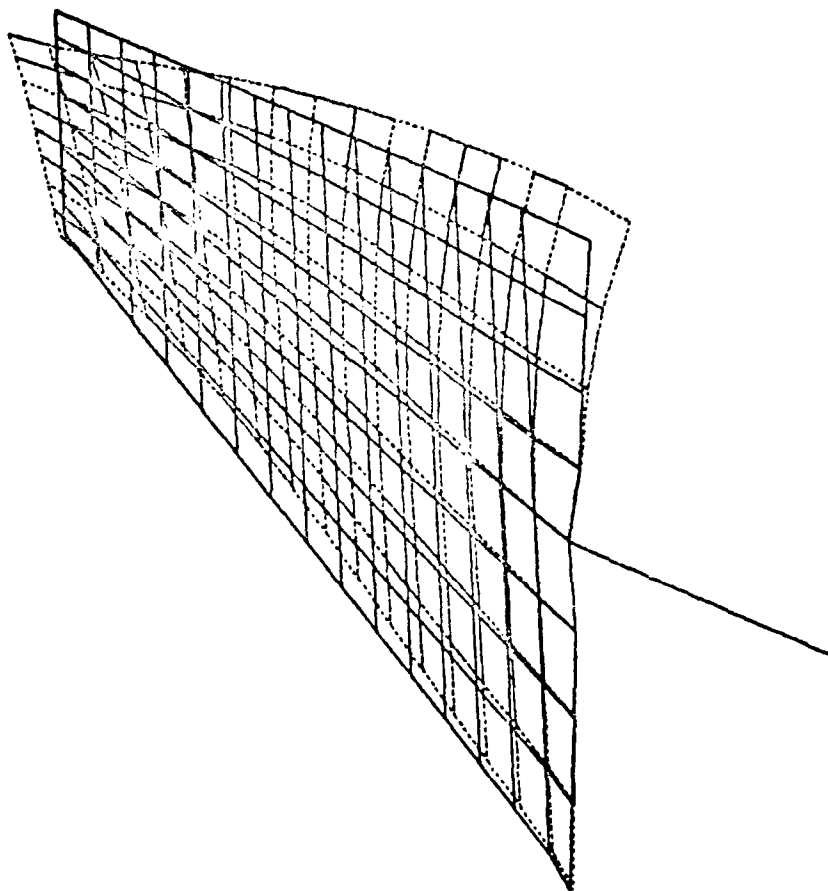


Figure 20. NASTRAN 2nd Bending 73.31 Hz

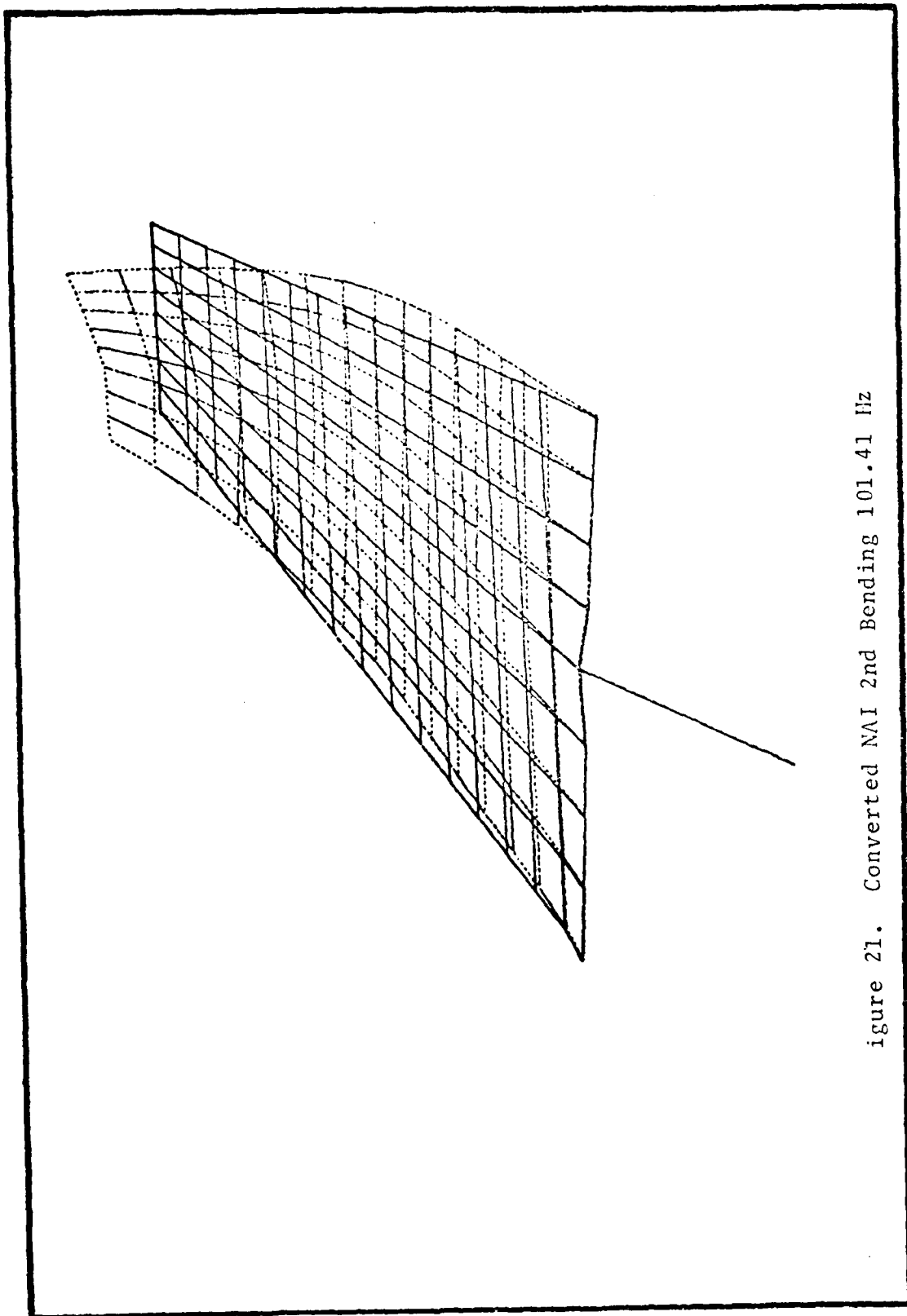


figure 21. Converted NAI 2nd Bending 101.41 Hz

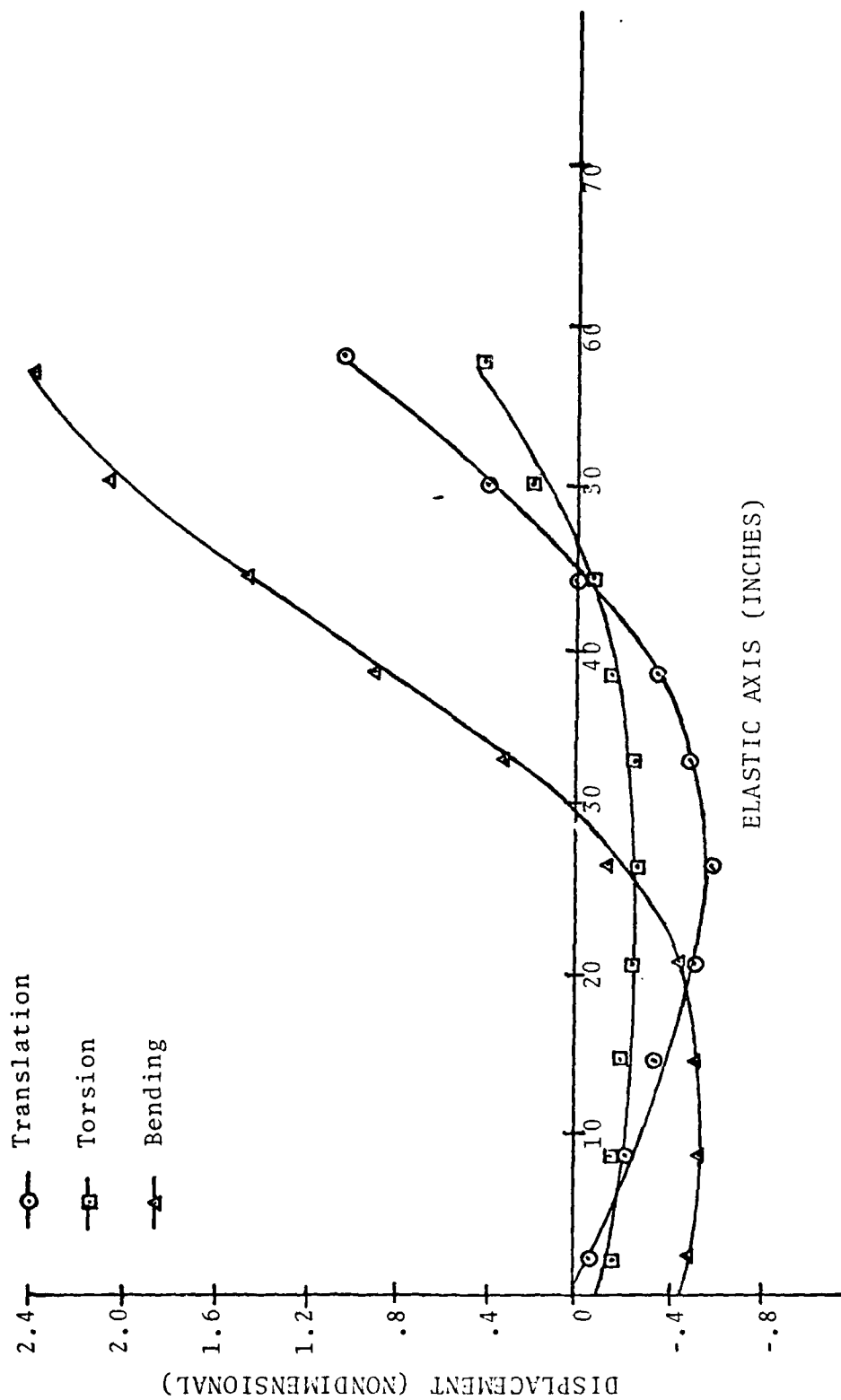


Figure 22. NAI Lump Parameter Model
2nd Bending (Ref 9:37)

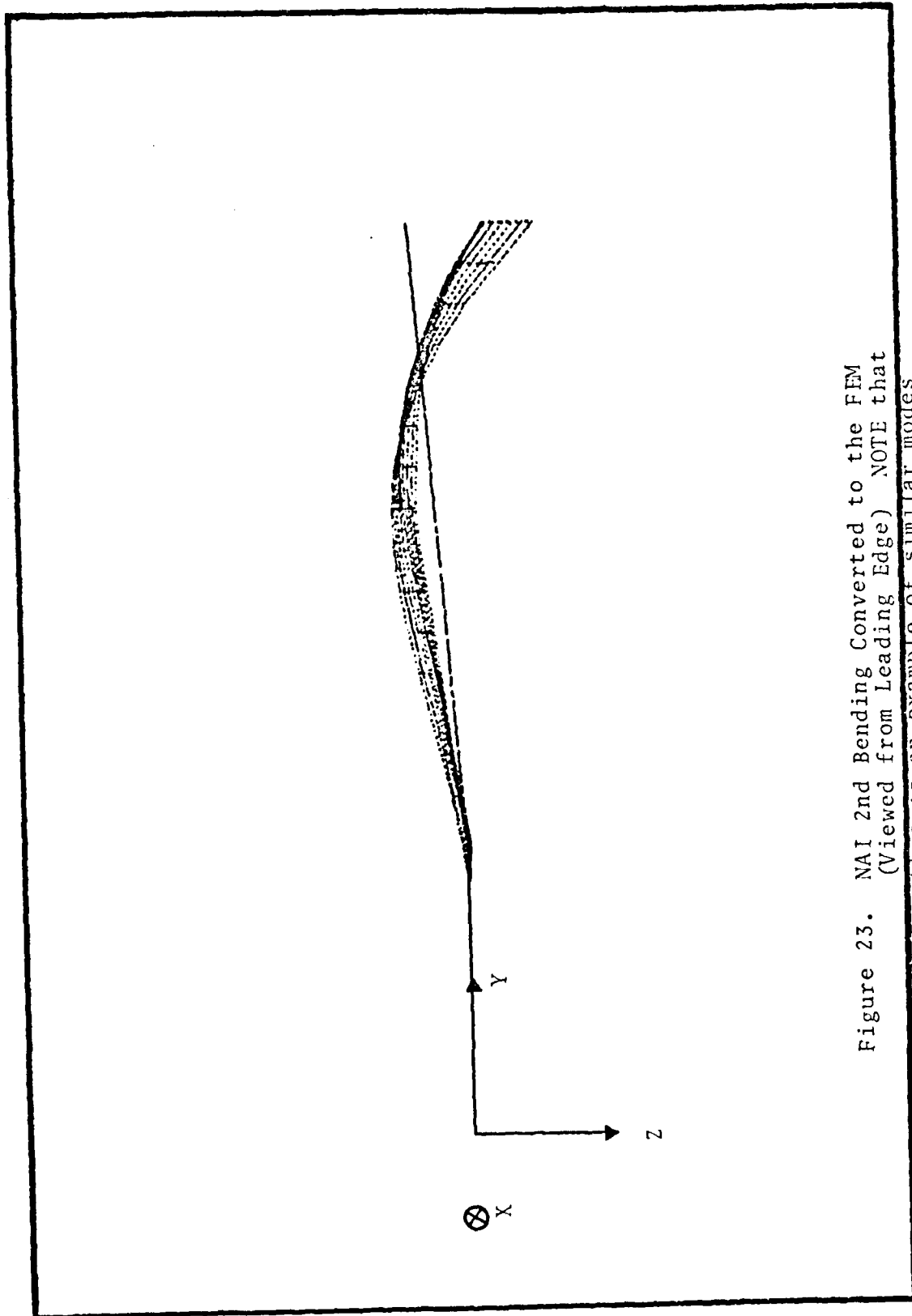


Figure 23. NAI 2nd Bending Converted to the FEM
(Viewed from Leading Edge) NOTE that
this is an example of similar modes
but opposite signs.

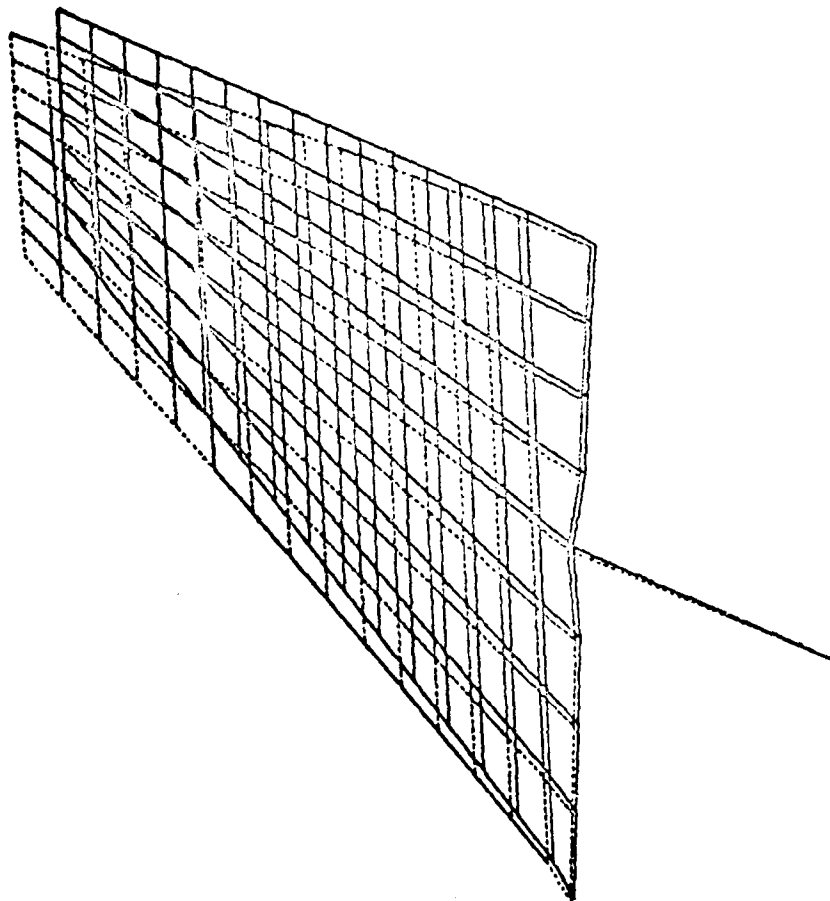


Figure 24. NASTRAN/GVT Torque Tube Bending 12.95 Hz

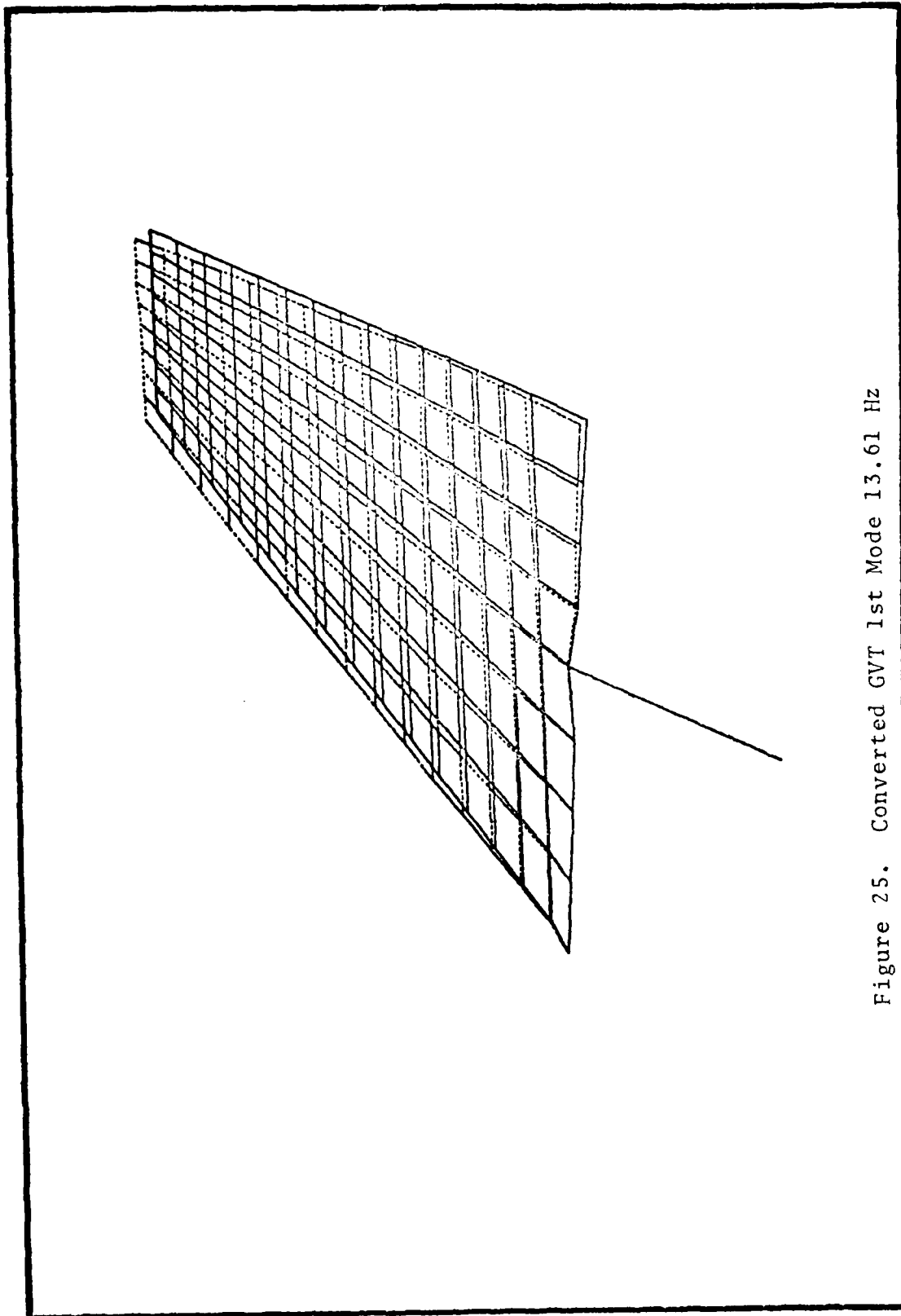


Figure 25. Converted GVT 1st Mode 13.61 Hz

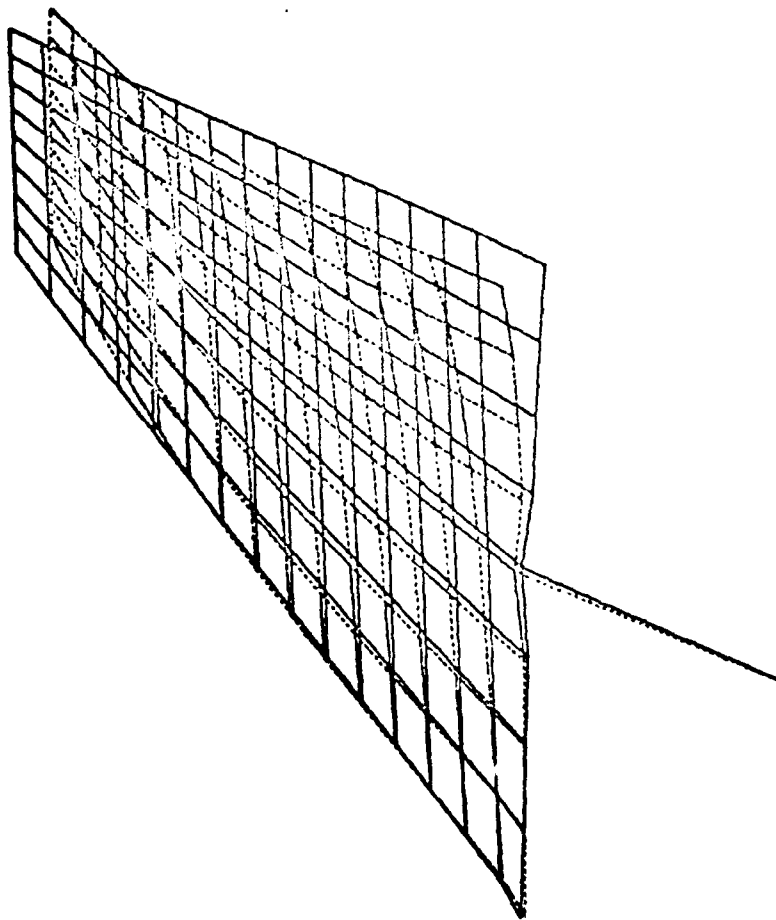


Figure 26. NASTRAN/GVT 2nd Binding 45.99 Hz

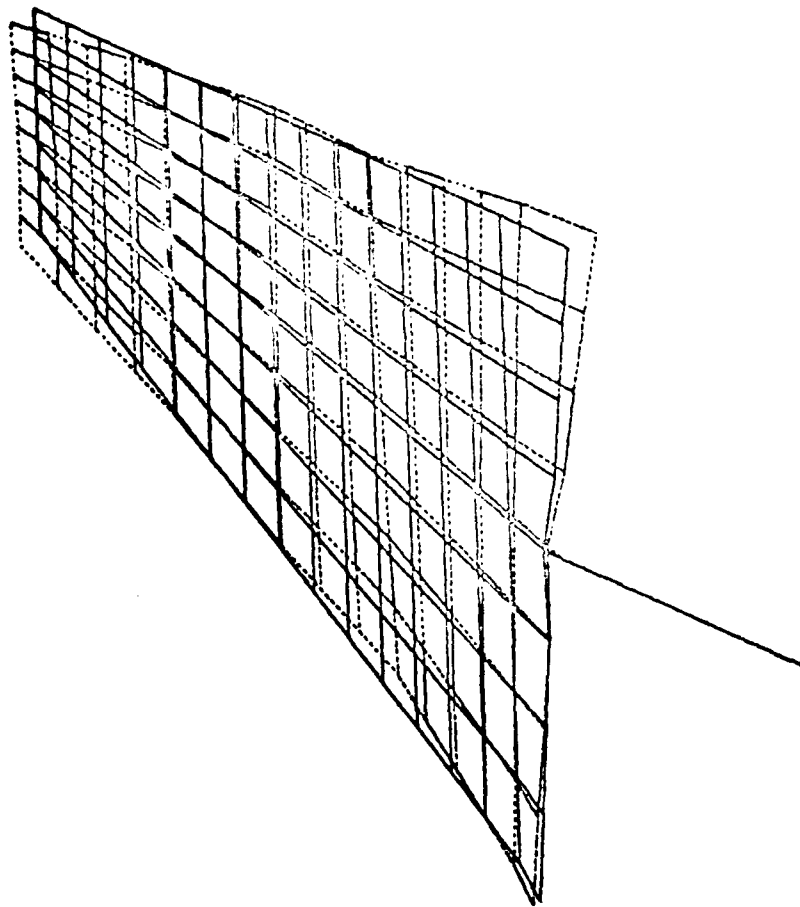


Figure 27. Converted GVT 2nd Mode 55.67 Hz

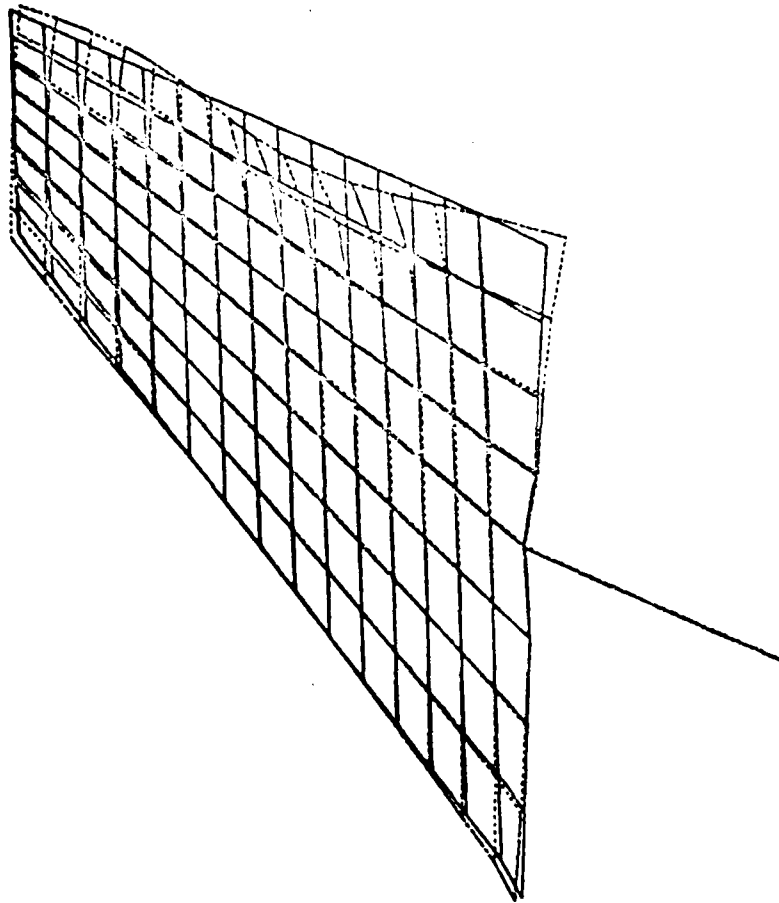


Figure 28. NASTRAN/GVT 3rd Torsion 116.49 Hz

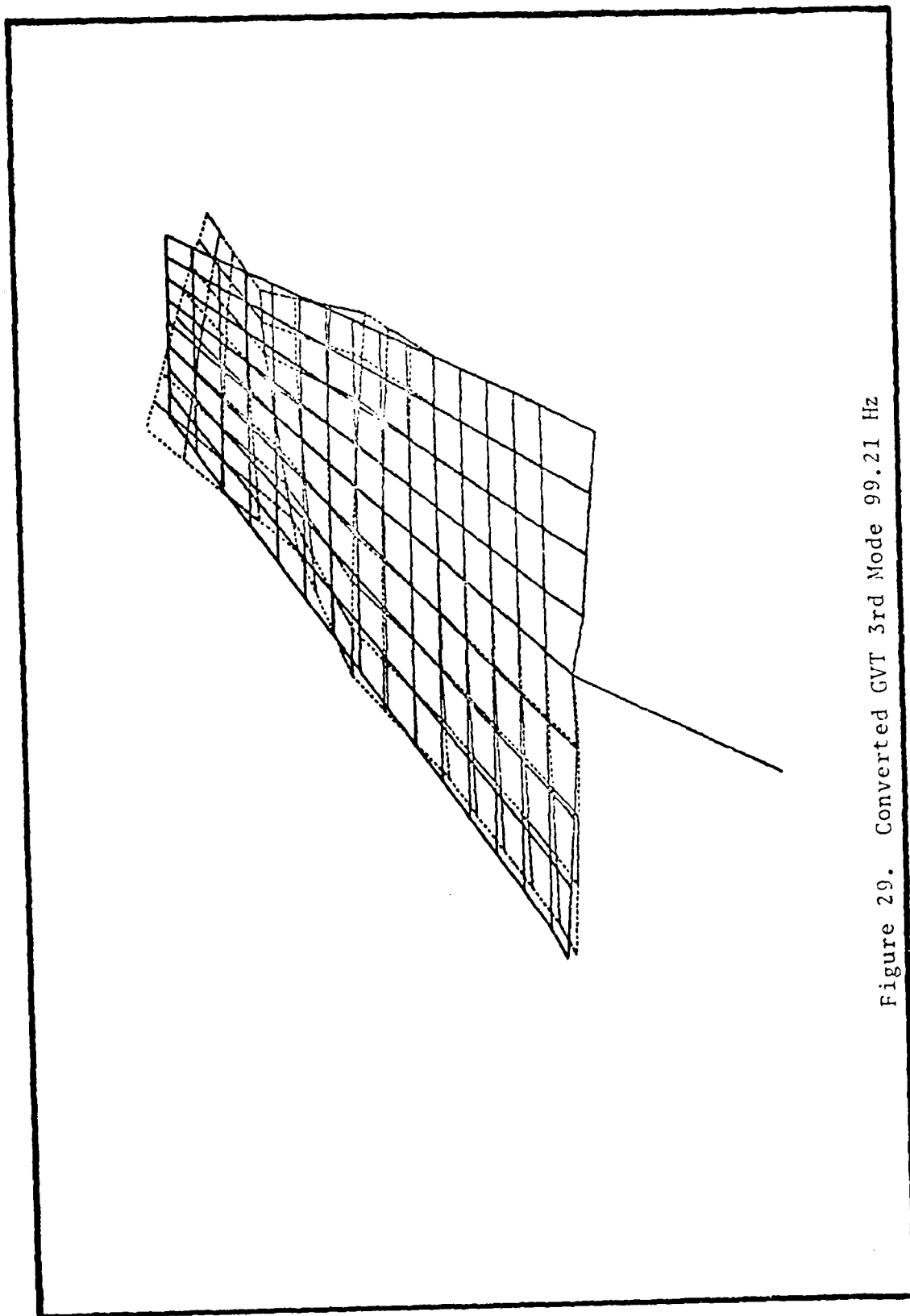


Figure 29. Converted GVT 3rd Mode 99.21 Hz

FLEXIBLE ROOT MODAL ANALYSIS

For this work, flexible root indicates that the hydraulic actuator assembly for the horizontal stabilator is taken into account in the modal analysis. The combined actuator assembly stiffness adds an external stiffness to the horizontal stabilator. Since the flutter analysis is to be performed on damaged horizontal stabilators in an actual flight condition, the effect of a pressurized hydraulic actuator assembly must be considered.

The equivalent stiffness of the actuator assembly-torque tube combination can be modeled in the FEM using several ways. As opposed to including the components and their degrees of freedom of the actuator assembly (Ref 11:4) in the FEM, the equivalent spring stiffness in pitch (degree of freedom 5 in NASTRAN) was included by using the CELAS2 card. This spring element was placed at the location of the actuator horn (see Figure 3). It is certain that the actuator assembly provides no constraints in the critical degrees of freedom which are 3, 4, and 5 in NASTRAN. Only the torque tube provides bending stiffness for this area.

Hydraulic actuator stiffness depends heavily upon the temperature and pressure of the hydraulic fluid. Reference 11 shows the method of determining the hydraulic cylinder linear spring rate and the system (actuator assembly) pitch stiffness. A pressure of 3000 - 3100 psi and a temperature between 100° F and 150° F is assumed to be a standard operating condition (Ref 5:33 and 12:2).

There are two separate hydraulic systems in the T-38. The "utility" system is powered by one engine and the "flight" system is powered by the other engine. In normal operating conditions, both systems are used. Both systems by themselves provide the same stiffness. Using the given hydraulic fluid temperature and pressure, equivalent pitch stiffness values were found. These values are

One system = 1.72×10^6 in-lbs/rad

Both systems = 2.54×10^6 in-lbs/rad

A pitch stiffness of 2.0×10^6 in-lbs/rad was also found for the actuator assembly in Reference 13, page 70. The results using all three values will be shown (Ref 11:11-12).

Since the torque tubes of the stabilators are near the engines, one may suspect that the heating of the torque tubes by the engines should be considered. Any decrease in the modulus of elasticity of the 43M30 steel torque tubes is considered small and this effect is neglected.

Both symmetric and antisymmetric mode shapes are considered in the modal analysis. For a flutter analysis, both of these should be included since flutter can occur in either or both conditions. The constraints for a symmetric boundary condition is given in the section concerning the influence coefficient study. For an antisymmetric boundary condition, degree of freedom 4 is replaced by degree of freedom 3.

Reference 9 shows the lump parameter model mode shapes for a flexible root. An emergency hydraulic power (only one system operating) in the actuator assembly is modeled. This worst case simulation is Case 1 in this NASTRAN modal analysis.

Case 2 shows the comparison of the FEM to the data contained in an AFFDL in-house study (Ref 14:5-8). The mode shapes in this report are also for a worst case simulation. Information from one of the authors indicated that the tab on the stabilator does not significantly affect the mode shapes needed for this comparison.

Case 3 uses the last value of the actuator pitch stiffness. Since the report that utilized this value (Ref 13) compared their results to the NAI results (Ref 9), this case is also for only one hydraulic system powered.

The Structural Dynamics Laboratory at Eglin Air Force Base, Florida, performed a modal analysis (GVT) of a horizontal stabilator which was on a Canadian CF-5 aircraft. Both the T-38 and the CF-5, which is the same as the United States Air Force F-5, have the series 3 stabilator. A five by five grid of deflection points was used to obtain both symmetric and anti-symmetric modes. The aerospace ground equipment that was used in this GVT powered both hydraulic systems. Case 4 of the flexible root modal analysis simulates this GVT.

The results for the four cases are shown in the following table and figures. The same FORTRAN programs that were used in the rigid root modal analysis are used here. Also, the same format in presenting the results is used.

TABLE VII
COMPARISON OF NASTRAN MODAL ANALYSIS RESULTS
TO THE CALCULATED AND GVT FLEXIBLE-ROOT CASES

CASE 1 - NASTRAN COMPARED TO NAI CALCULATED DATA

MODE	NAI MODE #	NAI FREQ (cps)	NASTRAN MODE #	NASTRAN FREQ (cps)
1st Bending	1	17.61	1	15.56
1st Torsion	2	44.89	3	32.47
2nd Bending	3	78.76	4	56.08

CONDITIONS: 1 hydraulic system operating, actuator pitch
stiffness is 1.72×10^6 in-lb/rad, symmetric
boundary conditions.

CASE 2 - NASTRAN COMPARED TO GVT DATA CONTAINED IN REF 14

MODE	AFFDL MODE #	AFFDL FREQ (cps)	NASTRAN MODE #	NASTRAN FREQ (cps)
1st Bending	1	18.0	1	15.56
1st Torsion	2	40.5	3	32.47
2nd Bending	3	61.2	4	56.08
2nd Torsion	5	104.3	5	79.42

CONDITIONS: Same as in Case 1.

TABLE VII (Cont'd)

CASE 3 - NASTRAN COMPARED TO CALCULATED FREQUENCIES LISTED IN REF 13

MODE	SWRI MODE #	SWRI FREQ (cps)	NASTRAN MODE #	NASTRAN FREQ (cps)
1st Bending	1	18.80	1	15.56
1st Torsion	2	44.56	3	32.47
2nd Bending	3	79.27	4	56.08

CONDITIONS: Same as in Cases 1 and 2 except actuator pitch stiffness is 2.00×10^6 in-lb/rad.

CASE 4 - NASTRAN COMPARED TO EGLIN GVT DATA

MODE	EGLIN MODE #	EGLIN FREQ	NASTRAN MODE #	NASTRAN FREQ
1st Bending	1	18.52	1	15.62
1st Torsion	3	50.20	3	35.37
2nd Bending	5	70.69	4	56.22

CONDITIONS: 2 hydraulic systems operating, actuator pitch stiffness is 2.54×10^6 in-lb/rad symmetric boundary conditions. The deflection points of the Eglin GVT were moved to the closest FEM grid point. The locations of the two sets of points differed by less than two inches.

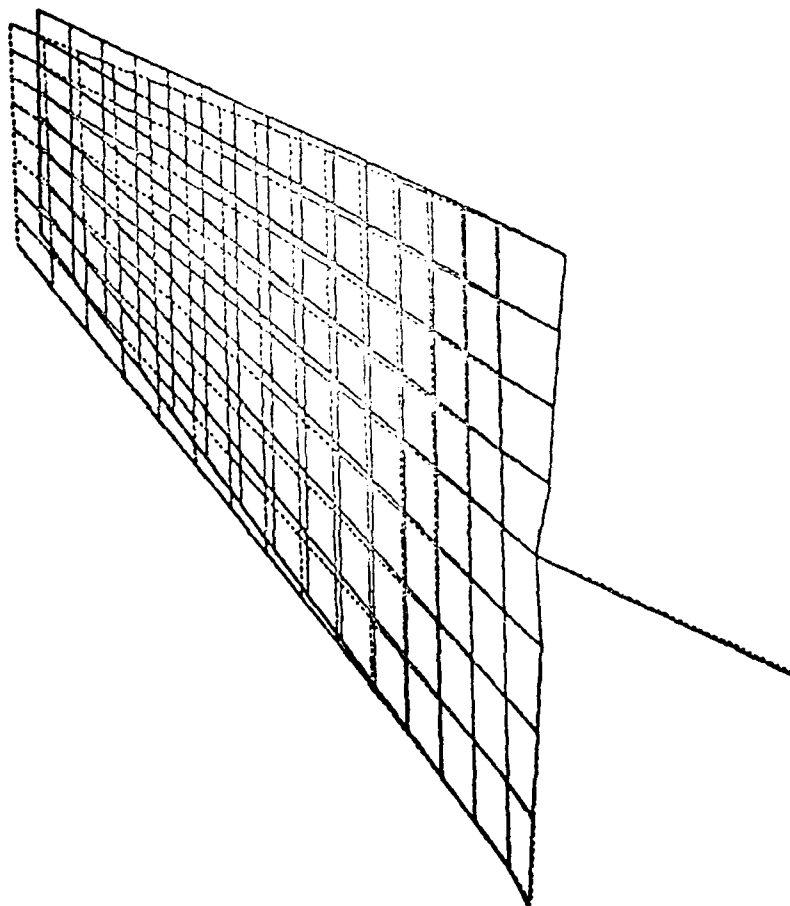


Figure 30. Case 1, NASTRAN 1st Bending, 15.56 Hz

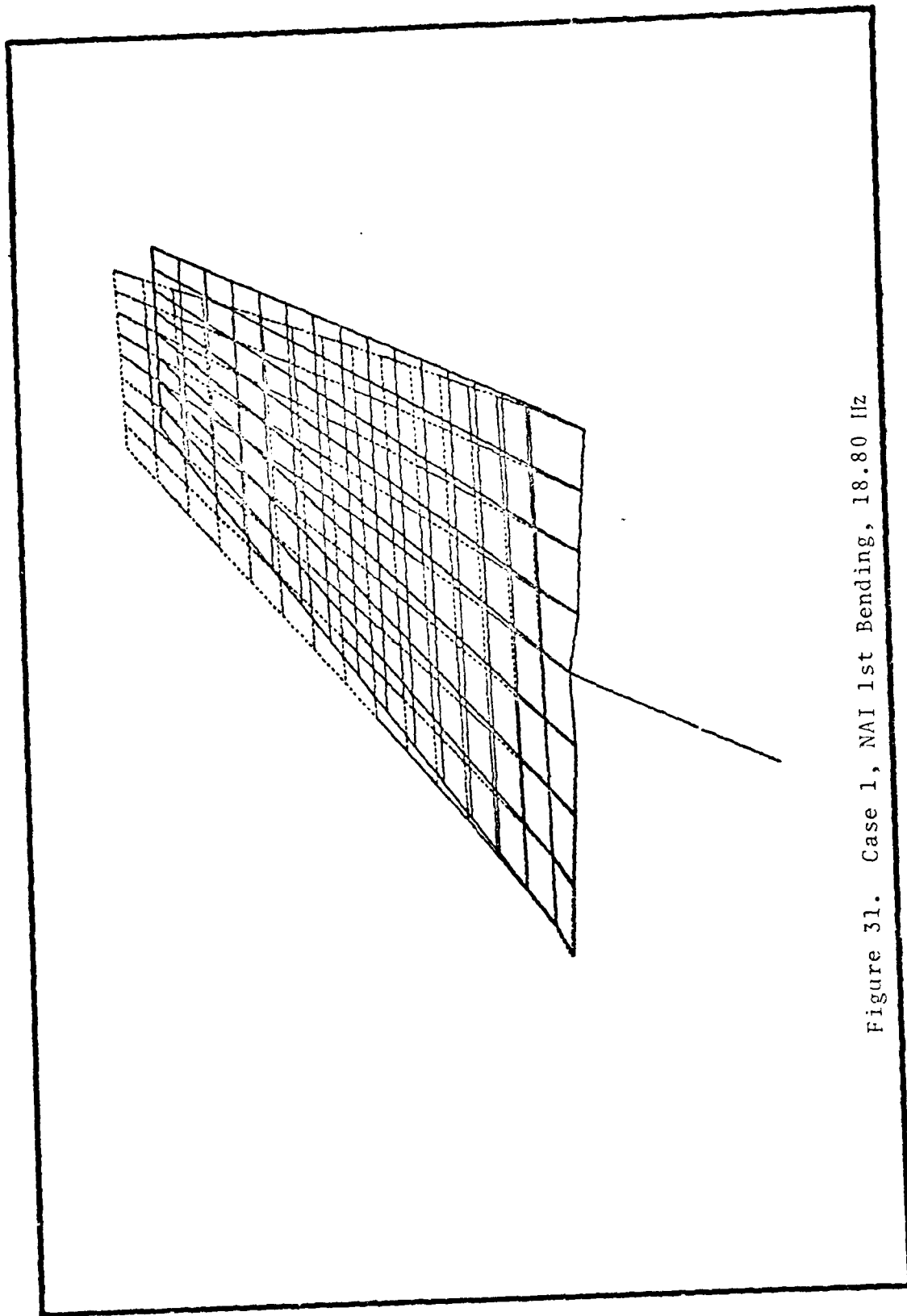


Figure 31. Case 1, NAI 1st Bending, 18.80 Hz

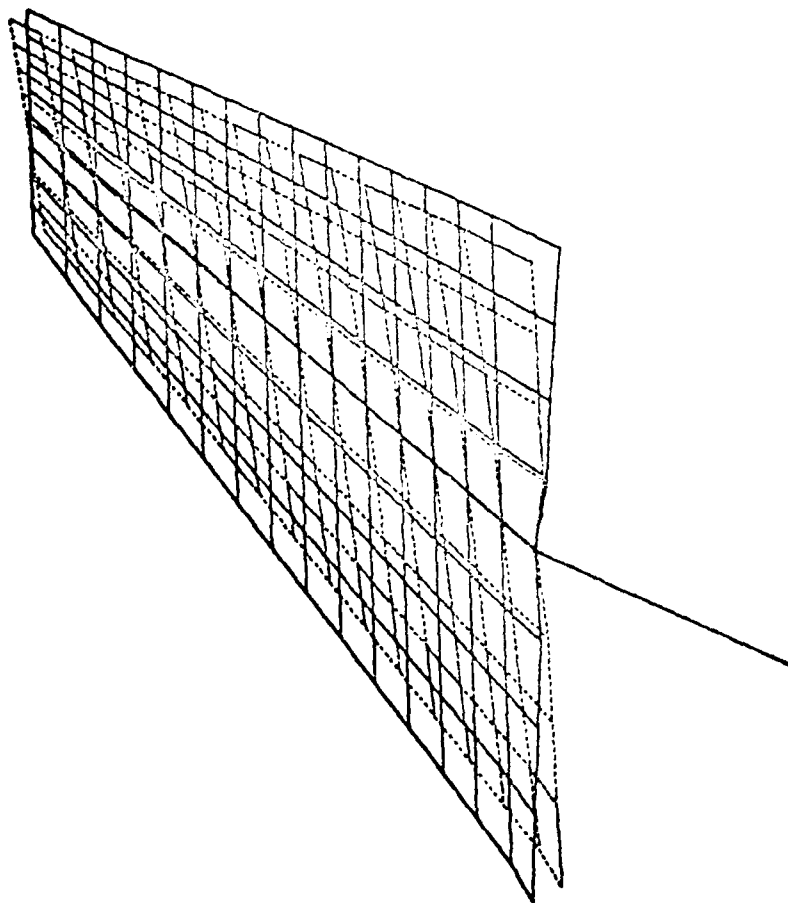


Figure 32. Case 1, NASTRAN 1st Torsion, 32.47 Hz

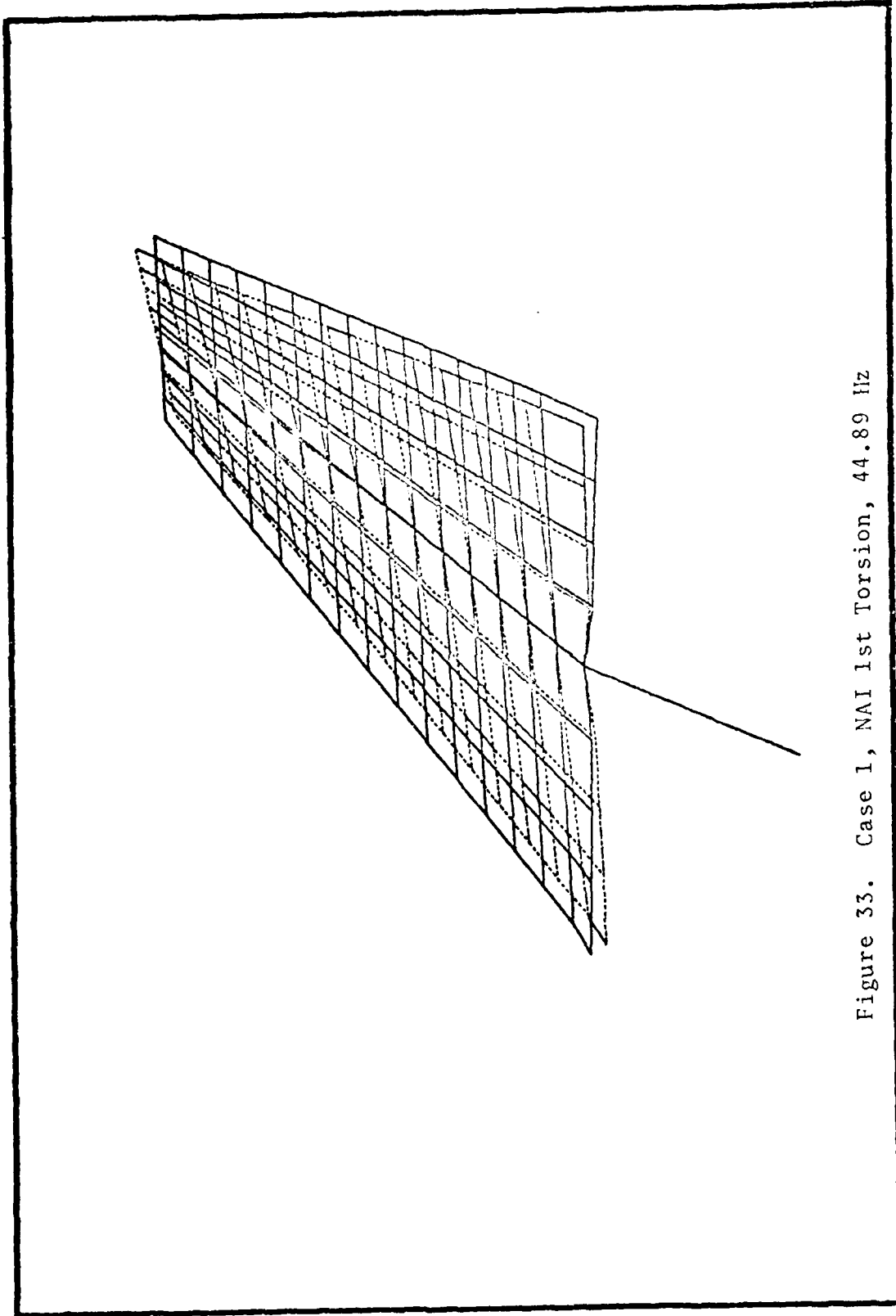


Figure 33. Case 1, NAI 1st Torsion, 44.89 Hz

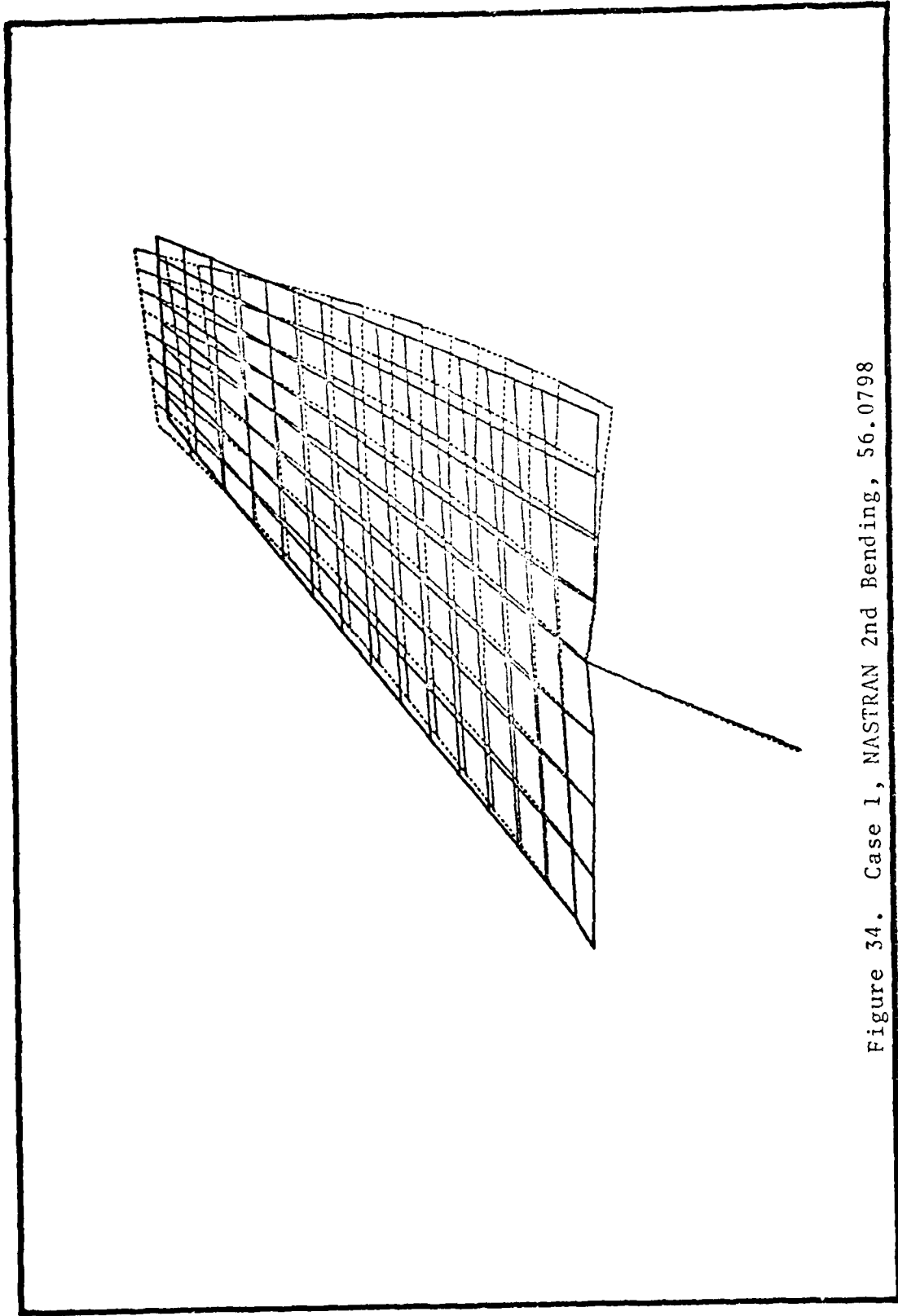


Figure 34. Case 1, NASTRAN 2nd Bending, 56.0798

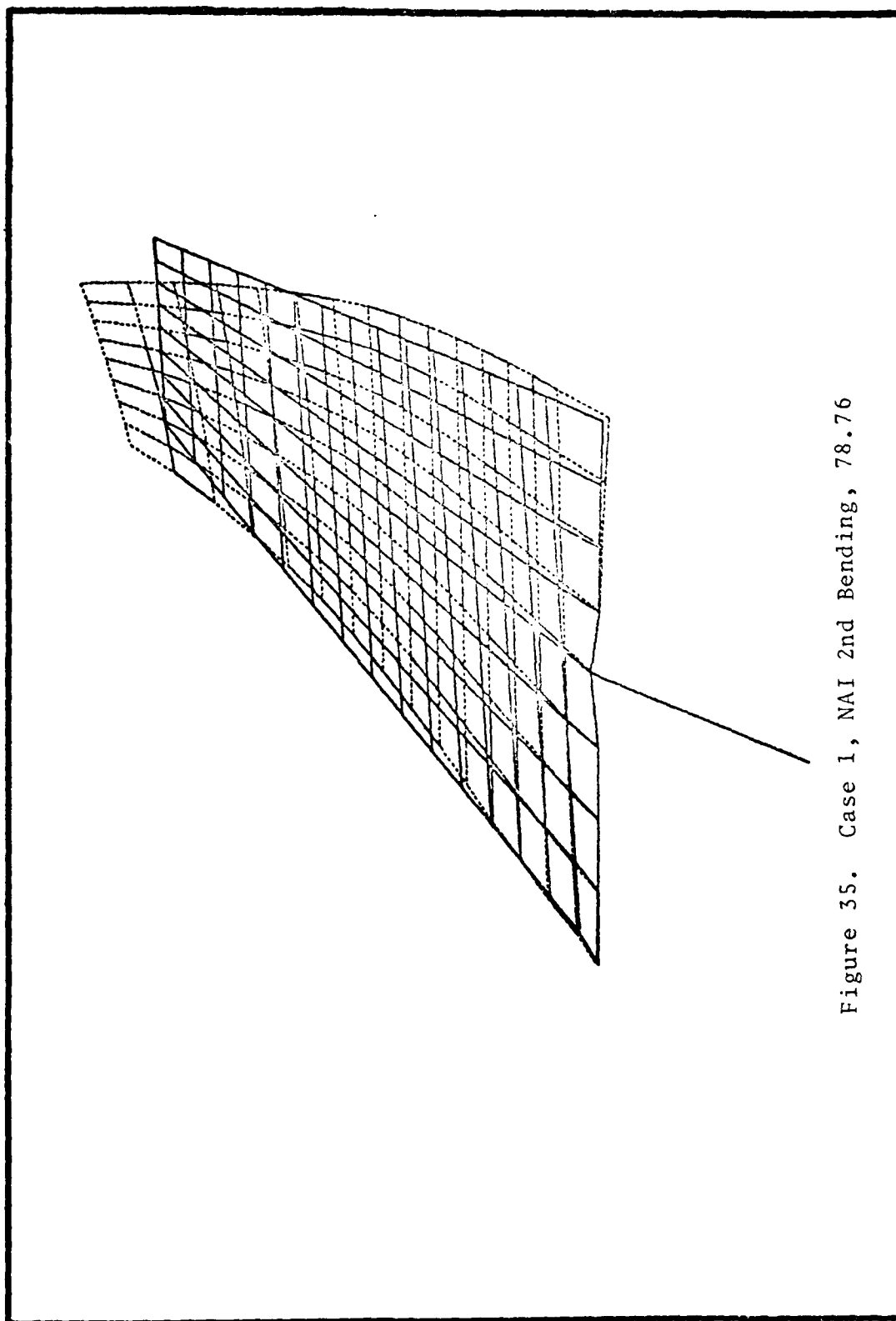
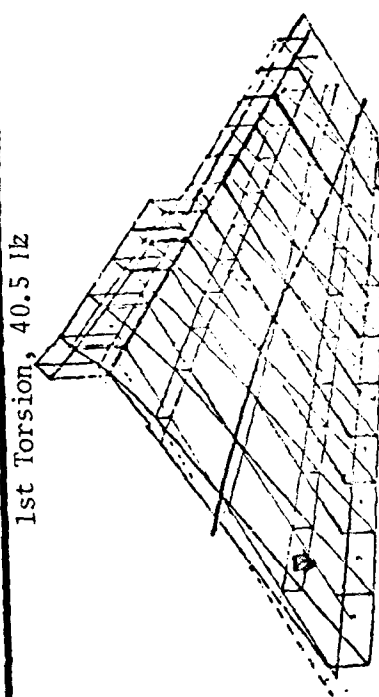
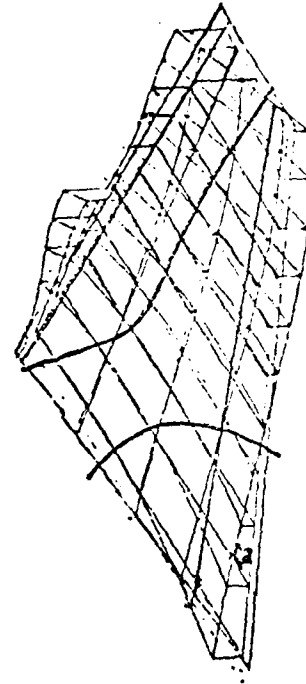


Figure 35. Case 1, NAI 2nd Bending, 78.76

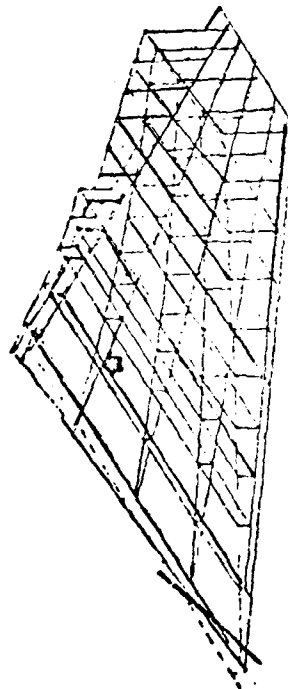


1st Torsion, 40.5 Hz

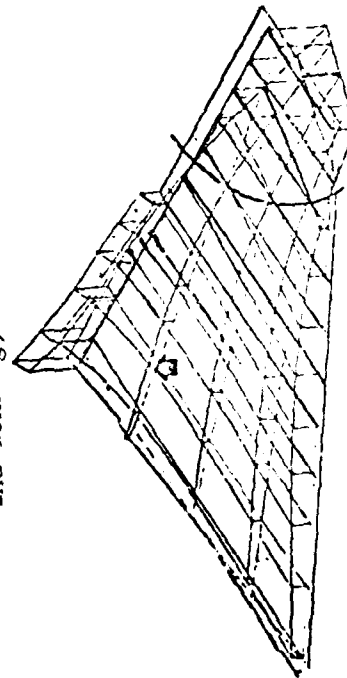


2nd Torsion, 104.3 Hz

1st Bending, 18.0 Hz



2nd Bending, 61.2 Hz



NOTE: Frequencies have been modified to approximate a stabilator with no tab.

Figure 36. Case 2, Measured Symmetric Flexible Root Modes (Ref 14:6-7)

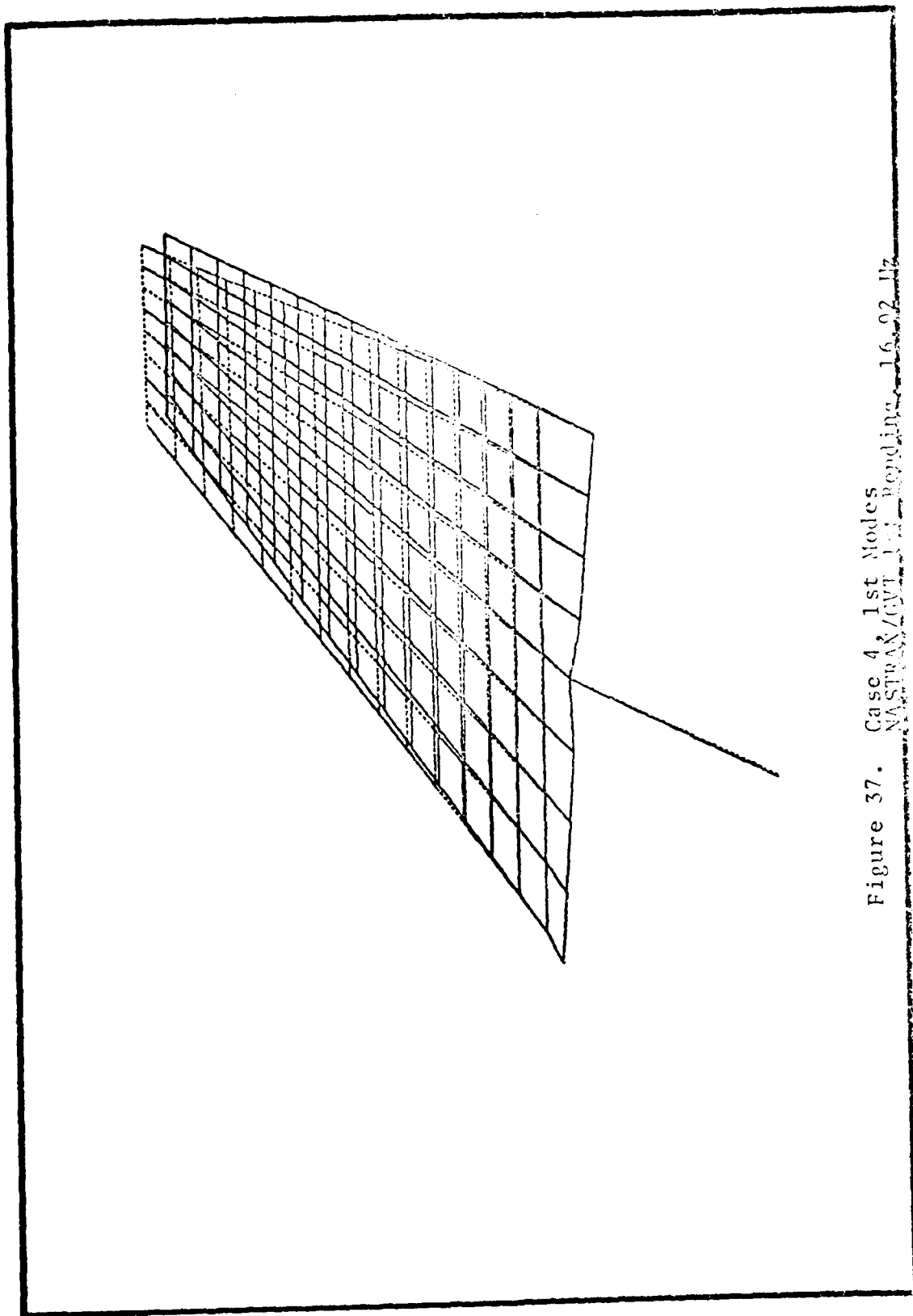


Figure 37. Case 4, 1st Modes
NASTRAN/CVT 1.00, Pending, 16.02.17

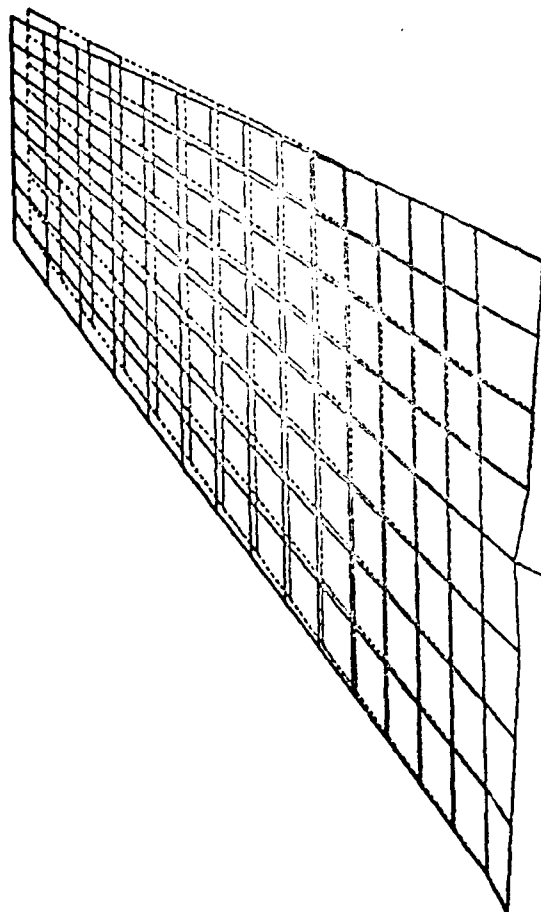


Figure 38. Case 4, 1st Modes
Eglin GVT 1st Bending, 18.52 Hz

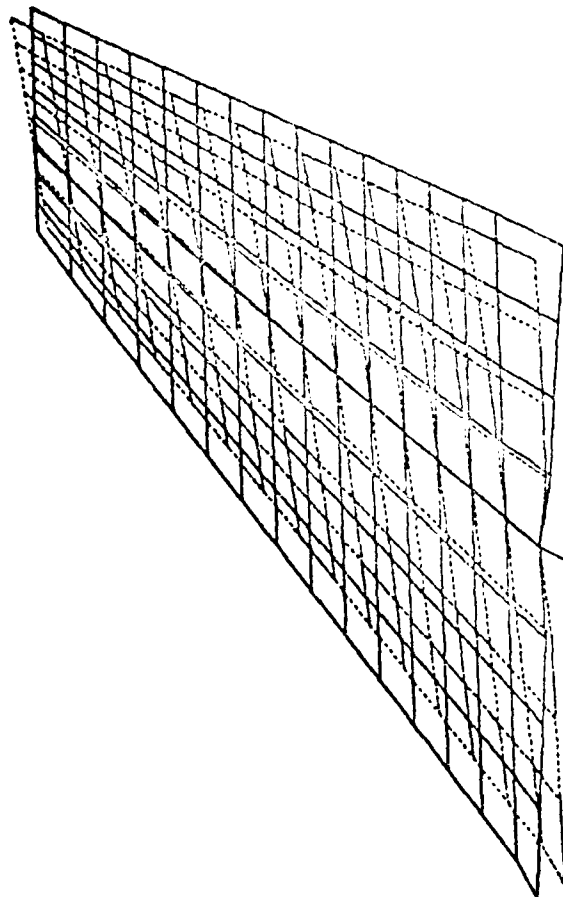


Figure 39. Case 4, 2nd Modes
NASTRAN/GVT 1st Torsion, 35.37 1/2

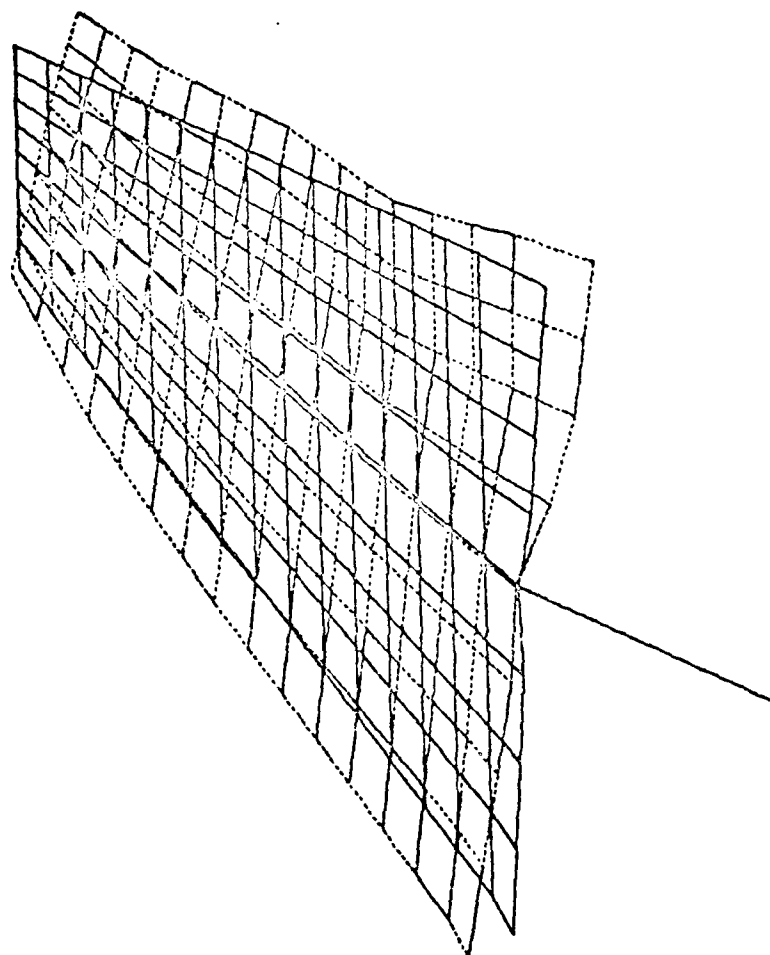


Figure 40. Case 4, 2nd Modes
Eglin GVT 1st Torsion, 50.20 Hz

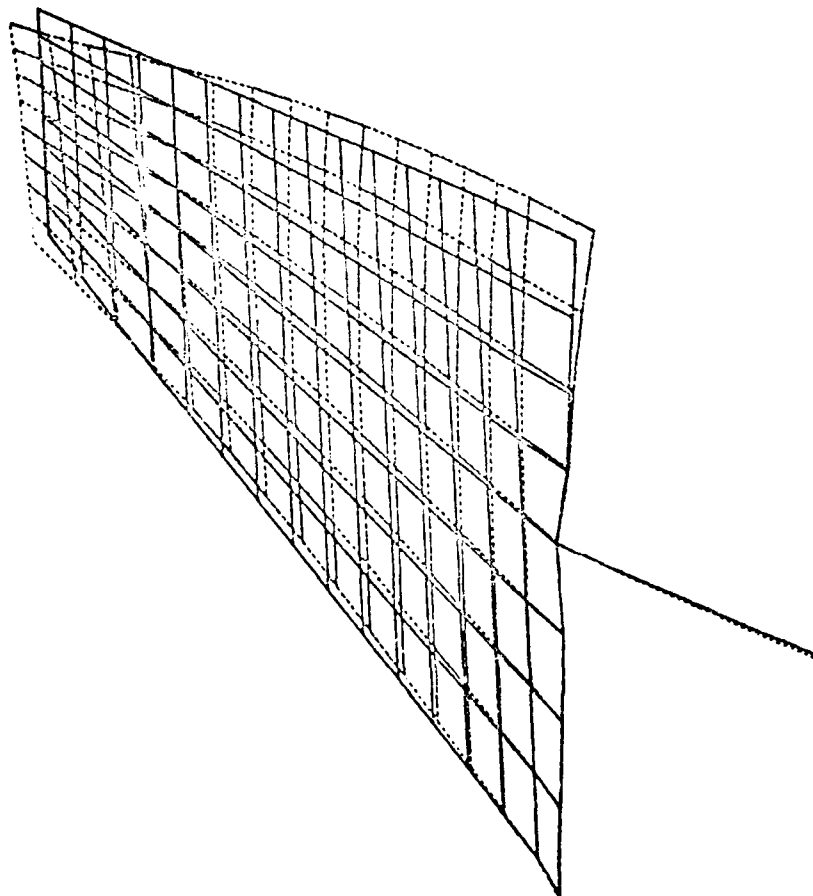


Figure 41. Case 4, 3rd Modes
NASTRAN/GVT 2nd Bending, 56.22 Hz

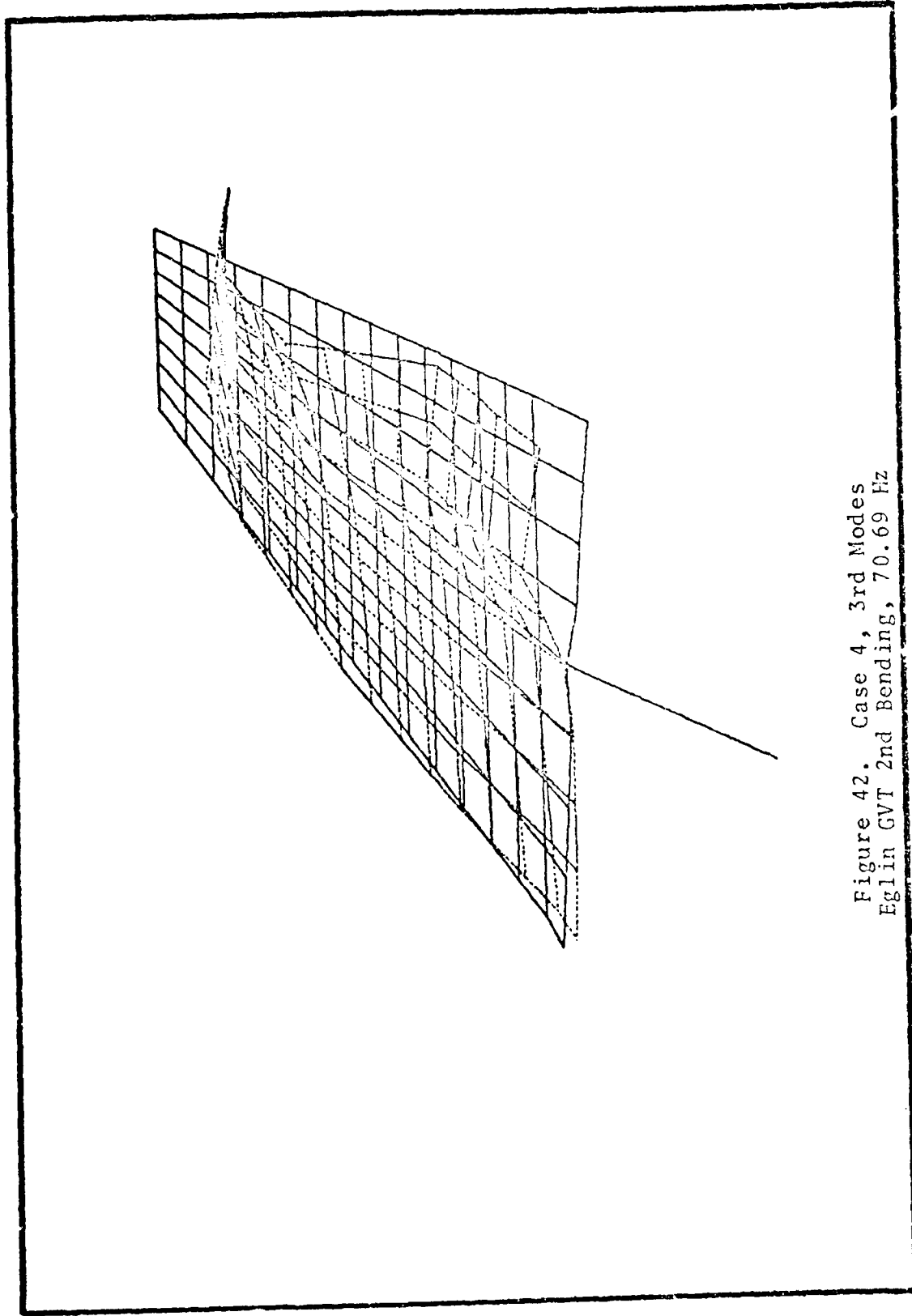


Figure 42. Case 4, 3rd Modes
Eglin GVT 2nd Bending, 70.69 Hz

AD-A082 168

AIR FORCE INST OF TECH WRIGHT-PATTERSON AFB OH SCH00--ETC F/G 20/4
INITIAL DEVELOPMENT FOR A FLUTTER ANALYSIS OF DAMAGED T-38 H0R1--ETC(U)
MAR 80 J O LASSITER

UNCLASSIFIED

AFIT/GAE/AA/80M-2

NL

2 of 2

AD-A082 168



END
DATE
FILMED
4-80
DTIC

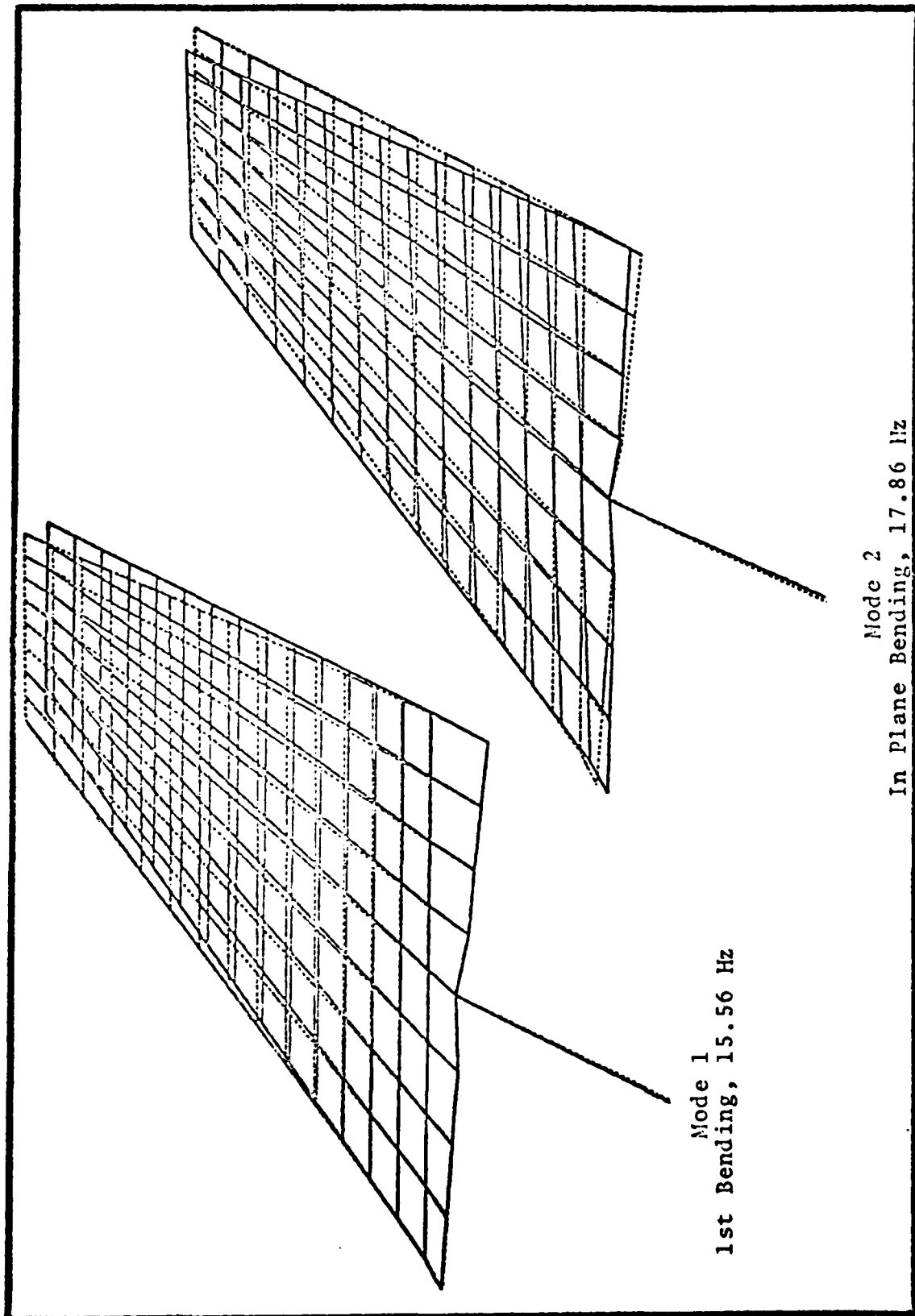


Figure 43. FEM Flexible Root Modes
Symmetrical Boundary Conditions
One Hydraulic System Operating

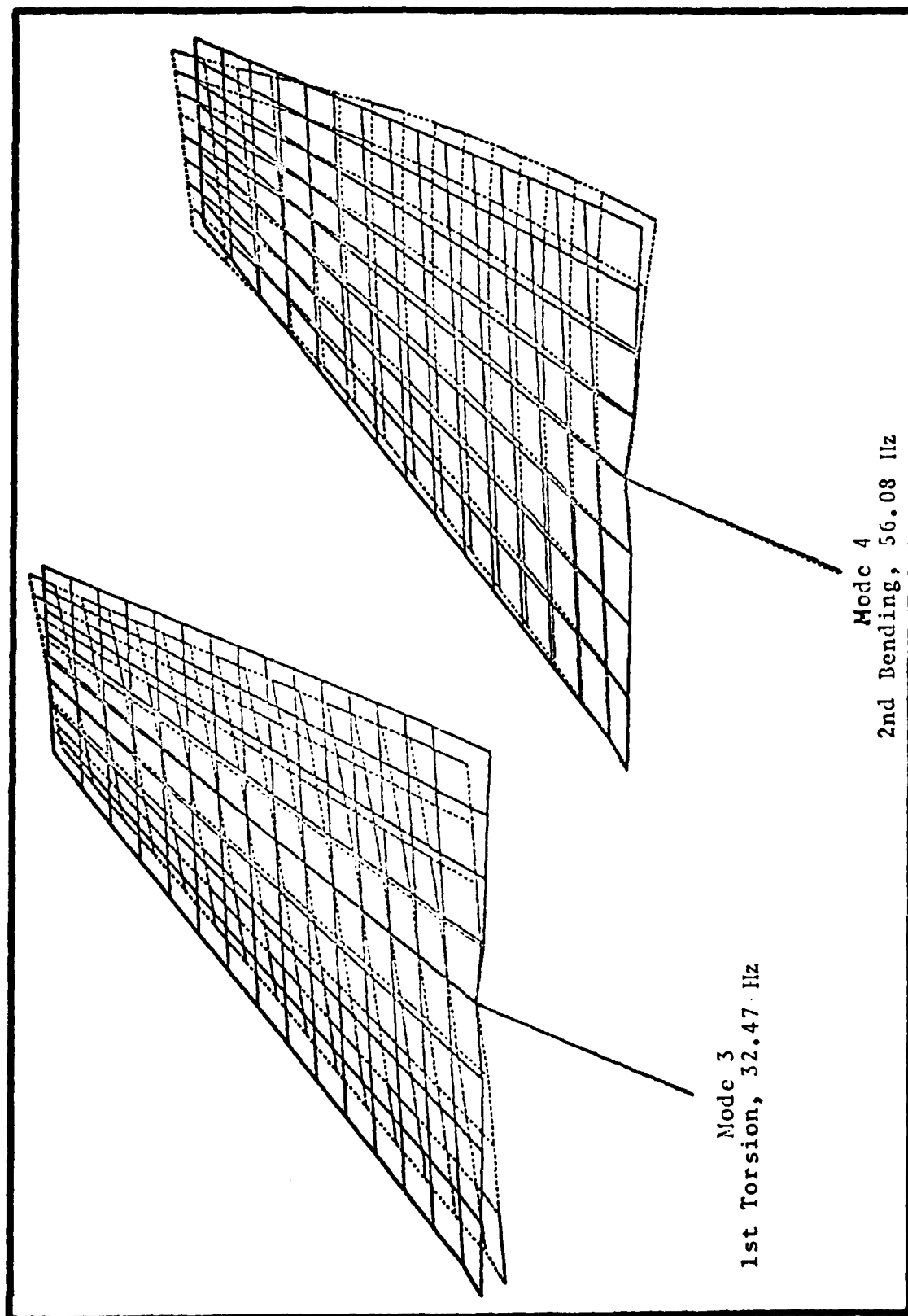


Figure 44. FEM Flexible Root Modes
Symmetrical Boundary Conditions
One Hydraulic System Operating

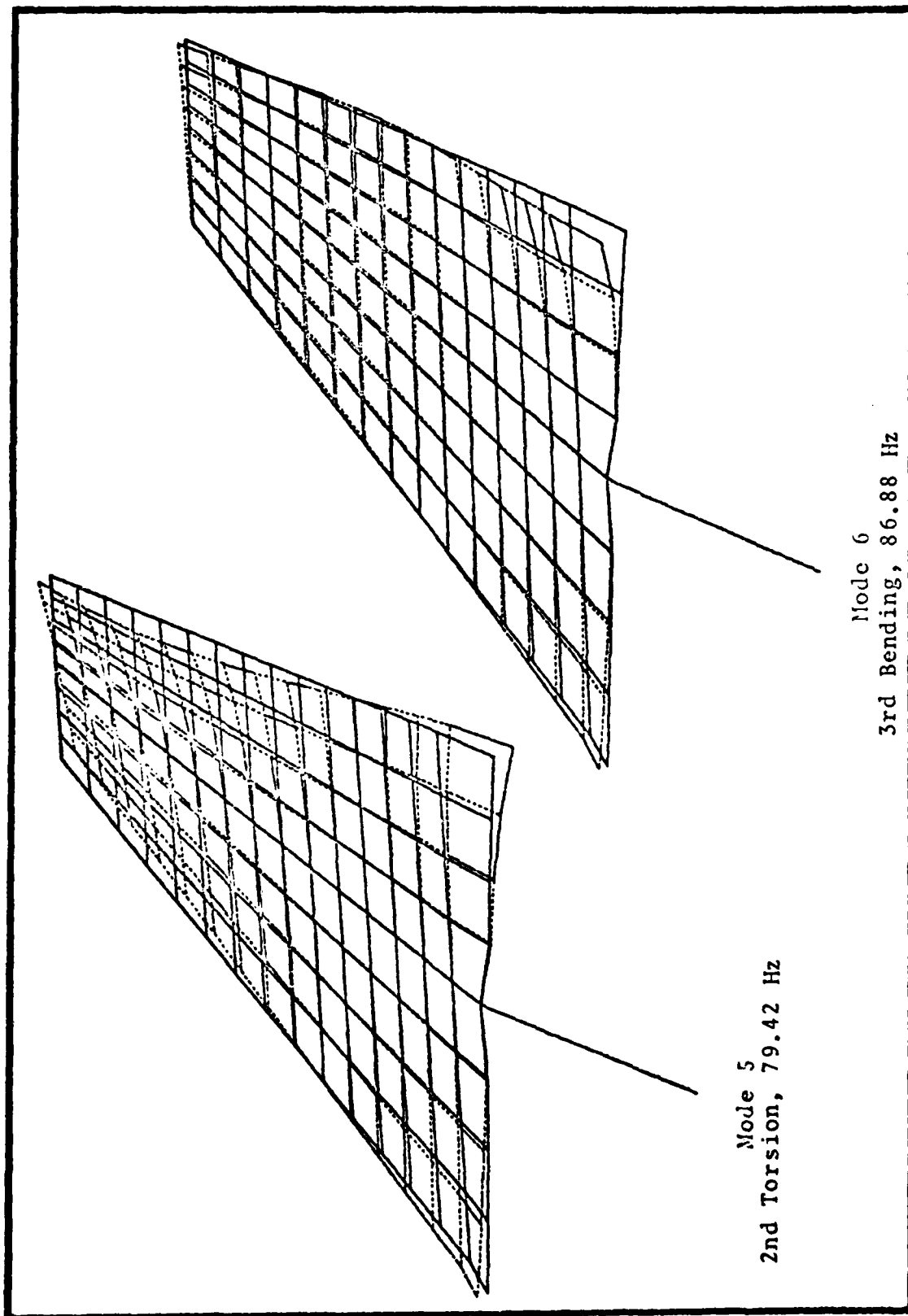
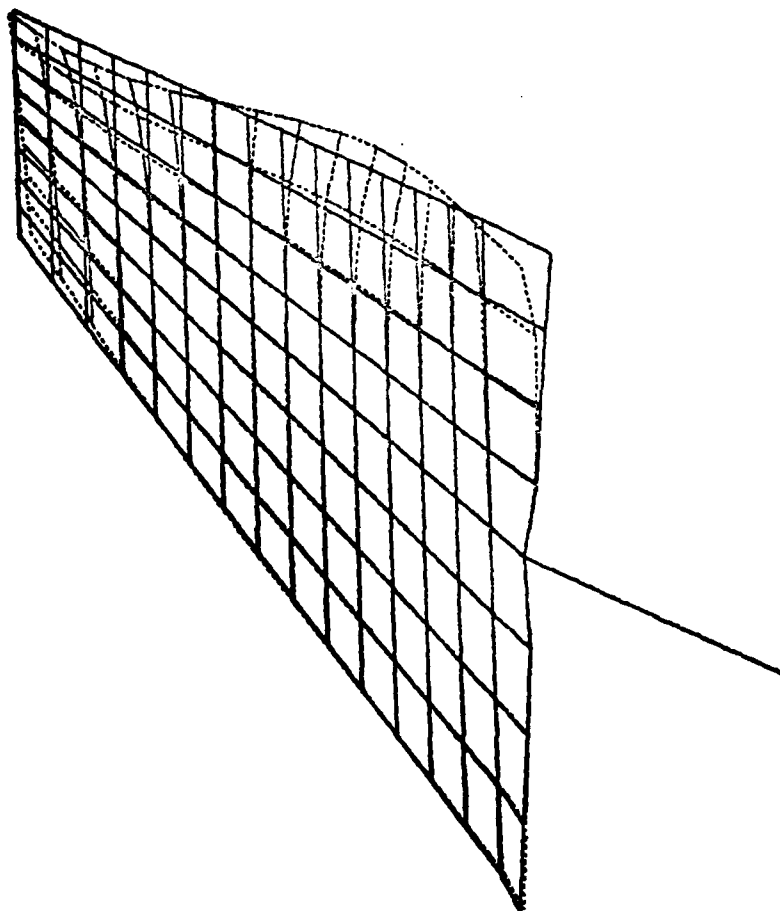


Figure 45. FEM Flexible Root Modes
Symmetrical Boundary Conditions
One Hydraulic System Operating



Mode 7
3rd Torsion, 118.13 Hz

Figure 46. FEM Flexible Root Modes
Symmetrical Boundary Conditions
One Hydraulic System Operating

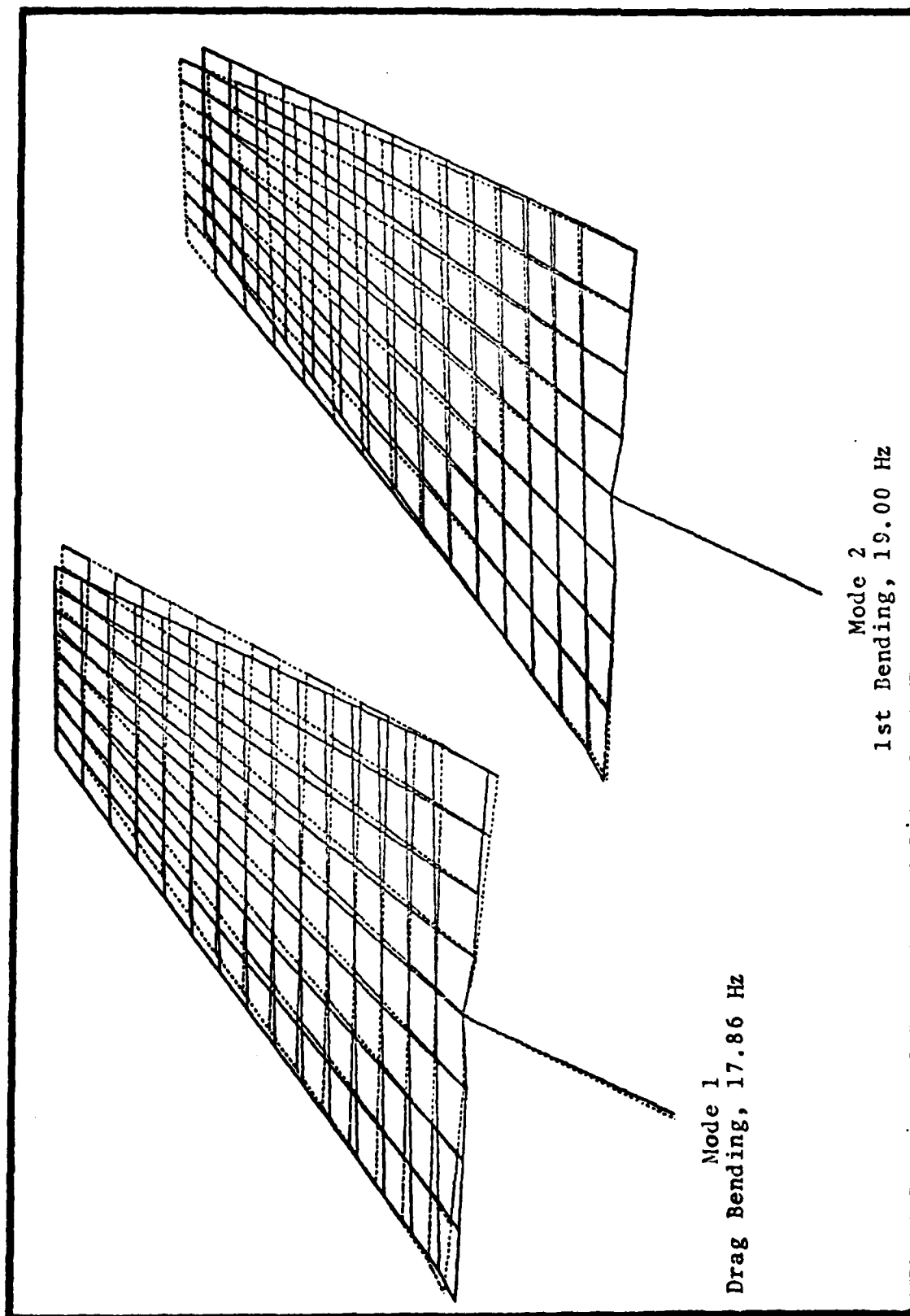


Figure 47. FEM Flexible Root Modes
Anti-Symmetrical Boundary Conditions
One Hydraulic System Operating

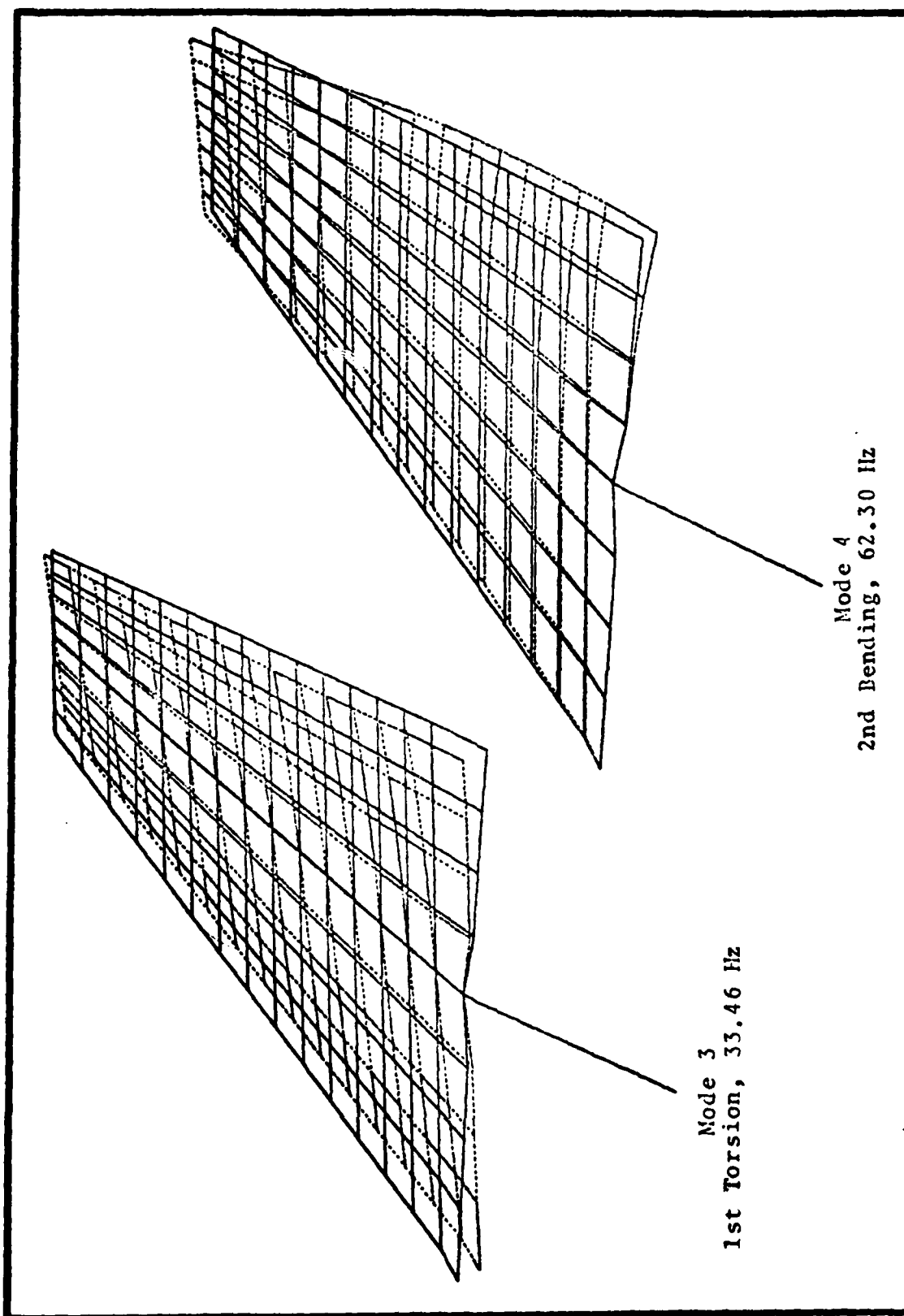


Figure 48. FEM Flexible Root Modes
Anti-Symmetrical Boundary Conditions
One Hydraulic System Operating

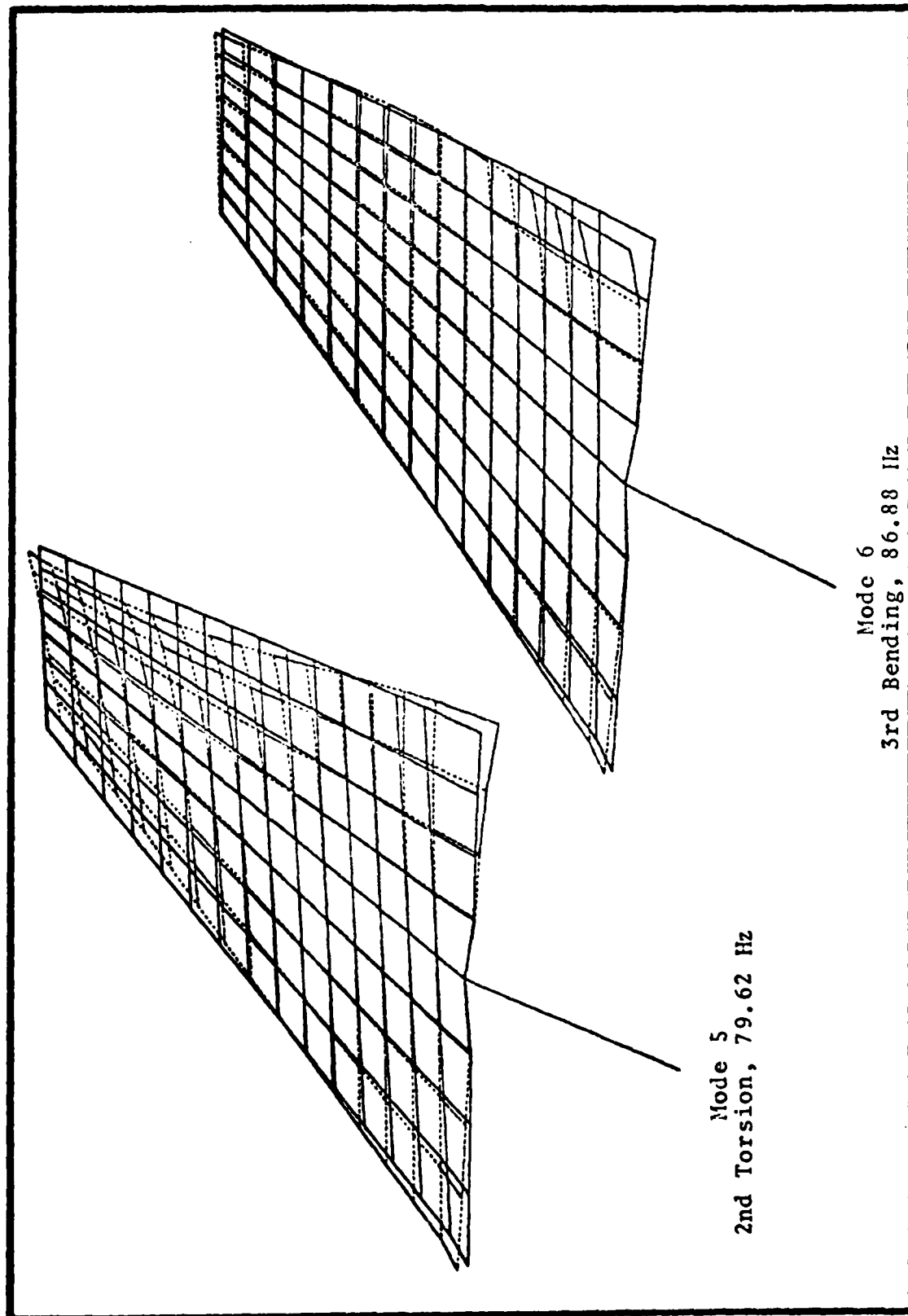
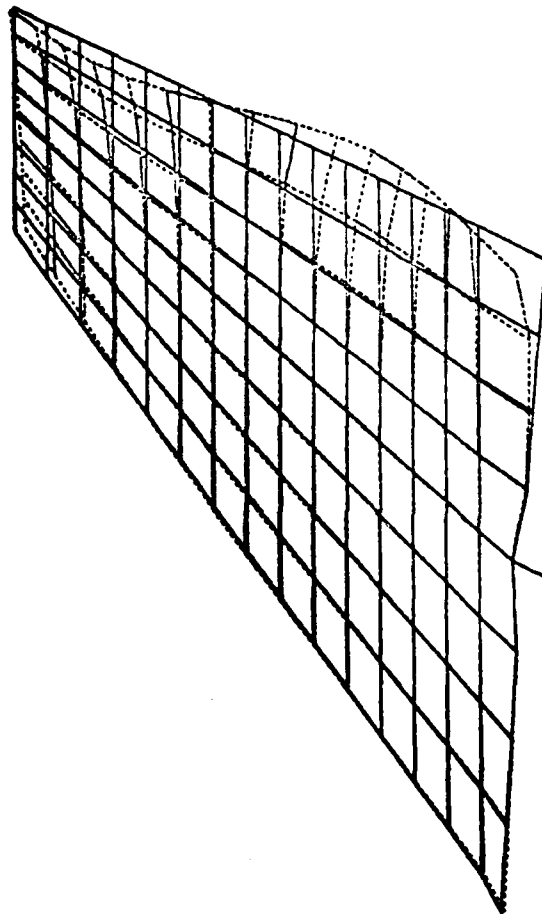


Figure 49. FEM Flexible Root Modes
Anti-Symmetrical Boundary Conditions
One Hydraulic System Operating



Mode 7
3rd Torsion, 118.44 Kz

Figure 50. FEM Flexible Root Modes
Anti-Symmetrical Boundary Conditions
One Hydraulic System Operating

CONCLUSIONS FROM MODAL ANALYSIS

From the rigid-root modal analysis as compared to the NAI study (Case 1), it is seen that the first two modes of the FEM agree to within an acceptable error in both frequency and mode shape. The most important criteria used in comparing mode shapes are relative displacements and location of node lines. It must be noted that two modes of opposite signs are compared in several instances. Also, the different magnitudes are due to the fact that the NASTRAN normalizing factor and STAGING scale factor are different. The third modes differ in frequency by over 20 cps, yet the mode shapes compare favorably.

In comparing the FEM to the GVT performed on one of the horizontal stabilators (Case 2), it is seen that correlation in the first two modes is achieved to within an acceptable error. Since the third modes are largely different, it is concluded that the FEM has only two comparable modes for this case.

A first bending frequency of 22.3 cps and a first torsion frequency of 45.6 cps is reported for the rigid root condition according to the report from SAALC (Ref 1:1-2). In comparing these measured frequencies to the FEM, it is seen that there is a better agreement with respect to the first torsion mode. It is concluded that the FEM has for the most part two modes which are similar to those of the actual horizontal stabilator with a rigid root condition.

As mentioned previously, the flexible-root mode shapes are the most critical. For these conditions, Case 1 shows the first two modes to be in agreement with an acceptable error. Case 2, which compares the FEM to measured flexible-root modes, shows good agreement up to the first three modes. The fourth modes agree closely when shapes are compared (especially node lines), but the frequencies are different by over 20 cps. By comparing frequencies only, Case 3 shows essentially the same results as in the previous two cases. Case 4 shows the first three modes being similar in shape and having acceptable differences in frequencies. Therefore, for the flexible-root condition, it is concluded that the FEM has three and possibly four modes that are similar to the actual structure. By referring to the modes of each case, it is seen that the range of actuator pitch stiffness used in this comparison does not alter the frequencies to a large extent as initially expected.

With the above conclusions, it is decided that the FEM can be used to start an initial development of a flutter analysis. From four to six flexible root modes for both symmetric and anti-symmetric boundary conditions will be used. These are shown in the previous figures. All are for the worst case (i.e., one hydraulic system operating) condition.

V. Doublet Lattice Aerodynamic Model and Flutter Analysis

INTRODUCTION

As mentioned previously, the flutter analysis requires that the finite element model be combined with an aerodynamic model. This section will describe the initial information needed to perform a flutter analysis on the basic finite element model.

DOUBLET LATTICE AERODYNAMIC MODEL

The Doublet Lattice Method is used for interfering lifting surfaces in uniform subsonic flow. Linearized aerodynamic theory is used for the theoretical basis of this method. All lifting surfaces are restricted to lie parallel to the flow.

The structure is divided into plane panels and each panel is further divided into boxes. These boxes should be arranged so that any fold or hinge lines lie along the box boundaries. To develop this model, the CAERO1 card is utilized. The two leading edge grid points (GP 1 and GP 136), the chord length at HSS 29.22 and the tip rib are used in the appropriate fields on this card in setting up the panel. In this case, the entire planform of the horizontal stabilator is a panel with sides parallel to the airstream (positive x) direction.

Additional model and aerodynamic data are supplied by the AERO card. It should be pointed out that the coordinate system for the aerodynamic model is the same as that for the FEM. The boxes of the panel are distributed in the same manner of the QUAD1 elements, that is 5 boxes spanwise and four chordwise. This distribution should be adequate for this structure.

For the interconnection between the structural model and the doublet lattice model, aerodynamic grid points are used. Each box of a panel has an aerodynamic grid point located at its center. The interpolation of structural deformation in particular mode shapes to these aerodynamic degrees of freedom is based on the theory of splines. Since the FEM is two dimensional, surface splines are used. The SPLINE1 card is used to accomplish this interpolation. For this problem, all the structural grid points are attached to this spline. It is quite possible that a smaller number of structural grid points can be used. Surface spline theory uses only the normal displacement (T3) degree of freedom (Ref 15:Section 1.11).

Any extensive verification of this aerodynamic model could be accomplished by using both steady and unsteady airloads. For the steady airloads, structural deformations at zero frequency are used. No attempts are made to do these types of verifications.

NASTRAN FLUTTER ANALYSIS OF AN UNDAMAGED HORIZONTAL STABILATOR

Rigid Format 10, Modal Flutter Analysis, is used for this part. The flutter theory that is chosen is the K method. Looping through three sets of parameters, density ratio, Mach number, and reduced frequency is allowed by this method. A Mach number of 0.8 and sea level density, which is considered a worse case situation, are used. For the reduced frequency, 15 values are used. Seven values in nearly equal increments above and below a particular reduced frequency make up the list of reduced frequencies that are used. The particular reduced frequency was found based on a reported flutter frequency. This flutter frequency, which is for first torsion flutter (Ref 16:55), is 44.9 Hz. For the reference chord length used in calculating the reduced frequency, the mean aerodynamic chord is used (Reference Appendix A). All of these parameters for the looping procedure are accomplished by supplying these data via the FLFACT and MKAERO1 cards.

As seen from the modal analysis, only three to four flexible root modes can be verified. The modes used in the flutter analysis are those for the flexible-root (one hydraulic system operating and symmetric boundary conditions). In order to reduce the size of the problem, only the vertical (T3) degree of freedom is allowed for each grid point (GP 1 to GP 144). The ASET1 card is used for this reduction in

degrees of freedom. These constraints do not indicate that the consistent or lump mass matrix is used. The ASET1 card, which is used by the flutter routine, eliminated the drag bending mode. Drag bending is essentially of no concern to this problem.

On the real and complex eigenvalue cards (EIGR and EIGC, respectively), it is indicated that only four modes are to be obtained. Since drag bending is one of these first five modes in the frequency range of 0.0 Hz to 80.0 Hz, it is eliminated by using the previously described ASET1 card. Therefore, only the first four modes which have been verified will be used. The Inverse Power Method is used for the real eigenvalue problem and the Upper Hessenburg Method for the complex.

It should be pointed out that no structural damping is considered in the analysis at this time. The velocity-damping diagrams can be used to find less conservative flutter speeds that indicate structural damping.

METHODS OF SIMULATING A DAMAGED HORIZONTAL STABILATOR

The more important flutter analysis is to be done for damaged horizontal stabilators. This part will briefly describe how damages or repairs can be simulated in the FEM.

Mass addition due to water absorption can be modeled by increasing the non-structural mass of the membrane element or elements where the water is located. Added mass

due to any type of repair (such as to fill a void) can also be simulated in a like manner. Other ways to add mass due to a repair is to increase the appropriate physical dimensions such as skin thickness or use concentrated masses at the grid points near the repair or damage.

A basic method of modeling stiffness changes due to a repair or damage is to increase (or decrease) the element's moment of inertia values which are caused by changes in dimensions. The changes in inertia can be found by inserting the appropriate modified dimension in the inertia algorithm.

VI. RESULTS

As an overview, it is seen that the static analysis of the FEM gave reasonably good answers, and they indicate that the results could improve if the number of elements was increased. Also, the FEM showed good agreement in weight, CG location, and mass distribution. For the modal analysis, it is indicated that three and possibly four modes for the flexible-root conditions have been verified.

For the flutter analysis, a flutter speed of approximately 175 knots was calculated. This is well below the reported flutter speed (Ref 16:55). No further flutter analysis runs were attempted.

The list of future aspects to be investigated, which is contained in the next section, is obtained from the results of this thesis.

VII. Conclusions

As indicated by the title, this thesis was designed to be an initial development for a flutter analysis of damaged or repaired horizontal stabilators. In the course of the present work done to develop this analysis, it was seen that several other aspects need to be addressed. These are listed as follows and they are taken to be the conclusions of this thesis. Most of the aspects presented will be considered in a follow-on thesis. Also most of the assumptions and restrictions in Part I will be utilized.

(1) The mesh size could be reduced and convergence characteristics can therefore be studied using a static or stress analysis.

(2) For a finite element model of this size, up to seven mode shapes should be verified.

(3) The effects of camber changes should be taken into account. Possibly excessive camber changes can be seen near the trailing edge - root rib area.

(4) Verification of the Doublet Lattice Model using both steady and unsteady airloads.

(5) Once a better verified FEM is obtained, the most critical types of damages and repairs should be investigated for flutter. All the previously studied constraints and conditions should be considered.

Bibliography

1. Golbitz, William C. Determination of the Decrement in Flutter Speed of The Horizontal Stabilizer of the T-38A Aircraft Modified with a Uniform Trailing Edge Repair, SAMME-ER-71-011. Kelly AFB TX: San Antonio Air Logistics Center, November 1971.
2. T.O. 1T-38A-3. "Horizontal Stabilator Damage Repair," T-38A Maintenance and Repair Manual. Kelly AFB TX: San Antonio Air Logistics Center.
3. Aperture Cards (Code Identification Number 76823). Blueprints for the T-38 Horizontal Stabilator. Kelly AFB TX: San Antonio Air Logistics Center.
4. NAI-57-59. T-38A Horizontal Stabilizer. Structural Analysis, Hawthorne CA: Northrop Aircraft, Inc., October 1958.
5. NOR-60-6. Static Test of Complete Airframe for the T-38A Airplane. Hawthorne CA: Northrop Aircraft, Inc., March 1960.
6. Schaeffer, Harry G. MSC/NASTRAN Primer Static and Normal Modes Analysis. Milford, New Hampshire: Wallace Press, Inc., 1979.
7. Halliday, David and Robert Resnick. Physics, Parts I and II. New York: John Wiley and Sons, Inc., 1966.
8. NAI-58-11. T-38A Flutter Characteristics Summary. Vibration and Flutter Analyses. Hawthorne CA: Northrop Aircraft, Inc., June 1960.
9. NAI-58-6. T-38A Vibration Mode Analyses of Empenage. Hawthorne CA: Northrop Aircraft, Inc., May 1959.
10. NASA SP-222(04). The NASTRAN User's Manual, Level 17. Washington DC: Scientific and Technical Information Division, National Aeronautics and Space Administration, December 1977.
11. NAI-58-813. Investigation of the Root Stiffness Properties of the T-38A Horizontal Stabilizer. Hawthorne CA: Northrop Aircraft, Inc., October 1958.

12. Rohlman, William H. CF-5 Horizontal Stabilizer Ground Vibration Test. Eglin AFB FL: Structural Dynamics Laboratory, Air Force Armament Test Laboratory, (AFATL/DLJCS), October 1979.
13. Burnside, O.H. Vibration Analysis of the T-38 Lead-In Fighter with the Addition of Fuselage Centerline Stores, Report No. 6. SWRI Project 03-3980. San Antonio TX: Southwest Research Institute, 1975.
14. Voelker, Leonard S. and Cooley, Dale E. Flutter Analysis of a Horizontal Tail with a Tab, AFFDL-TM-75-119-FYS, Wright-Patterson AFB OH: Air Force Flight Dynamics Laboratory, August 1975.
15. NASA SP-221(03). The NASTRAN Theoretical Manual. Washington DC: Scientific and Technical Information Division, National Aeronautics and Space Administration, March 1978.
16. Report Number 3435-75-48. F-5F Horizontal Stabilizer Plus Trailing Edge Tab, Flutter and Vibration Results. Hawthorne CA: Northrop Corporation, Aircraft Division, May 1975.

APPENDIX A

STABILATOR PHYSICAL PROPERTIES

AND NASTRAN BULK DATA DECK GENERATING PROGRAM

As mentioned in the text blue-prints of the series 3 stabilator (Ref 3) and NAI-57-59 (Ref 4) were relied upon to a great extent during the process of verifying the FORTRAN program that generates the NASTRAN Bulk Data Deck. Also, the horizontal stabilator repair manual (Ref 2) was also used to check certain dimensions. The purpose of this appendix is to briefly describe the physical properties of the stabilator that have not already been shown. Also, the steps used in checking the FORTRAN program will be included.

Figure 51 shows the planform of the finite element model of the stabilator. Included in this figure are the dimensions that are usually given for such a structure. All of these dimensions are obtained from the FEM.

In addition to the basic dimensions, the algorithms that describe the shape of the leading edge, spar, trailing edge, skin thickness forward of the spar and the chord are given in Figure 51. These algorithms are used in the FORTRAN program. Note that all of these algorithms are a function of HSS.

The FORTRAN program is divided into 8 modules (or sections). Each section performs a specific task which

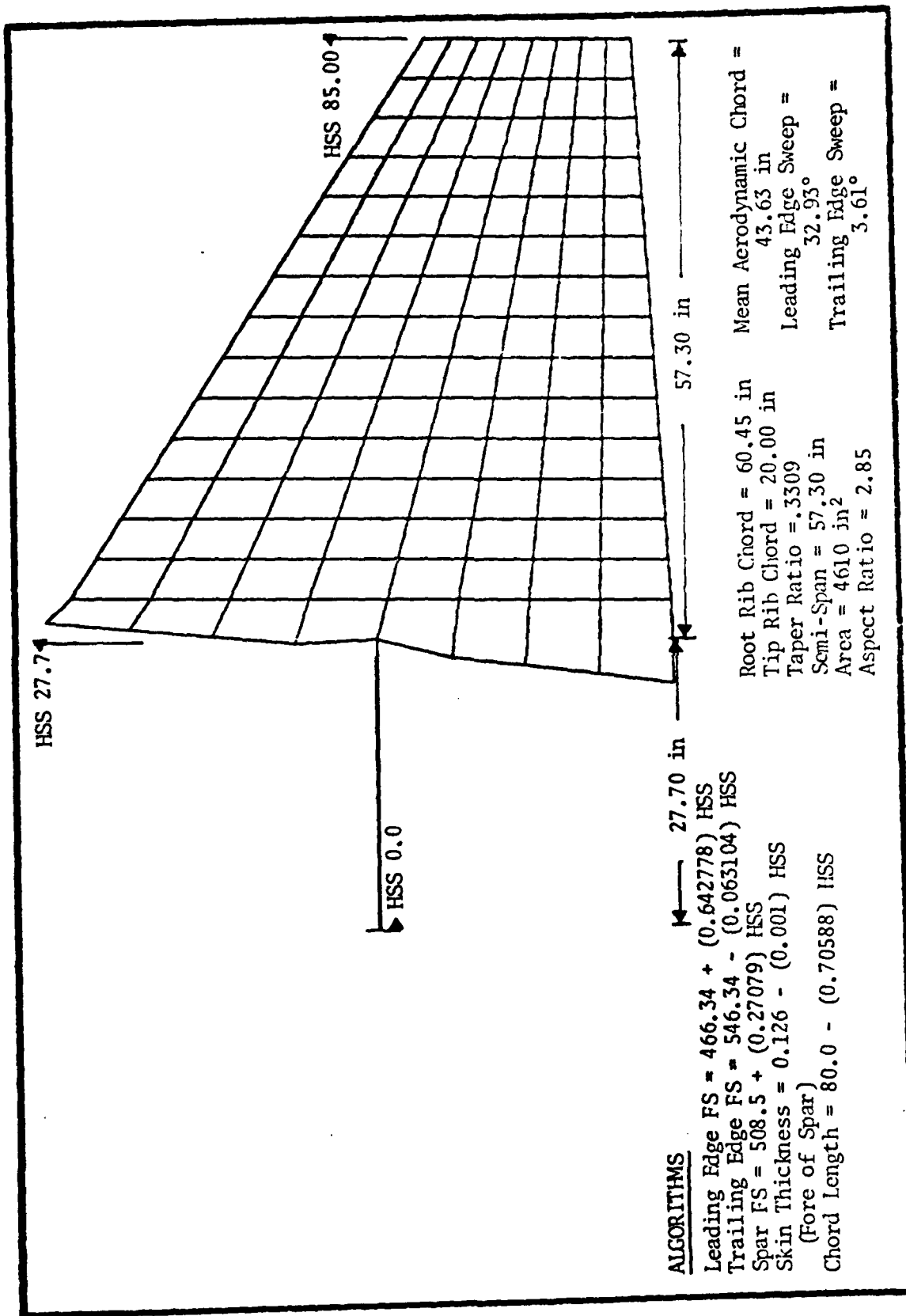


Figure 51. Horizontal Stabilizer Physical Dimensions and Properties

is either indirectly or directly related to the production of most of the cards contained in the Bulk Data Deck.

These modules are listed in order of occurrence as follows:

- Module 1 - Input of data statements for particular dimensions and algorithms
- Module 2 - Set up grid point mesh, calculate coordinates (FS and HSS) of each grid point. The coordinates of grid points on the root rib are found from interpolating values.
- Module 3 - Sequencing of grid points for QUAD1 elements. Development of connectivity and property cards for QUAD1 elements.
- Module 4 - Sequencing of grid points for BAR elements that represent the main spar. Development of associated property and connectivity cards.
- Module 5 - Development of the cards for the root rib bar elements (similar to Module 4).
- Module 6 - Development of cards for the trailing edge BAR elements (similar to Module 4).
If modules for the leading edge and tip rib BAR elements were included, they would be in this section of the program.

Module 7 - Output of grid cards.

Module 8 - Formulation of material (MAT1) cards.

The primary methods of calculating the dimensions of a stabilator component (for example, skin thickness, airfoil thickness, spar web thickness, etc.) which are used in determining the properties of an element (area, volume, moment of inertia) are the above algorithms and data statements. The data statements are used in conjunction with a one dimensional subroutine. For instance, once the center of an element is found in terms of HSS and percent chord, the needed dimension is found from interpolating values of that dimension. Of course, these interpolating values are based on HSS value and/or percent chord. A particular dimension and its associated HSS values or percent chord values is found from the blueprints.

Most of the algorithms of properties for a particular component have a constant dimension. An example of this aspect appears on the forward root rib. Going chordwise, the flange width remains essentially constant. Dimensions of this nature were found from the blueprints.

Important dimensions for each component were verified using the FORTRAN program. These checks were accomplished by printing out a particular dimension and its respective HSS value or percent chord. Most of these dimensions do

not appear explicitly in the output. For an example, a spar web thickness is used in finding the moment of inertia for a bar element, yet this property and not the dimension appears on the element's property card. The lists of values were compared to those for the particular components using the associated blueprint. Errors were corrected by using the appropriate interpolating values. Errors in constant values of algorithms were also verified and changed where necessary.

Appendix B

EXPERIMENTAL MODAL ANALYSIS

A ground vibration test was performed on one of the stabilators obtained from SAALC. Rigid root conditions were simulated by clamping the torque tube near the location of the aircraft centerline (GP 146 on Figure 3). The stabilator was hung vertically from the side of a large I-beam mounted in concrete.

The grid point mesh size was drawn on the stabilator and locations of grid points were indicated. For the modal analysis, a five by five array of deflection points was utilized. For HSS values of 35.34, 46.80, 58.26, 69.72, and 81.18, five deflection points were used. The deflection point percent chord values for each HSS are 0.1317, 0.2635, 0.5270, 0.7630, and 0.8817. Small aluminum pads were glued to each location in order to attach standard accelerometers to the stabilator. For the modal analysis, a Hewlett-Packard 5423A Structural Dynamics Analyzer was utilized. A hammer and load cell set-up enabled the stabilator to be subjected to an impulsive load. Only three to four samples were taken at each deflection point. These samples yielded the frequencies and converted mode shapes that are shown in this thesis.

VITA

John O. Lassiter was born on 5 December 1955 in Gadsden, Alabama, where he spent the first 18 years of his life. He then spent four years at the University of Alabama in Tuscaloosa, and graduated from there on 14 May 1978 with a Bachelor of Science degree in Aerospace Engineering. On that same day, he received his commission into the United States Air Force through the ROTC program. Lt Lassiter was then assigned to the School of Engineering, Air Force Institute of Technology, to earn a Master's Degree in Aeronautical Engineering. His next assignment after graduation is at the Air Force Armament Laboratory, Aircraft Compatibility, Eglin Air Force Base, Florida.

Permanent Address: 2109 Argyle Place
Gadsden, Alabama 35901

UNCLASSIFIED

SECURITY CLASSIFICATION OF THIS PAGE (When Data Entered)

REPORT DOCUMENTATION PAGE		READ INSTRUCTIONS BEFORE COMPLETING FORM
1. REPORT NUMBER	2. GOVT ACCESSION NO.	3. RECIPIENT'S CATALOG NUMBER
AFIT/GAE/AA/80M-2		
4. TITLE (and Subtitle)		5. TYPE OF REPORT & PERIOD COVERED
INITIAL DEVELOPEMENT FOR A FLUTTER ANALYSIS OF DAMAGED T-38 HORIZONTAL STABILATORS USING NASTRAN		AFIT THESIS
		6. PERFORMING ORG. REPORT NUMBER
7. AUTHOR(s)		8. CONTRACT OR GRANT NUMBER(s)
John O. Lassiter 2d Lt USAF		
9. PERFORMING ORGANIZATION NAME AND ADDRESS		10. PROGRAM ELEMENT, PROJECT, TASK AREA & WORK UNIT NUMBERS
Air Force Institute of Technology (AFIT/EN) Wright-Patterson AFB, Ohio 45433		
11. CONTROLLING OFFICE NAME AND ADDRESS		12. REPORT DATE
		March 1980
		13. NUMBER OF PAGES
		109
14. MONITORING AGENCY NAME & ADDRESS (if different from Controlling Office)		15. SECURITY CLASS. (of this report)
		Unclassified
		15a. DECLASSIFICATION DOWNGRADING SCHEDULE
16. DISTRIBUTION STATEMENT (of this Report)		
Approved for public release; distribution unlimited		
17. DISTRIBUTION STATEMENT (of the abstract entered in Block 20, if different from Report)		
18. SUPPLEMENTARY NOTES		
Approved for public release; IAW AFR 190-17 Joseph P. Hipps, Major, USAF Director of Information		
19. KEY WORDS (Continue on reverse side if necessary and identify by block number)		
NASTRAN Finite Elements Mode Shapes Flutter Analysis		
20. ABSTRACT (Continue on reverse side if necessary and identify by block number)		
<p>This thesis demonstrates the development and response of a finite element model of the T-38 horizontal stabilator using NASTRAN. The finite element model is to be used in a flutter analysis of damaged or repaired stabilators. The objective of the flutter analysis is to determine absolute values and degradations of the flutter speed due to different types of damages and repairs.</p> <p>Development of a finite element model with two dimensional quadralateral</p>		

~~UNCLASSIFIED~~

SECURITY CLASSIFICATION OF THIS PAGE(When Data Entered)

and bar elements is described. For verification, a static analysis of the finite element model yielded for the most part qualitatively agreeable values in comparison to an influence coefficient study.

For showing the dynamic response of the finite element model, a modal analysis using both rigid and flexible root boundary conditions is used. The rigid root analysis shows agreement between the first two modes and the flexible root compares favorably up to three and possibly four modes. With these results, it is decided to use the finite element model in an initial flutter analysis.

In the flutter analysis a doublet lattice aerodynamic model is combined with the finite element model for an undamaged stabilator. Poor agreement of the NASTRAN flutter speed with other available data indicates possible camber effects and the need for a verification of the aerodynamic model using steady and unsteady airloads. A brief description of a method of simulating repairs and damages of a horizontal stabilator is included.

~~UNCLASSIFIED~~

SECURITY CLASSIFICATION OF THIS PAGE(When Data Entered)